



Centre Technique Industriel  
de la Construction Métallique

Domaine de Saint-Paul  
102, route de Limours  
F-78471 Saint-Rémy-lès-Chevreuse Cedex  
Tél : 33 (0)1 30 85 25 00 Fax : 33 (0)1 30 52 75 38  
cticm@cticm.com  
www.cticm.com

---

**Ref. CTICM**

SRI – 07/xxx - CR/PB

---

Affair: 04-905

**Division** : Fire Safety and Certification

**Section** : Fire Research

Tél : + 33 (0)1 30 85 25 23 Fax : + 33 (0)1 30 85 37 29

E-Mail : chrenaud@cticm.com

# **Contract RFS-04048 “Stainless Steel in Fire”**

## **WP2 : COMPOSITE MEMBERS IN FIRE**

### **FINAL REPORT**

**August 7<sup>th</sup>, 2007**

---

**Author**

Christophe RENAUD

---

**Number of pages:** 72



Établissement certifié qualité ISO 9001 : 2000, le CTICM assure un suivi de chaque étude conformément à ses procédures qualité

## **1 EXECUTIVE SUMMARY**

The present research work was focused on both experimental and numerical investigation of the mechanical behaviour of composite members with austenitic stainless steel. Within the experimental investigation, a number of fire tests have been carried out on both rectangular hollow section columns filled with concrete and partially protected floor beams with exposed part in stainless steel and concrete protected part in carbon steel. Based on these fire tests, corresponding numerical analysis has been made using advanced calculation models to check, on the one hand, the validity of these models, and on the other hand, to perform parametric studies with the purpose of developing simple calculation methods providing a practical rule for daily design of composite members with austenitic stainless steel. It has been shown through the comparison with numerical results and fire tests that the proposed calculation methods are suitable to predict with a good precision the fire resistance of composite columns with hollow stainless steel section and partially protected floor beams with exposed part in stainless steel.

## 2 CONTENTS

1 EXECUTIVE SUMMARY .....	2
2 CONTENTS.....	3
3 INTRODUCTION .....	4
4 OBJECTIVES.....	4
5 EXPERIMENTAL WORK.....	4
5.1 TESTING PROGRAMME ON COMPOSITE COLUMNS .....	4
5.1.1 TEST SPECIMENS.....	4
5.1.2 TEST ARRANGEMENTS .....	7
5.1.3 TEST RESULTS.....	10
6 NUMERICAL ANALYSIS.....	14
6.1 ASSUMPTIONS FOR NUMERICAL SIMULATIONS.....	14
6.2 RESULTS OF NUMERICAL SIMULATIONS.....	15
6.2.1 THERMAL RESPONSE .....	15
6.2.2 MECHANICAL RESPONSE.....	19
6.3 SYNTHESIS OF RESULTS .....	21
7 DEVELOPMENT OF DESIGN GUIDANCE.....	23
7.1 COMPOSITE COLUMNS.....	23
7.1.1 PARAMETRIC STUDY OF ULTIMATE BUCKLING LOAD OF COMPOSITE COLUMNS .....	23
7.1.2 PROPOSED DESIGN METHOD .....	28
7.1.3 FIELD OF APPLICATION .....	33
7.1.4 COMPARISON BETWEEN THE PROPOSED DESIGN METHOD AND THE NUMERICAL MODEL .....	33
7.1.5 COMPARISON BETWEEN FIRE TEST RESULTS AND SIMPLIFIED METHOD .....	37
7.2 FLOOR BEAMS WITH CONCRETE FIRE PROTECTION .....	38
7.2.1 PRELIMINARY PARAMETRIC STUDY .....	38
7.2.2 PROPOSED DESIGN METHOD FOR SIMPLY SUPPORTED BEAMS.....	41
7.2.3 COMPARISON BETWEEN THE PROPOSED DESIGN METHOD AND THE NUMERICAL MODEL .....	44
8 COMPARAISON BETWEEN STAINLESS STEEL AND CARBON STEEL .....	47
9 CONCLUSIONS.....	53
10 RECOMMANDATIONS FOR FURTHER WORKS.....	53

### 3 INTRODUCTION

Although many European research projects have already shown its great fire resistance, the use of high-strength austenitic stainless steel as steel-concrete composite members remains not very used in practice because of the lack of knowledge on the fire behaviour of this type of structural members. Due to its good behaviour at elevated temperature, stainless steel could become a practical alternative solution to conventional structural carbon steel reducing for example the cross-section size of steel profiles or the ratio of additional reinforcing bars which are often needed with carbon steel to achieve the required fire resistance. So, in order to investigate the fire behaviour of composite members with austenitic stainless steel, a total of nine fire tests have been carried out, included both rectangular hollow section columns filled with concrete and partially protected slim-floor beams with exposed part in stainless steel and concrete protected part in carbon steel. All test members were grade EN 1.4404 stainless steel currently used in construction. Based on fire tests, corresponding numerical analysis have been made using an advanced finite element model able to simulate the mechanical behaviour and resistance of composite members exposed to fire. This model was proved already to be in good agreement with several fire tests performed on composite members with conventional structural carbon steel. Reasonably good agreement has been obtained between the test results and numerical analysis. Globally, the comparison between failure times ascertained either numerically or experimentally shows a divergence less than 15%, what is reasonable considering uncertainties inherent to tests data, such as the uniformly heated length of members, the degree of rotational restraint at the ends, unintentional eccentricity of load, .... Once the finite element models were validated as good as possible against the available test data, parametric study has been performed to develop design rules for composite columns and floor beams. The proposed design methods are consistent with the general flow chart in EN 1994-1-2 used to check the other types of composites members but including some specific characteristics.

The present report describes tests, numerical modelling and the development of design guidance for investigated composite members with stainless steel.

### 4 OBJECTIVES

The present Work Package aims at:

- Providing available data on the basis of an experimental investigation (on fire behaviour of both concrete filled RHS columns and beams with concrete fire protection) and a series of parametric studies using advanced calculation models validated against above experimental results.
- Developing design guidance for both concrete filled hollow stainless steel column and partially protected floor beams.

### 5 EXPERIMENTAL WORK

Fire tests on seven columns and two beams were carried out in France (Fire station of CTICM in "Maizières-Les-Metz") for the purpose of studying the structural behaviour of stainless steel-concrete composite members subjected to fire

#### 5.1 TESTING PROGRAMME ON COMPOSITE COLUMNS

##### 5.1.1 Test specimens

The main structural properties of tested composite columns are collected in **Table 1**. All columns were square hollow steel sections with cross-section sizes ranging from 150x8 to 300x8 mm. Columns were filled with either reinforced or non-reinforced concrete core. Additional reinforcement, if used, was defined by four identical longitudinal bars, with a diameter chosen to achieve a ratio of reinforcement  $A_s/(A_s+A_c)$  of approximately 2% and an axis distance of reinforcing bars  $u_s = 30$  mm. The stainless steel grade of hollow section was EN 1.4401. The length of the column was 4000 mm.

Table 1: Structural details of composite columns with hollow steel section

Column	Cross-section	Stainless Steel grade	Rebars		Loading		R (min)	Length (mm)
	b×e (mm)		diameter	Cover* (mm)	Load (KN)	eccentricity		
n°1	150×8	EN1.4401	none	-	400	5 mm	30	4000
n°2	200×8	EN1.4401	none	-	240	0.25×b**	60	4000
n°3	200×8	EN1.4401	4Φ14	30	630	5 mm	30	4000
n°4	200×8	EN1.4401	4Φ14	30	240	0.25×b**	60	4000
n°5	300×8	EN1.4401	none	-	750	0.5×b**	30	4000
n°6	300×8	EN1.4401	4Φ22	30	1000	0.125× b**	60	4000
n°7	300×8	EN1.4401	4Φ22	30	800	0.25× b**	60	4000

\* distance between the axis of longitudinal reinforcements and the border of concrete core

\*\* external side of hollow steel section

All columns were tested under eccentric load. A small eccentricity of loading of 5 mm was applied to both column ends in order to induce an overall flexural buckling mode of failure under the fire condition.

The main structural properties of tested beams are reported in **Figure 1** and

**Table 2.** Beams were simply supported hybrid I-section (stainless steel lower flange, carbon steel web and top flange) of 5m span (this value corresponds to the existing testing capabilities for beams at CTICM). Two different I cross-sections have been tested. The first beam consisted of ½ HEA 450 and 15mm thick × 500 mm stainless wide plate. The second beam consisted of carbon steel HEB 200 and 15mm thick × 360 mm stainless wide plate. Beams were partially encased with concrete. Concrete was reinforced by stirrups welded to the web of the H profile and four longitudinal reinforcing bars of diameter  $\phi=6\text{mm}$ . The loading was applied in two points so as uniform bending moment was present in mid-span area of beams. The load  $P$  applied on beams was 100 kN and 75 kN respectively.

It should be noted that the dimensions of the chosen beams are close to the IF and SF beams product by ARCELOR.

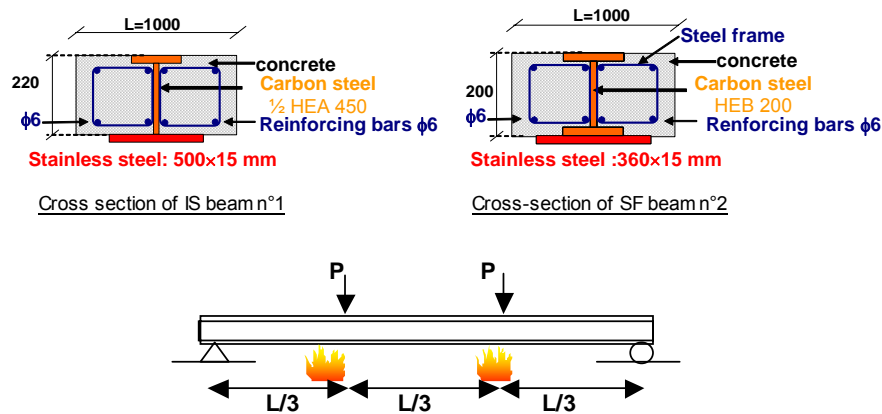
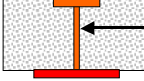
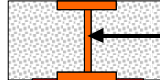


Figure 1. Structural details of tested beams.

Table 2: Structural details of composite beams

Beam	Cross-section	Stainless steel grade	Load P (KN)	R (min)	Length (m)
n°1	 <p>carbon steel 1/2 HEA 450</p> <p>Stainless steel: 500x15 mm</p>	EN1.4401	-100.0	60	4.90
n°2	 <p>carbon steel HEB 200</p> <p>Stainless steel :360x15 mm</p>	EN1.4401	-75.0	60	4.90

Test loads applied on columns and beams were evaluated by preliminary numerical analyses to achieve a fire rating of 30 or 60 minutes. As the results of the material tests were not available, initial design of the loads were performed assuming the following mechanical properties:

- Stainless steel grade EN1.4401 with yield strength:  $f_y=240$  MPa,
- Yield strength of reinforcing steel (column):  $f_{sk} = 500$  MPa,
- Compressive strength of concrete:  $f_c=30$  Mpa.
- Carbon steel grade E24 with yield strength:  $f_y = 235$  MPa,

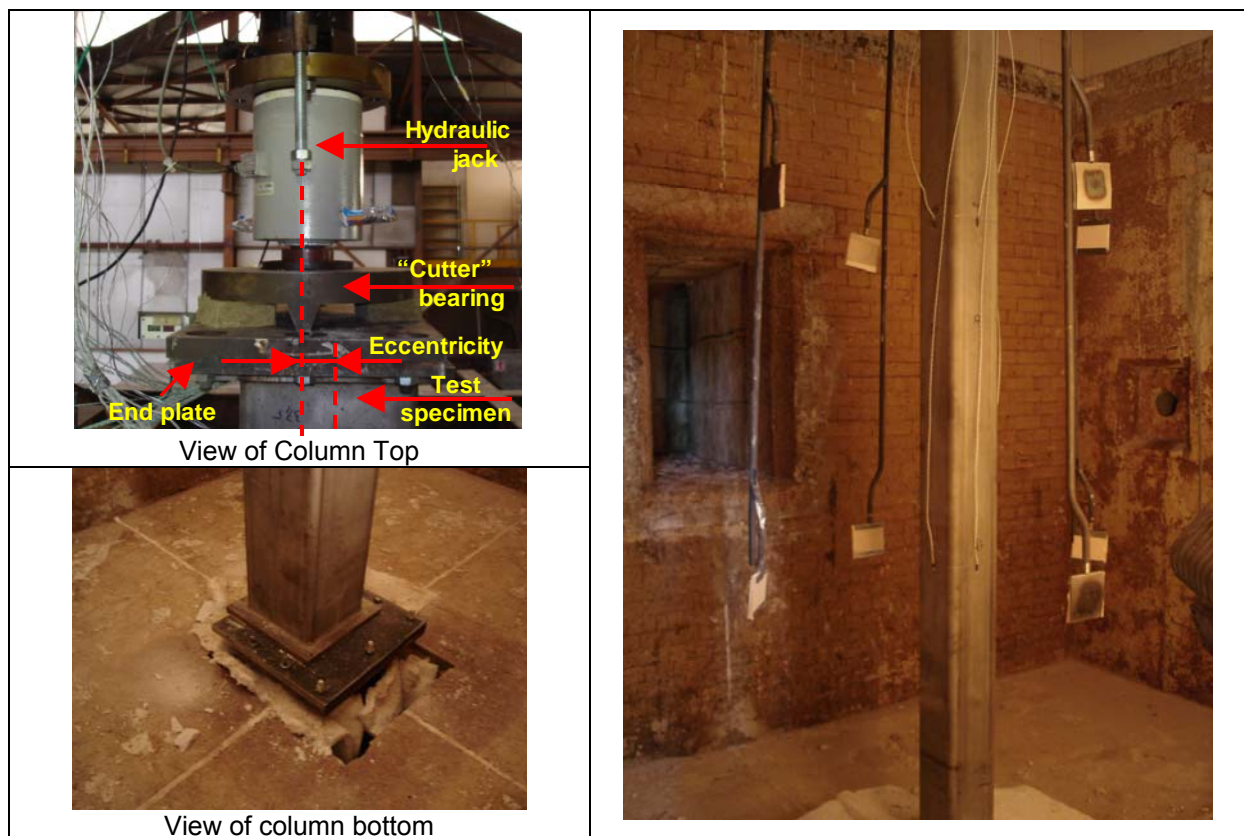
Mechanical properties of member components (hollow section, concrete, reinforcing bars, carbon steel profile) were checked after fire tests by doing material tests which have lead to real mechanical properties indicated in paragraph 5.1.3.

### 5.1.2 Test arrangements

Test set-up of column is described on **Figure 2**. Each column was located at the centre of the furnace and was subjected to a compressive load, applied before fire test and kept constant during the test until the failure. Columns were exposed to heating controlled in such a way that the average temperature inside the furnace follows, as closely as possible, the ISO-834 standard fire curve. Columns were tested with both ends hinged. For that, support conditions at the top end and the bottom end of columns were built-up from additional end plates and cutter bearings (see **Figure 3**).

Moreover, to obtain eccentric load, cutter bearings were shifted in comparison to the gravity center of the cross-section. Both ends of the specimens were free to rotate about the axis perpendicular to cutters bearings but restrained to rotate about the other axis. Loading was applied by a hydraulic jack of capacity one hundred tons located outside and above the furnace chamber. The load was controlled manually and measured using pressure transducers.

View of one of the tested columns and their end support are shown in **Figure 3**.



During all tests, the furnace temperature will be continuously measured with twelve plate thermometers on four sides of the specimen at 100 mm from the surface of the specimen. Thermocouples were also installed on the hollow steel section and the reinforcing bars as well as in the concrete core: Three cross-sections were equipped with thermocouples along the column length (at  $L/4$ ,  $L/2$  and  $3L/4$ ) in order to measure the temperature field. Details about the column length which was directly exposed to fire during the test are given in **Figure 4**. In fact, only three-quarter of the columns were heated (which correspond to the testing capabilities of CTICM). Moreover, the top of the column should be outside the furnace to allow its loading.



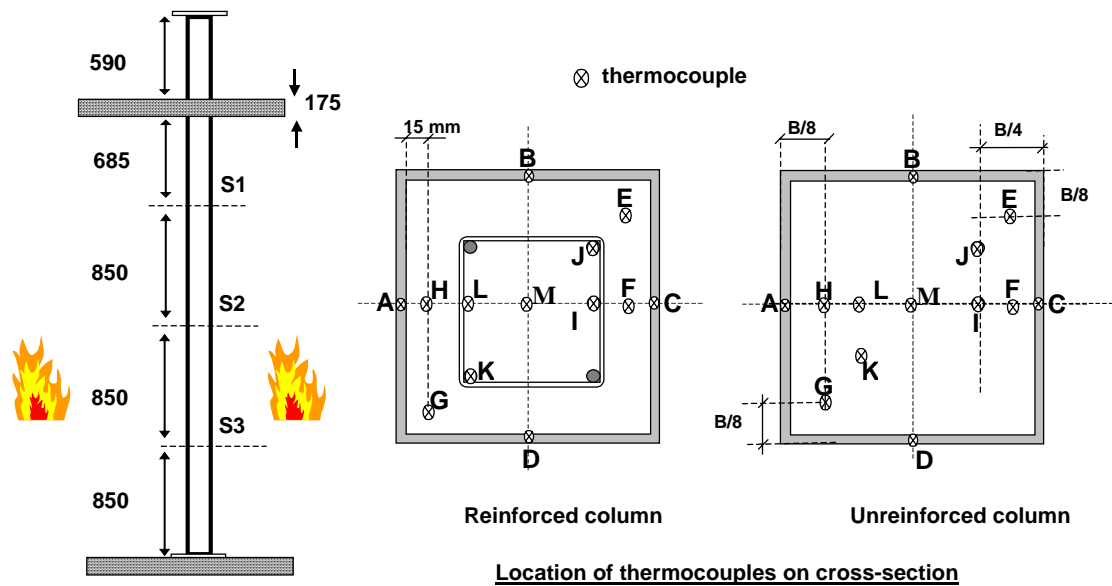


Figure 4 : Thermocouple location in the steel and concrete core

Axial deformations of the test specimen were determined by measuring the displacement of the top of the column (outside the furnace) using transducers. The rotations of the lower supporting end plate along two axes were also measured during the test by two inclination sensors. Failure time measured during all the test corresponds to the condition when each column could not bear the applied load any more.

Specimens from steel profiles, reinforcing bars and concrete were used to determine the real mechanical properties (yield and ultimate tensile strengths of steel and compressive strength of concrete).

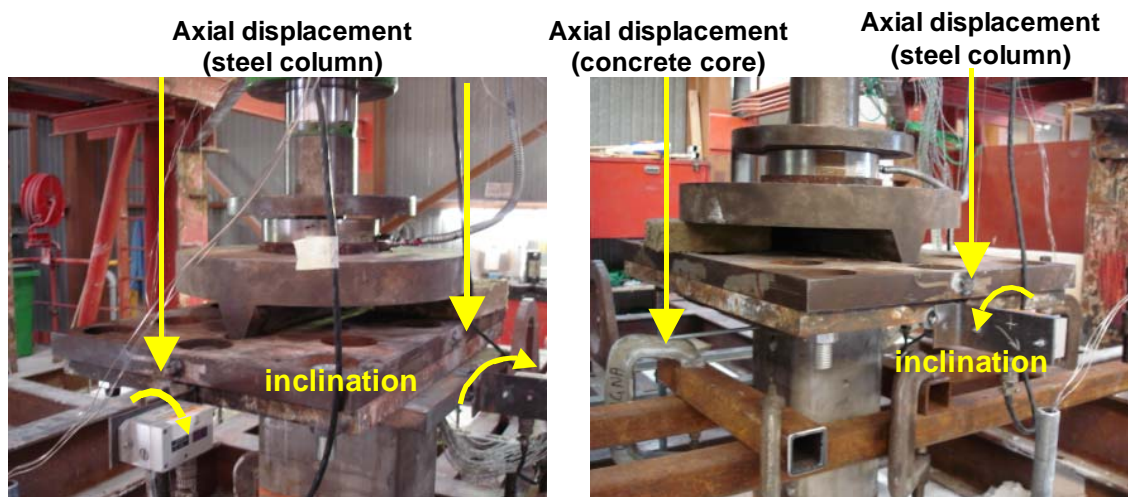


Figure 5: Location of displacement measures

The experimental set-up for the beam is shown in **Figure 6**. The ISO-834 standard fire curve was followed inside the furnace to heat the test beam. The load was applied to the beam at least 15 minutes before the heating period and was maintained until the beam failed.

During the tests, heating of the beams has been measured on five sections (S1, S2, S3, S4 and S5), uniformly distributed along the beams by means of thermocouples located at several points over the cross-section: The position of thermocouples is shown in Figure 6.

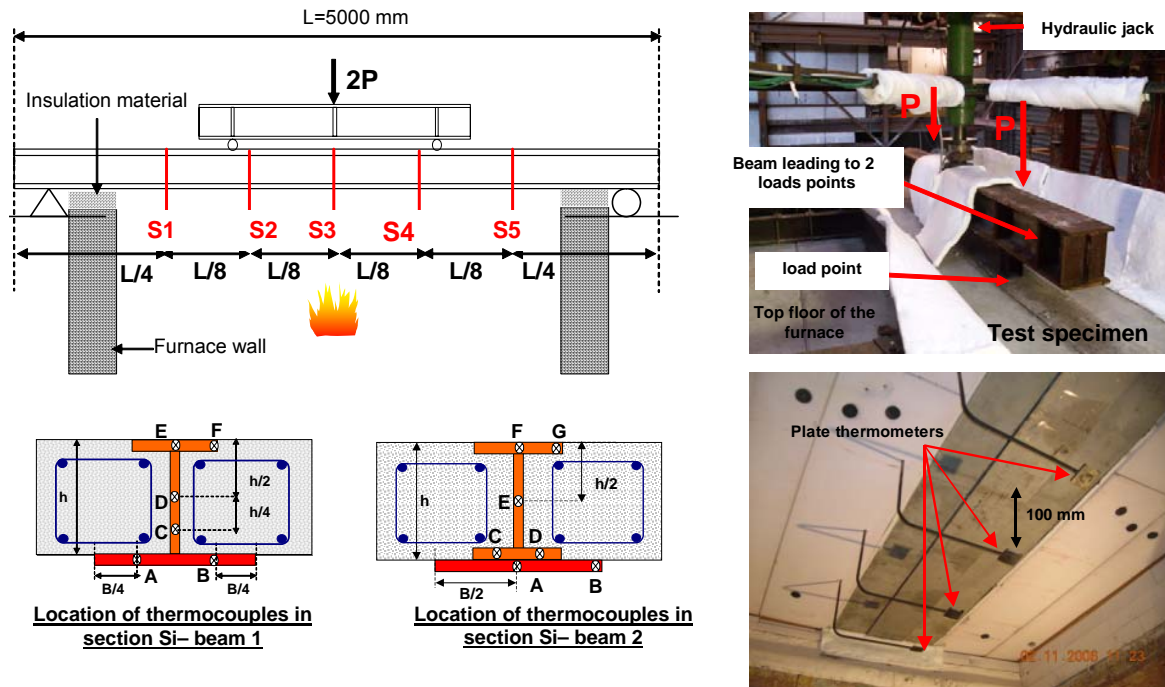


Figure 6 : Thermocouple location in the steel profile and concrete

Furnace temperatures will be recorded using five plate thermometers located at the level of the five preceding sections (one per section). Moreover, two linear displacement transducers were positioned above the mid-span of the beam to measure the central deflection of the beam during the test.

### 5.1.3 Test results

#### Fire behaviour of columns:

Failure times measured during the tests are reported in **Table 3**. They correspond to the condition where columns could no longer bear the applied load any more. It can be noted that all failure times were higher than the expected fire ratings (R30 or R60). Reasons are that initial design of columns was made using the nominal values of the mechanical properties of materials and assuming a uniform temperature distribution along the full column height.

Table 3: Measured failure time of tested composite columns

Column	Load ratio*	Failure time (min)	Temperature in the hollow section (°C)	Failure mode
N°1	0.42	42	775	Flexural buckling
N°2	0.22	59.5	850	Flexural buckling
N°3	0.31	56	835	Flexural buckling + local buckling
N°4	0.20	71	910	Flexural buckling + local buckling
N°5	0.46	38	700	Flexural buckling + local buckling
N°6	0.29	70.5	890	Flexural buckling + local buckling
N°7	0.29	62	850	Flexural buckling + local buckling

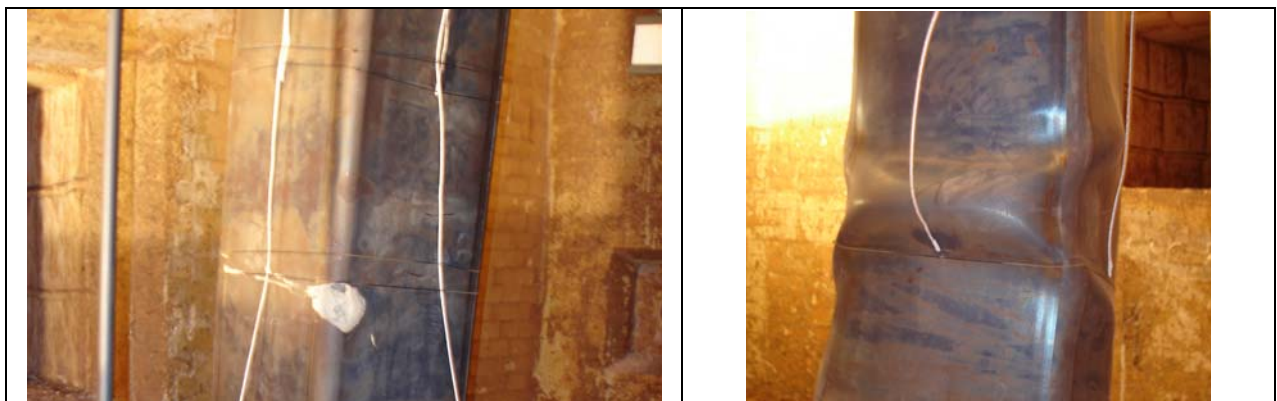
\* As there is no available design method to check the buckling resistance of stainless steel composite column at room temperature, the load level of columns is defined here as  $N_{appl}/N_{Rd}$ , where  $N_{appl}$  is the test load and  $N_{Rd}$  is the buckling resistance (according to the eccentricity of the load) calculated in accordance with numerical model.

Photographs of some columns after the fire tests are given in the following figures. Column failures were through flexural buckling or through flexural buckling combined with local buckling. After the test, the actual maximum deflection of the column was observed to be located close to the bottom (lower part of the column) or near the mid-height of the specimen. For specimens with the larger cross-section (300x8mm), maximum deflection was observed on the lower part of the columns (due to the non-uniform heating of columns during fire tests). The thermocouple recordings on other RHS columns showed that columns can be considered to be uniformly heated. In this case, the maximum deflection was observed near the mid-height of the specimen.

Observation of the bending deflections has shown that local buckling had formed along the hollow steel section of tested columns with the higher cross-section sizes (200x8mm and 300x8mm). This local buckling may be explained by the fact that these columns have excessive wall slenderness. As an example, only one local buckling had formed in the lower part of the column n°5 (near the bottom) as shown in **Figure 8**. No local buckling had formed along the column with smaller cross-section sizes (150x8mm).



Figure 7 : View of composite column after test n°2



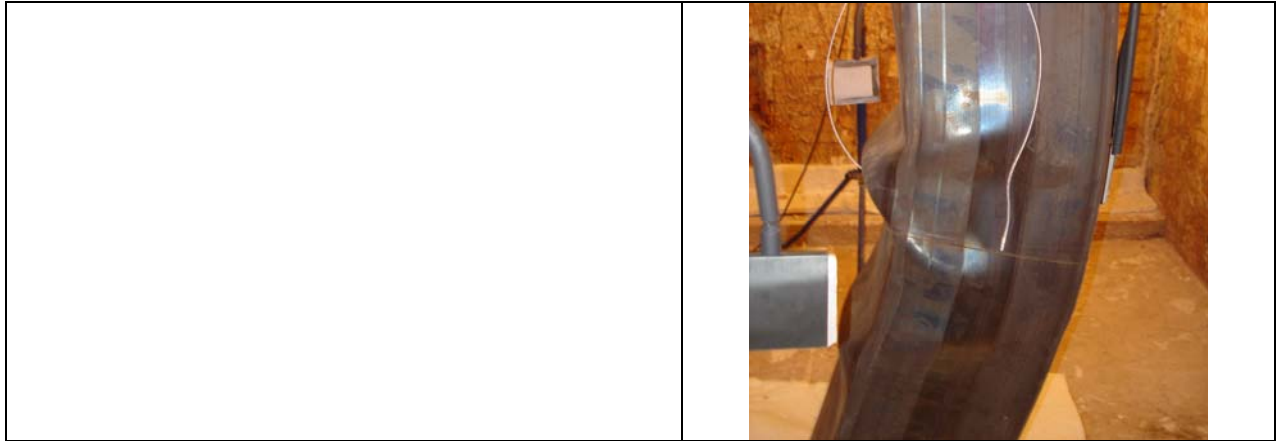


Figure 8 : View of composite column after test n°5

Specimens from the tested members (steel hollow section, reinforcing bars and concrete) were used to obtain their actual mechanical properties (yield and ultimate tensile strengths of both stainless and carbon steel and compressive strength of concrete).

Material tests showed that the actual compressive strength of the concrete was higher than the one assumed (Class C30) for the design of columns. As an example, after 90 days the compressive strength of the concrete has been measured as  $f_c=41.5$  MPa (mean value). Moreover, material properties of hollow steel section were determined at room temperature by tensile tests on three specimens taken from three different slender columns. The actual yield strength of the hollow steel section was higher than the one assumed for the design of columns ( $f_y=240$  MPa) as shown in Table 4. Material tests showed that the actual yield strength of the reinforcing bars (mean value  $R_{p0.2\%}=440$  N/mm<sup>2</sup>) was lower than the one assumed for the design of columns.

Table 4: Results of material tests on hollow steel section

Section	$R_{p0.2\%}$ (N/mm <sup>2</sup> )				$R_m$ (N/mm <sup>2</sup> )			
	Actual			Average	Actual			Average
150x8mm	340	382	387	370	594	607	619	607
200x8mm	306	381	305	330	596	613	592	600
300x8mm	403	324	302	343	608	589	595	597

#### **Fire behaviour of beams:**

Measurements during tests showed that temperature fields were relatively uniform along the length of the beams. Elapsed time of the fire tests carried out on beams and their failure times are reported in **Table 5**. The beams are deemed to have failed when they no longer supports the test load. This is taken as a deflection of  $L/20$  is exceeded (where  $L$  is the span of the specimen). The first beam reached the limiting deflection just after 79 minutes. Just before the imposed load was removed (at 90 minutes), the rate of deflection reached a maximum value of 15mm/min. The second beam reached the limiting deflection just after 76 minutes. Just before the imposed load was removed (at 86 minutes), the rate of deflection reached a maximum value of 10mm/min.

Table 5: Failure time of tested beams

Beams	Load ratio*	Fire duration (min)	Failure time (min)
N°1	0.43	90	79
N°2	0.65	86	76

\* the load ratio is defined as the ratio between the maximum moment due to applied loads and the moment resistance at room temperature obtained from numerical analysis.



All measured failure times are higher than the expected fire ratings (R60). The reason is that initial design of beams was made using nominal values of mechanical characteristics of materials and assuming the same emissivity, namely  $e_m=0.7$ , for the stainless steel plate and the concrete slab.

Photographs of the beams after the fire tests are given in the following figures.



Figure 9 : View of beam after the test n°1



Figure 10 : View of beam during and after the test n°2

Material properties of stainless steel were obtained from three tensile material tests carried out on offcuts from the steel plate used to fabricate the beams. The actual yield strength of stainless steel plate was higher than the one assumed for the design of beams, namely  $f_y=240$  Mpa. (see **Table 6**).

Table 6: Results of material tests on stainless steel plate

Section	$R_{p0.2\%}$ (N/mm <sup>2</sup> )				$R_m$ (N/mm <sup>2</sup> )			
	Actual			Mean value	Actual			Mean value
500x15mm	343	277	345	321	467	414	470	450
360x15mm	290	335	254	293	445	468	573	493

## 6 NUMERICAL ANALYSIS

The mechanical behaviour of tested composite members has been simulated using the FEM model SISMEF. Temperature distributions in members have been obtained separately, either from 2D heat transfer analysis (based on finite difference or finite element method) or from test data. These temperatures have been used as input data to numerical model to therefore allowing the influence of temperature on mechanical properties of materials.

### 6.1 ASSUMPTIONS FOR NUMERICAL SIMULATIONS

In addition to the loading, boundary and heating conditions described in the previous paragraph, the fire behaviour of both composite columns and beams has been analysed adopting the following assumptions:

- Columns are hinged at both ends and subjected to a compressive load kept constant during the fire exposure.
- The thermal and mechanical materials properties of concrete and reinforcing steel bars as a function of temperature were taken in accordance with EN 1994-1-2. Material models for stainless steel were taken from EN 1993-1-2. It may be underlined that the creep strains of steel and concrete are implicitly included in the stress-strain relationships at elevated temperature. Moreover, effects of residual stresses are neglected.
- Temperature distributions have been assumed uniform over the column height, except at the top of the column where a temperature gradient has been taken into account. The reason is that the top of the column was outside the furnace during the test and was not exposed directly to fire. Temperature distribution over the cross-section of column has been computed separately from 2D heat transfer analysis. To calculate the heat flow transmitted to the surface of hollow steel section during the fire exposure, it is necessary to introduce into the model the values of the convection factor ( $h_c$ ), the emissivity of fire ( $\epsilon_f$ ) and the emissivity of steel ( $\epsilon_m$ ). In practice, whatever the nature of materials, the convection factor inside the furnaces is taken equal to  $h_c=25$  W/m<sup>2</sup>K. In EN 1991-1-2 and EN 1993-1-2, the emissivity of the fire is taken in general as unity. In the present study, the emissivity of the fire is also assumed as unity. The surface emissivity of the column is applied in accordance with EN 1993-1-2, namely  $\epsilon_m = 0.4$ . Moreover, additional calculations have been performed adopting  $\epsilon_m = 0.2$  and  $h_c=35$  W/m<sup>2</sup>K. in accordance with all other project partners. The same moisture content, ie. 4% has been taken into account for all tests. The influence of moisture is considered in a simplified way in calculating the transient temperature state of fire exposed columns by assuming that all moisture evaporates, without any moisture transfer, at the temperature 100°C or another temperature within a narrow range with the heat of evaporation giving a corresponding change in the enthalpy-temperature curve. Direct heat transfer was assumed between stainless steel hollow section and concrete core (no gap due to differential thermal elongation of materials).

- Temperature distribution has been assumed uniform along the beam length. The temperature development of the two beam tests was modelled numerically with advanced calculation model ANSYS, adopting the same parameters as those used for columns and an emissivity of 0.7 for the concrete slab. In accordance with all other project partners, thermal analysis has been also performed adopting  $\epsilon_m=0.2$  for stainless steel plate and  $h_c = 35 \text{ W/m}^2\text{K}$ .
- To investigate the effects of the mechanical interaction between the hollow steel section and the concrete core on the fire behaviour of columns, calculations have been performed with two different assumptions: on the one hand a full interaction (no slipping between steel and concrete) and on the other hand none interaction (slipping is assumed to occur without significant bond between steel and concrete).
- Beams are simply supported. Contribution of the concrete slab on the mechanical fire resistance of beam has been neglected.

## 6.2 RESULTS OF NUMERICAL SIMULATIONS

### 6.2.1 Thermal response

#### 6.2.1.1 Composite columns

The measured temperature rise on composite members has been systemically compared to the predicted temperature rises assuming emissivity values of 0.2 and 0.4 and using upper limit of thermal conductivity of concrete. As example, following figures show comparisons for three columns.

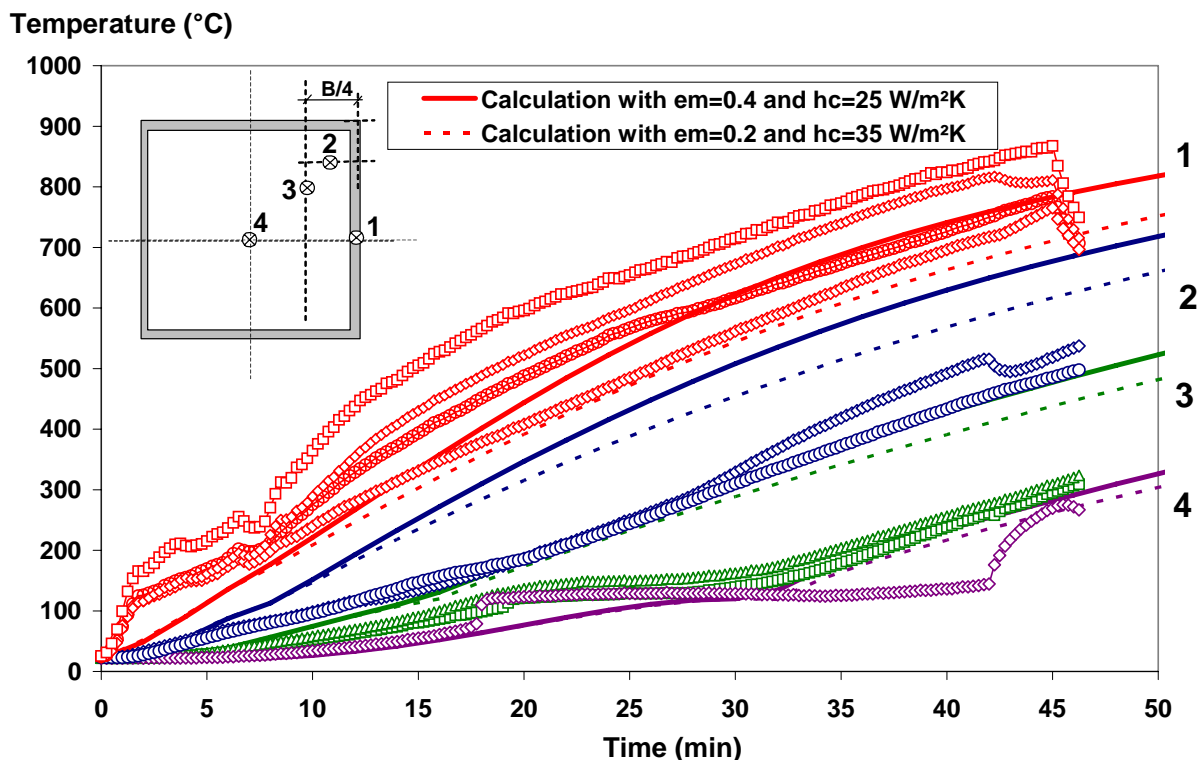


Figure 11 : Calculated and measured temperatures in the column cross-section n°2 of test n°1

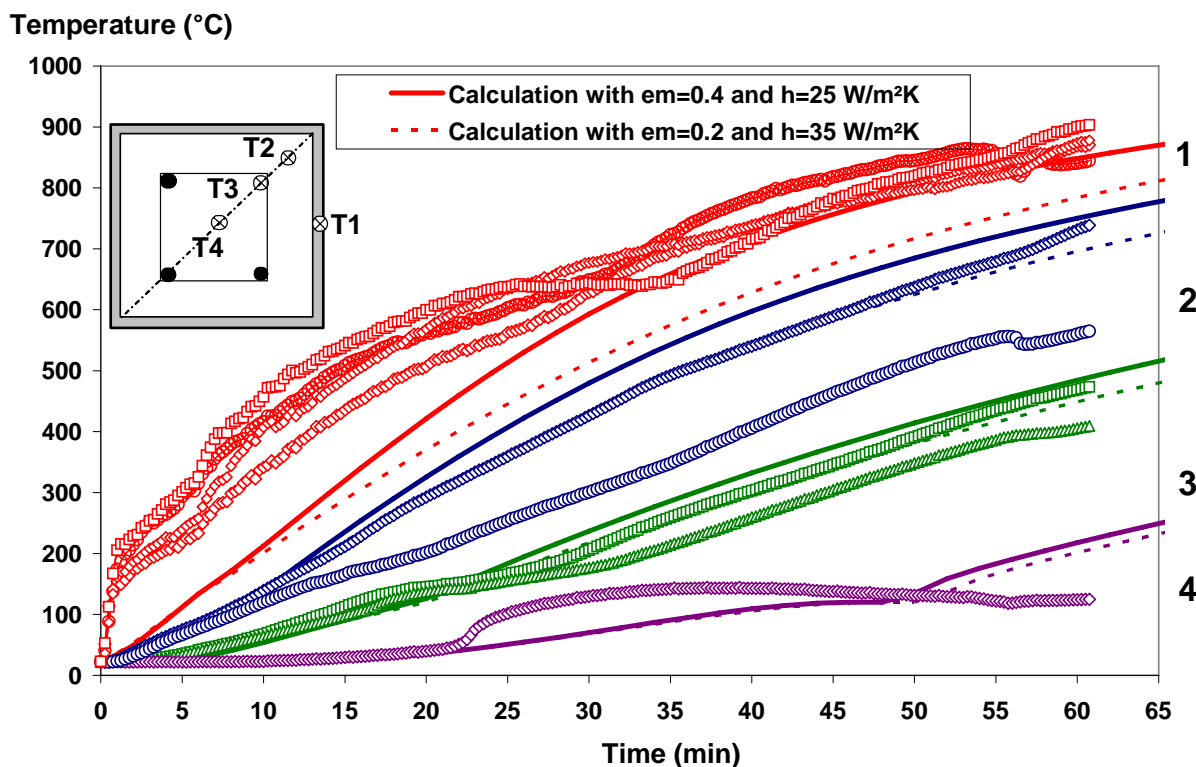


Figure 12 : Calculated and measured temperatures in the column cross-section n°2 of test n°3

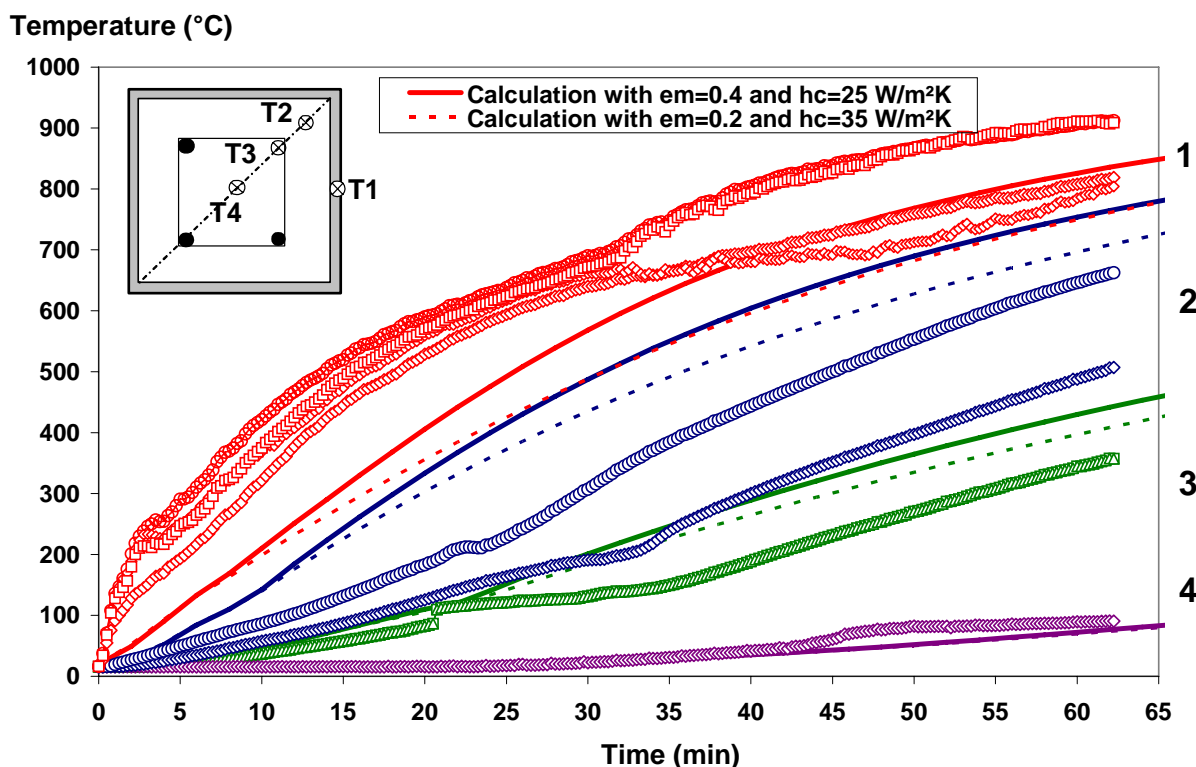


Figure 13 : Calculated and measured temperatures in the column cross-section n°2 of test n°7

The following comments can be drawn:

- The test results are more closely simulated when values of 0.4 and 25 W/m²K are assumed for the emissivity and convection factor. Globally, all calculated temperatures remain on the side safe.



- Assuming the thermal parameters recommended in EN 1993-1-2 for stainless steel ( $\epsilon_m = 0.4$  and  $h_c = 25 \text{ W/m}^2\text{K}$ ), the temperature rises predicted for the hollow steel sections are in good agreement with the measured ones. However, figures show fairly large discrepancies between the predicted temperatures and the measured temperatures, particularly for the first 20 minutes. In fact, predicted temperatures rise more slowly. The difference remains lower than  $150^\circ\text{C}$  during the early stage of the tests and decreases quickly with the fire duration. The faster rise in temperature of the hollow steel section might be explained by the role of “heat shield” played by the gap which occurs usually between the hollow section and the concrete core of heated composite columns. This gap is due to the differential thermal elongation of materials (steel and concrete) in the radial direction. It interrupts direct heat conduction between the steel wall and the concrete core. The concrete core is heated only by the thermal radiation from the heated hollow steel section.
- For reinforced columns, temperature rise of longitudinal reinforcing steel bars are simulated satisfactorily between  $0$  to  $100^\circ\text{C}$ . Once the temperature of  $100^\circ\text{C}$  is reached close to the reinforcement, calculated temperatures becomes appreciably more important than those measured (the maximum difference is about  $200^\circ\text{C}$ ). Globally, the predicted curve of temperature rise is analogous to those observed in experiments, but somewhat translated towards lower times. This translation between the curves is due, on the one hand to the delaying effect as a result of the gap between the hollow steel section and the concrete core (not taken into account in the thermal analyses), and on the other hand to the time necessary to the vaporisation of water really enclosed in the concrete.
- With regard to the point inside the concrete core, the agreement is not so good, but can nevertheless be regarded as satisfactory. Difference between theoretical curves is without too significant consequences: for low temperatures, the concrete mechanical are not affected and for higher temperatures the calculated curve is on the safe side.

Finally, assuming the thermal parameters recommended in EN 1993-1-2 for stainless steel ( $\epsilon_m = 0.4$  and  $h_c = 25 \text{ W/m}^2\text{K}$ ), the temperature rises predicted for the hollow steel sections are in good agreement with the measured ones. Globally, all calculated temperatures remain overall on the side safe.

#### 6.2.1.2 Beams

**Figure 14** and **Figure 15** compare the temperature rises measured during tests to the predicted curves assuming an emissivity value of 0.2 and 0.4 for the exposed stainless steel plate.

From these figures, it can be observed that:

- As seen during tests, the bottom of the beams (stainless steel plate and lower flange of the carbon steel profile) heated up faster than the top, due to fire protection given by the concrete slab.
- Assuming an emissivity of 0.4, the temperatures of stainless steel plates obtained from the numerical model are higher than the test results between 10 to 70 minutes. Then, they become quite close to the measured temperatures. The largest temperature difference in this case is about  $100^\circ\text{C}$  at 45 minutes. Assuming an emissivity of 0.2, the temperatures calculated for the stainless steel plates are in good agreement with the test results until 60 minutes ; then, they become lower than the measured values. One reason for this difference might be that the surface properties of the stainless steel plate undergo some changes, which could affect the value of emissivity during the fire exposure.
- On the contrary, it can be seen that the temperatures calculated for the carbon steel profile are very close to the measured values. However, there are some discrepancies between the predicted curves and the measured temperatures for the upper flange of the carbon steel profile. In this case, predicted temperatures increase more quickly. This faster rise in temperatures might be explained by a gap which could occur between the stainless steel plate and the upper flange. This gap stops the heating of the carbon steel profile.

Comparison shows that test results are more closely simulated when a value of 0.4 is assumed for the emissivity of the stainless steel plate. In this case, numerical results remain on the safe side during the majority of the tests.

### Temperature (°C)

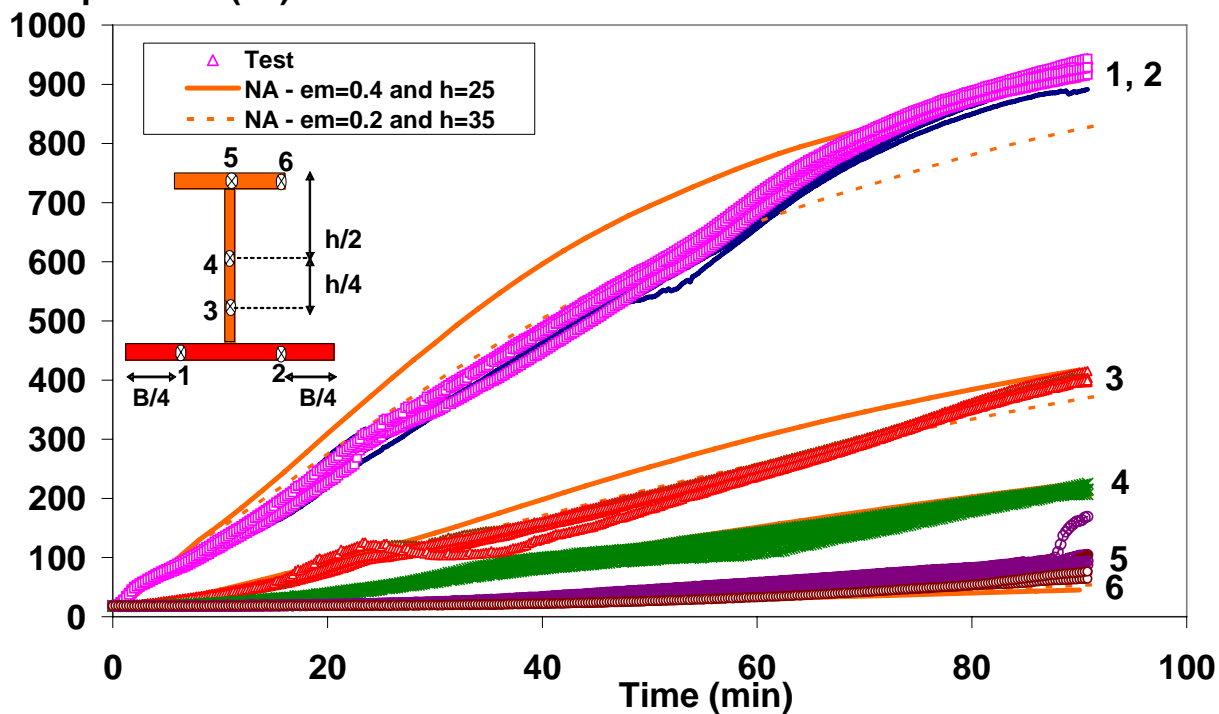


Figure 14: Calculated and measured temperatures for beam n°1

### Temperature (°C)

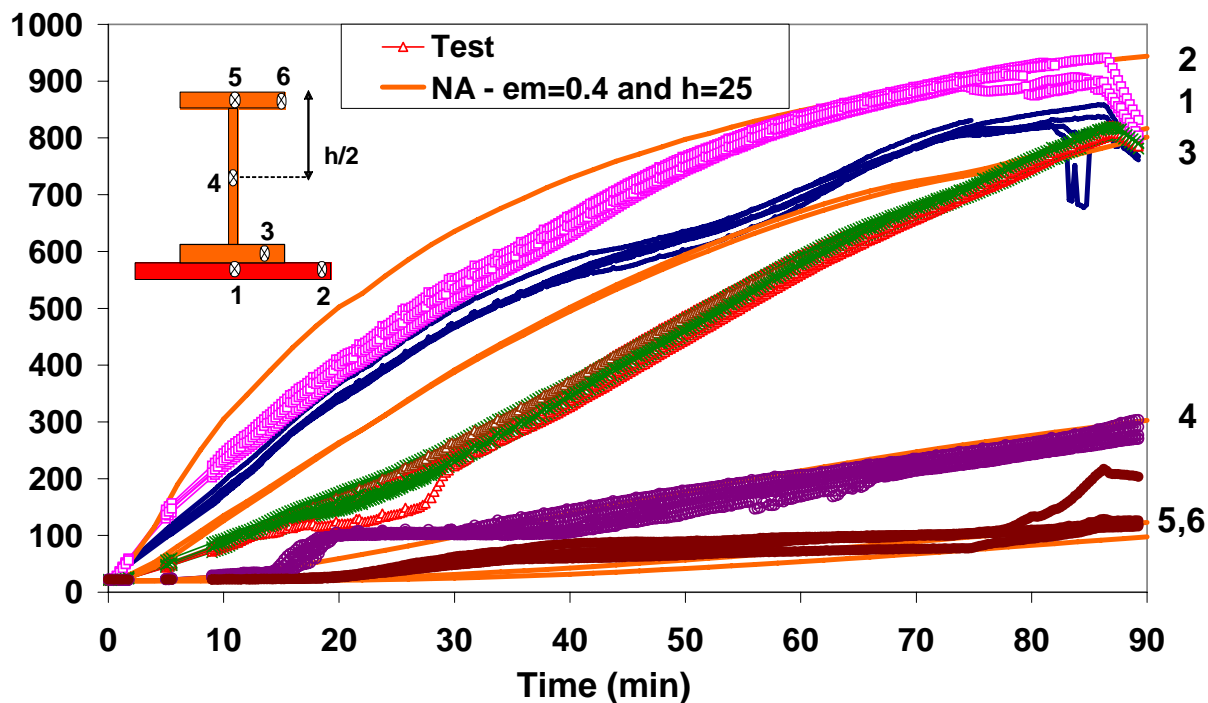


Figure 15 : Calculated and measured temperatures for beam n°2

## 6.2.2 Mechanical response

### 6.2.2.1 Composite columns

The many temperature rises recorded during the test allowed introducing temperature fields of sufficient accuracy in the mechanical simulations. So, calculated as well as experimental temperature fields have been systematically used to check the mechanical analyses conducted with SISMEF.

As an example, the evolution of the vertical displacement calculated at the top of the non-reinforced column n°2 is shown in **Figure 16**. This displacement is compared to the test values. The lateral deflection at mid-height has not been the subject of measurement during the test, so that no comparison with the model is possible.

The same comparison is given in **Figure 17** for reinforced columns n°7. Only the displacements calculated from predicted temperature assuming an emissivity value of 0.4 are presented here. In fact, comparisons between test and numerical results have shown that temperature fields obtained from 2D thermal analysis using an emissivity value of 0.2 lead to a fire resistance more important than the test values.

From these figures, it can be noted that there is a reasonable agreement between measured and calculated displacements. The numerical model SISMEF replicated the deformation behaviour of the tested composite columns to a satisfactory level of accuracy. During the early stages of the fire exposure, axial displacement of columns increases rapidly due to the quick heating of the external unprotected hollow steel section. As the steel column expands more rapidly than the concrete core, it carries the entire applied load. With increasing temperatures, the load becomes critical due to the decrease of steel strength at elevated temperature. Then the steel (as well as the column) suddenly contracts with local buckling. At this time, the concrete core is loaded almost suddenly and carries a progressively increasing portion of the load with temperature rises. The concrete, due to its lower thermal conductivity and higher heat capacity, loses its strength more slowly than steel. It provides the fire resistance of the column at these later stages of fire exposure. If the concrete core is reinforced, the composite column can remain stable and the axial displacement decreases more slowly (see figure 10). The strength of the concrete also decreases with time and ultimately, when the concrete core can no longer support the load, failure occurs by buckling. When concrete core are non-reinforced, the vertical displacement increases approximately linearly and reaches a maximum just before failure occurs, whereupon it reduces very rapidly as the column buckles (see **Figure 17**).

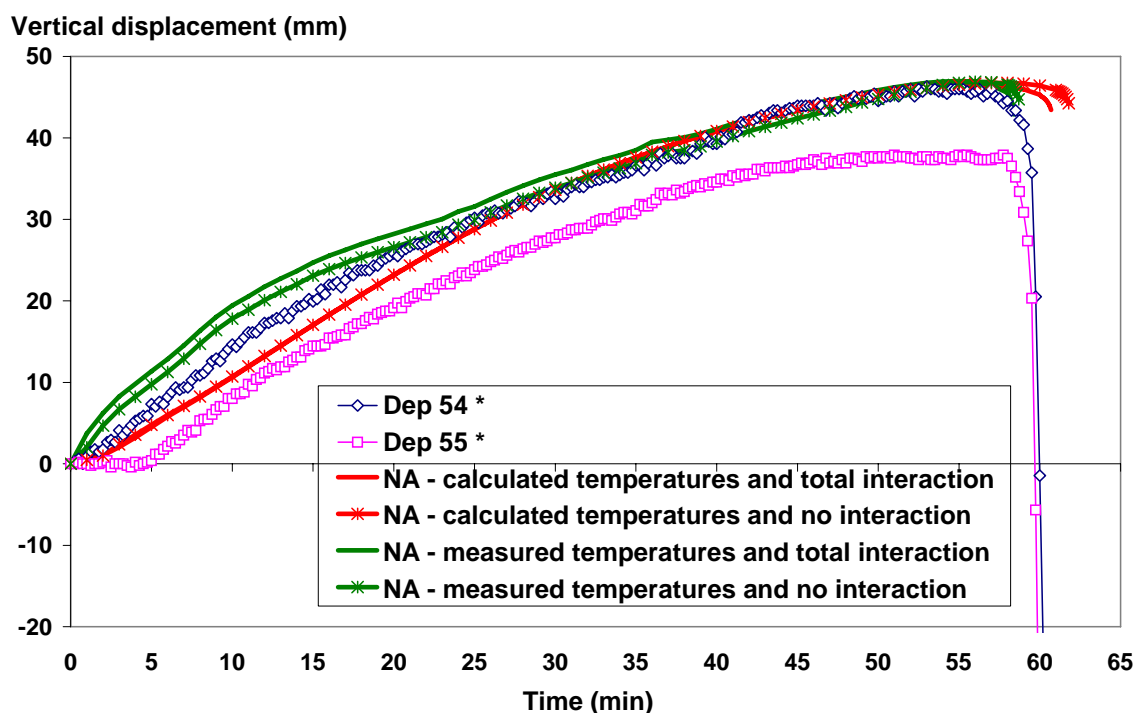


Figure 16: Vertical displacement at the column top of test n°2

Vertical displacement (mm)

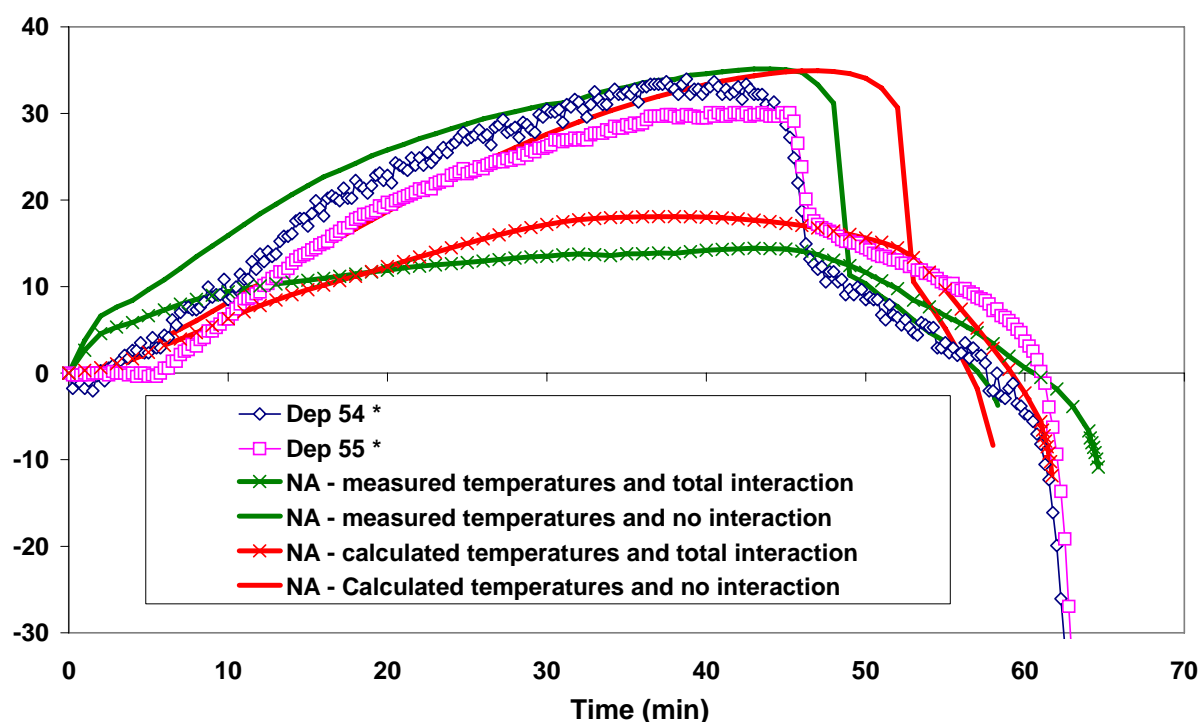


Figure 17: Vertical displacement at the column top of test n°7

#### 6.2.2.2 Beams

**Figure 18** and **Figure 19** show the results of the IF beam and SF beam respectively. Both graphs compare the fire test results with the FE analysis results. It can be seen that there is a good correlation between the predicted and the measured curves. The agreement is quite good during the first stage of test and some differences are observed at the end of the test.

Vertical displacement (mm)

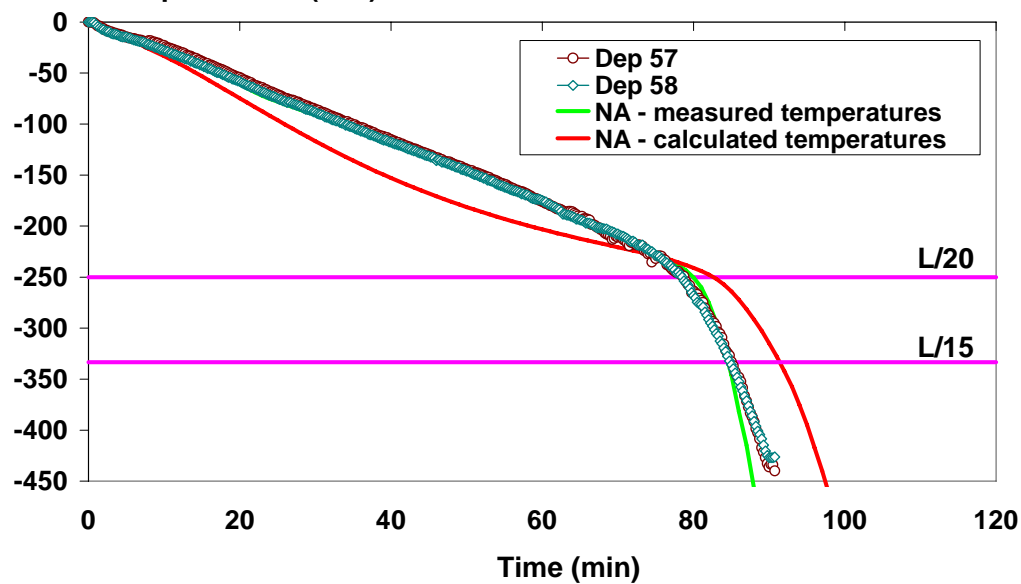


Figure 18: Vertical displacement at mid-span of beam n°1

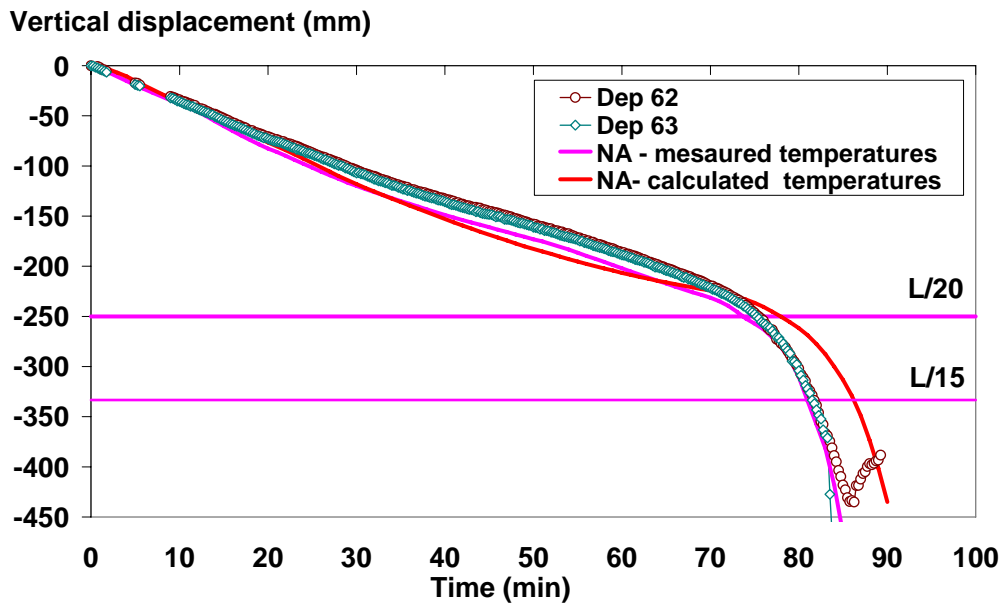


Figure 19::Vertical displacement at the column top of test n°2

### 6.3 SYNTHESIS OF RESULTS

Globally, there is a reasonably agreement between measured and calculated displacements, in particular when the slip is taken into account (no mechanical interaction between the hollow steel section and the concrete core). The numerical model SISMEF replicated the fire behaviour of tested columns to a satisfactory level of accuracy.

All calculated failure times of the composite members are reported in the following tables and in Figure 20. They are very far from the test failure times. They are very far from the test failure times. Reasonably good agreement has been obtained between the test results and numerical analysis. Globally, the comparison between failure times ascertained either numerically or experimentally shows a divergence less than 10%, what is reasonable considering uncertainties inherent to tests data, such as the uniformly heated length of members, the degree of rotational restraint at the ends, unintentional eccentricity of load for columns and the initial out-of straightness.

Moreover, all numerical results confirm that the slip has no significant influence on the failure time of composite columns, provided that the hollow section is filled with reinforced concrete. However, it leads to a more realistic evolution path of the displacements (vertical displacement and deflection) during the first period of heating.

Comparison shows also that test results were more closely simulated adopting material properties of stainless steel defined in EN 1993-1-2. Thus, these currently values have been adopted in following parametric studies of the fire resistance of composite members with stainless steel.

Table 7: Comparison of fire tests and FE analyses

Column	Test failure time (min)	Calculated failure time assuming experimental temperature field		Calculated failure time assuming numerical temperature field	
		Total interaction	No interaction	Total interaction	No interaction
N°1	42	43.6	43.7	43.4	43.3
N°2	59.5	58.4	58.7	60.7	61.8
N°3	56	48.5	52.8	46.5	52.4
N°4	71	65.5	68.4	62.2	66.4
N°5	38	40	39.4	39	36
N°6	70.5	62	70.7	61	56.6
N°7	62	53.6	58.3	61.7	58

Table 8: Comparison of fire tests and FE analyses

Beam	Test results		FE results	
	Failure time (min)	Maximal temperature in stainless steel plate (°C)	Failure time (min)	Maximal temperature in stainless steel plate (°C)
N°1	79	880	83* (80**)	883
N°2	76	908	78* (74**)	915

\* failure time calculated from calculated temperature fields and assuming that failure occurs when a deflection of  $L/20$  is exceeded (where L is the span of the specimen)

\*\* failure time calculated from experimental temperature fields and assuming that failure occurs when a deflection of  $L/20$  is exceeded (where L is the span of the specimen)

#### Numerical model (min)

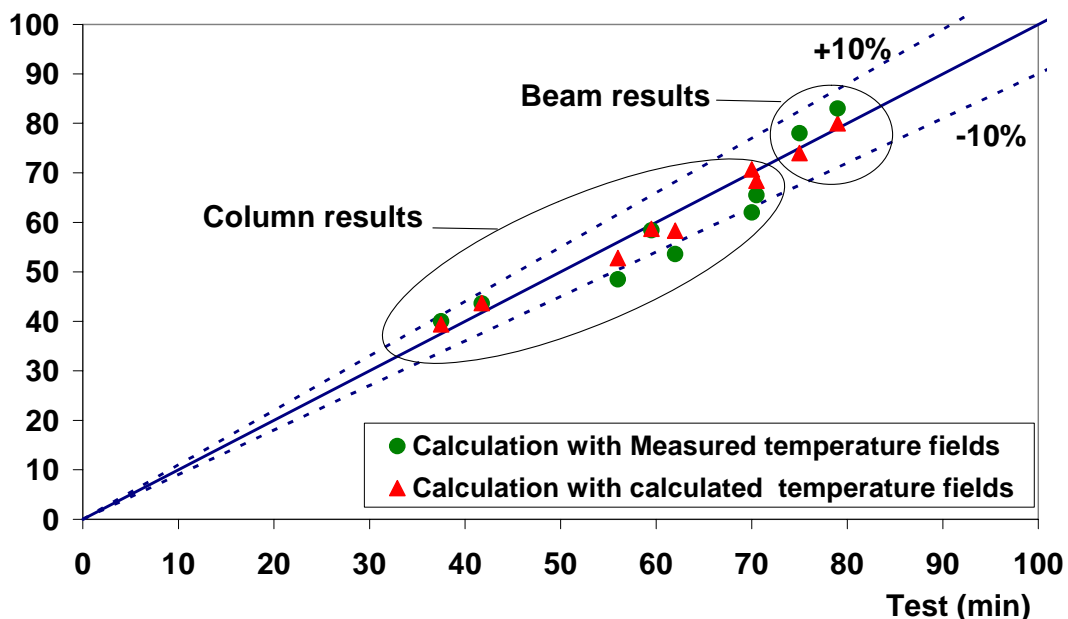


Figure 20 : Comparison between fire resistances between numerical model and test

## 7 DEVELOPMENT OF DESIGN GUIDANCE

Experimental investigations constitute an essential aspect for the verification of validity of developed simple calculations methods. However, it is impossible to cover all application domains by experimental way. A useful solution is to use advanced numerical models to make up experimental limitation.

### 7.1 COMPOSITE COLUMNS

#### 7.1.1 Parametric study of ultimate buckling load of composite columns

In order to obtain design rules to predict the mechanical resistance of composite columns under fire situation, a parametric study has been performed by varying different main parameters susceptible to affect the fire resistance of columns, such as cross-section size, eccentricity of loading, buckling length, percentage of reinforcements, ...

Numerical simulations of composite columns have been conducted in the following way:

- In a first step, the temperature distribution over the cross-section of columns has been calculated separately from 2D heat transfer analysis using a numerical model based on the finite difference method and taking into account the thermo-physical properties of materials (which was proved to simulate the thermal behaviour of composite columns appropriately and to provide a good estimation of the temperature field);
- In a second step, a mechanical calculation to evaluate the ultimate buckling load of the columns, taking into account the mechanical characteristics of materials at elevated temperature, is performed using the FEM model SISMEF.

The load-bearing capacity of composite columns was calculated by firstly submitting the column to the ISO fire curve for a given duration of fire exposure (30 and 60 min). Once this was reached, the corresponding temperature distribution in the cross section was kept constant and an axial vertical load was applied incrementally to the column up to failure. To improve the accuracy of this load (which is only an approximate value of the effective ultimate load of the column), neighbouring axial loads, more or less increased or reduced, were applied at room temperature and the column was heated progressively under constant load until the required fire resistance was obtained.

##### 7.1.1.1 Calculations assumptions:

The mechanical behaviour of composite columns has been conducted adopting the following assumptions:

- Columns are hinged at both ends.
- Columns are subject to concentric or eccentric load, kept constant during the fire;
- The thermal and mechanical material properties of concrete and reinforcing steel are those given by EN 1994-1-2. Effects of residual stresses are assumed negligible. The creep strain of steel and concrete is considered to be implicitly included in their stress-strain relationships at elevated temperatures;
- Material models for stainless steel were taken from EN 1993-1-2.
- Temperature distributions have been assumed uniform over the column height. The net heat flux transferred to the column by convection and radiation was calculated basing on a convection coefficient  $\alpha_c = 25 \text{ W/m}^2\text{K}$  and a global emissivity coefficient  $\varepsilon_m = 0.4$  accordingly to EN 1991-1-2 and 2-2. Moreover, calculations have been carried out using the upper limit of thermal conductivity of concrete, specified in EN 1994-1-2. Effects of possible gap (thermal resistance) between the hollow steel section and the concrete core on the heating of columns core have been neglected.
- An out-of-straightness of  $L/500$  is used in simulations (tolerance given by the manufacturing standards for cold forming), which will have an additional effect to the eccentricity of loading.

- In each column, the bond-slip between concrete core and hollow steel section is assumed negligible (assumption of full interaction between the hollow steel section and the filled concrete).

Moreover, the main parameters adopted in this study are the following:

- Cross-section Sizes: 5 square hollow steel sections with size ranging from 150 to 500 mm. For each section, the choice has been made of two thickness; namely 4 and 8 mm.
- Yield stress of the steel section: Only steel grades 1.4301, 1.4401 and 1.4571 have been considered with a 0.2% proof strength taken as  $f_{0.2p} = 240$  Mpa and an ultimate strength,  $f_u = 2.04 \times f_{0.2p}$
- Fire duration: Two fire ratings, namely 30 and 60 minutes, have been considered; The possibilities of using stainless steel seem quite realistic when the fire resistance time is lower than 60 minutes according to the ISO 834 standard fire temperature curve;
- Compressive strength of concrete: Only the concrete class C30 has been considered. C30 is the minimum quality suggested in EN 1994-1-2 to be used for composite columns;
- Reinforcing steel: Five reinforcement ratios have been considered, namely 0, 1, 2, 3 and 5 %. Only the quality S500 has been considered in this research because it is now the most commonly used reinforcing steel. Moreover, high strength reinforcement is the most interesting for composite sections submitted to fire. Concrete cover (i.e. distance between the axis of longitudinal reinforcements and the border of concrete core) was fixed at 30 mm. Moreover, the width of the hollow steel section must be higher than 150 mm to allow a good concrete filling. For this reason, cross-section size of investigated reinforced column has been limited to 150 mm.
- Column lengths: for each section, 9 different lengths have been considered, with the reduced slenderness ratios at room temperature equal to 0.2, 0.3, 0.4, 0.5, 0.8, 1, 1.2, 1.5, 2.0
- Eccentricity of load: For each section, 4 different load eccentricity values, namely 0,  $0.125 \times b$ ,  $0.25 \times b$  and  $0.5 \times b$ , have been considered. The chosen load eccentricity covers fairly well the application range in buildings.

#### 7.1.1.2 Results of parametric calculations

In order to illustrate the effect of restrained thermal stresses (due to differential thermal elongation of various materials) on the load bearing capacity of composite columns, additional calculations have been carried out considering two distinct mechanical modelling:

- On one hand, a first modelling that explicitly takes into account the differential thermal elongation as function of temperature rise (assuming in addition a full interaction between the hollow steel section and the filled concrete), and
- On other hand, a second modelling that takes into account only the lost of mechanical properties at elevated temperature of materials without considering their interaction (The thermal elongation of each material is assumed to be zero).

To facilitate the presentation of results, both modelling will be designated by DTS (modelling with differential thermal stresses) and NDTS (modelling without differential thermal stresses). Moreover, results are given in the form of buckling coefficients as a function of the relative slenderness evaluated for temperature distributions at the ultimate state. The buckling coefficient is defined as  $N_{fi,\theta} / N_{fi,pl,R}$ , where  $N_{fi,\theta}$  is the load bearing capacity of the columns obtained from the numerical model and  $N_{fi,pl,R}$  is the design plastic resistance to axial compression at elevated temperature according to EN 1994-1-2 at the same elevated temperatures distribution.

It is specified at this stage of investigation that the relative slenderness  $\bar{\lambda}_\theta$  is calculated according to EN 1994-1-2 with the use of reduction coefficients  $\phi_{i,\theta}$  taken as 0.8 for concrete and 1.0 for both steel materials. Moreover, the design plastic resistance to axial compression is calculated using the 0.2% proof strength as characteristic strength of stainless steel.

Comparisons with analytical buckling curves "c" and "d" specified in EN 1993-1-1 are also given. It should be noted that EN 1994-1-2 recommends design buckling curve "c" to check the fire resistance of other types of composite column (as partially encased columns,...).



As an example, Figure 21 presents some results obtained (as function of buckling length) for non-reinforced composite columns. **Figure 22** gives others results for reinforced columns.

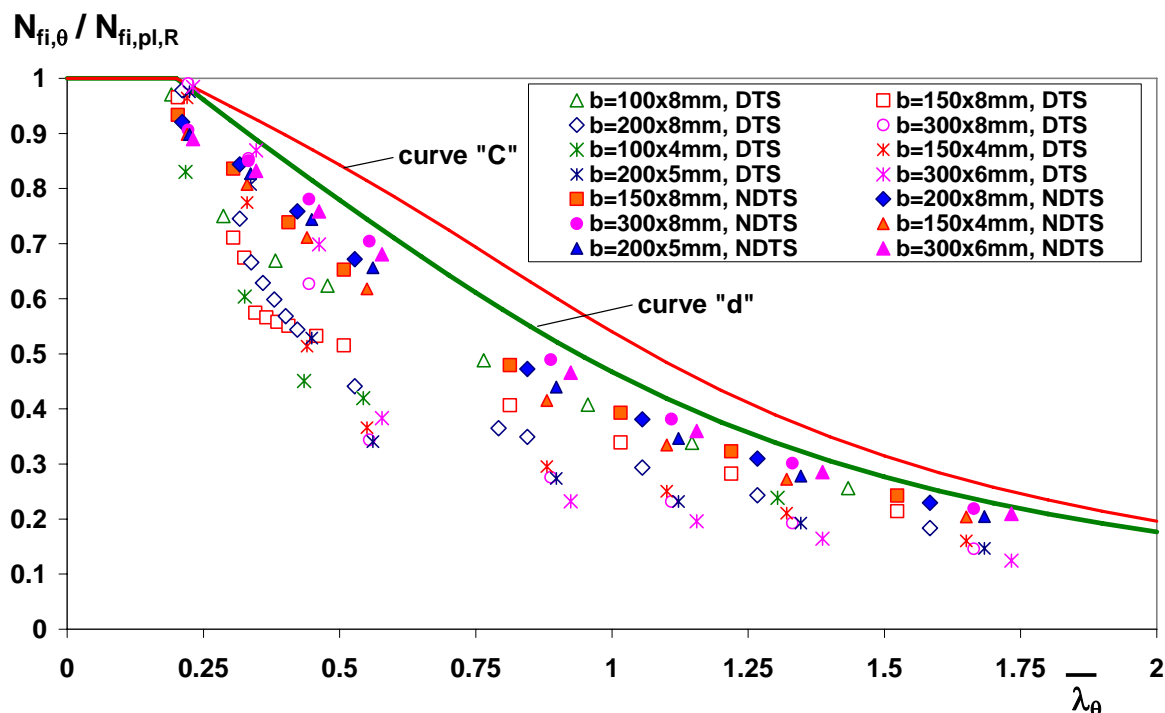


Figure 21 : Thermal stress effects on fire behaviour of non-reinforced columns

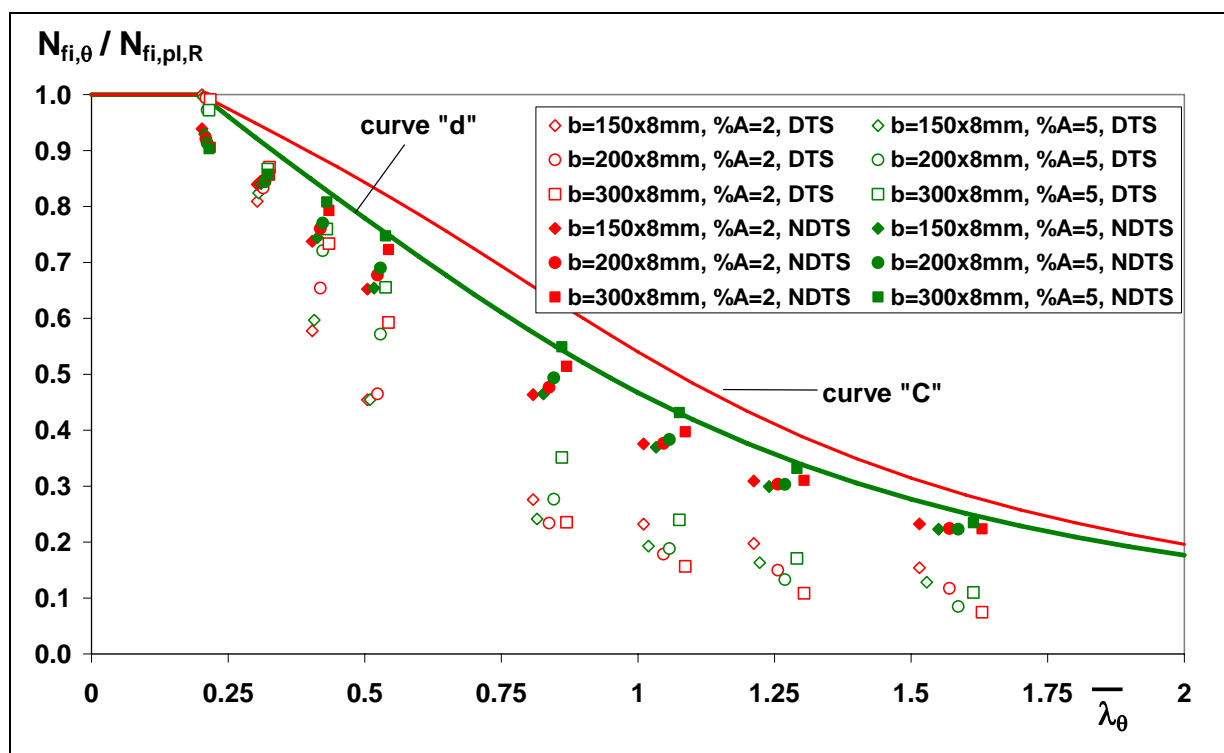


Figure 22 : Thermal stress effects on fire behaviour of reinforced columns

From these results, the following comments may be drawn:

- The dispersion of buckling coefficient may be large between both assumptions. Restrained thermal stresses have little effects on the behaviour of short columns ( $\bar{\lambda}_\theta < 0.3$ ). Globally, these additional internal stresses increase slightly the fire resistance of columns. On the other hand, for higher values of the relative slenderness (slender columns), restrained thermal stresses may have an unfavourable effect on the column resistance. As an example, for a relative slenderness equal to 0.5, buckling coefficients can be found between 0.3 and 0.7 according to the modelling assumption (DTS or NDTs).
- Where thermal elongation is neglected, the shape of buckling curves derived from numerical results is close to the shape of buckling curve “d” provided by EN 1993-1-1. On the other hand, when restrained thermal stresses are taken into account, numerical buckling curves differs clearly from available design buckling curves of Eurocodes, which are too optimistic for both non-reinforced and reinforced columns. Generally, these curves lead to buckling load values which may be quite on the unsafe side when the column slenderness increases.
- Assuming differential thermal elongation in calculations, numerical buckling curves start approximately at  $\chi=1.0$  for  $\bar{\lambda}_\theta = 0.2$  and decrease quickly when increasing relative slenderness. It should be pointed out the singular shape of the curve showing a more or less discontinuity on both sides of a certain value  $\bar{\lambda}_{\theta, transition}$  of the relative slenderness  $\bar{\lambda}_\theta$ . When the relative slenderness  $\bar{\lambda}_\theta$  is less than  $\bar{\lambda}_{\theta, transition}$  the column works as a composite element with significant interaction between steel and concrete while the fire resistance of columns is progressively provided by the concrete core only (when high additional ratio of reinforcement is used) or by the hollow steel section (for non-reinforced columns or columns with low ratio of reinforcement) when  $\bar{\lambda}_\theta$  exceeds  $\bar{\lambda}_{\theta, transition}$ . As shown in Figure 23, non-reinforced columns as well as columns with low additional ratio of reinforcement behave gradually as simple steel columns when the relative slenderness increases. It should be noted on this figure that both relative slenderness and buckling coefficient of steel columns have been calculated assuming an equivalent composite columns to allow the comparison of fire behaviour. This behaviour is mainly explained by the enhanced material properties and the favourable relationship between strength and stiffness of stainless steel that makes hollow steel columns show higher buckling resistance than the filled concrete core despite of the elevated temperatures.

Behaviour differences between short and slender columns may be explained by the more or less favourable effect of restrained thermal stresses on the load bearing capacity of columns. The resulting differential thermal elongations are a consequence of Bernoulli's assumption for any cross-section and the assumption of a full interaction between the hollow steel section and the filled concrete. For short columns, thermal stresses usually have a positive effect on the fire behaviour of columns with a pre-stressing in tension of a certain core of the concrete cross-section. Generally, failure occurs by plastic crushing when the cumulated axial resistance of the materials falls under the applied load. In fact, the concrete core contributes for an important part to the load bearing capacity as well as the stability of the column. As the column length increases, failure becomes progressively more related to instability considerations. The unequal temperature distribution within the cross-section leads to the same restrained thermal stresses as before but the distribution of total stresses in each part (steel hollow section, concrete and reinforcing bars) is affected by column deflection. In addition, the evolution of the stress levels during the fire exposure (with a stress redistribution towards the colder parts of the cross-section) creates a more heterogeneous distribution of rigidity within the cross-section (which is emphasized by the non-linear material behaviour at elevated temperature, by a certain bending moment and by a possible cracking of concrete). Consequently, the position of the neutral axis moves progressively during the fire exposure and the resulting eccentricity of the applied load leads to create more deflection and therefore more important additional bending moment which precipitates the failure of the column. As a consequence, mean slender columns may not carry an important applied load which explains the higher decrease of buckling coefficient in the range of intermediate slenderness.

Finally, the fire behaviour of composite columns appears very complex in relation with several phenomena, such as the fast thermal elongation due to the direct exposure of the stainless steel hollow section to fire; the abrupt shortening of the column length due to the loss of axial stiffness after some fire duration; at the same time, the development of self equilibrated differential thermal stresses in both steel and concrete parts of any cross-section; the possible occurrence of large slip at the steel concrete interface and the amplification of the transverse initial imperfection by 2nd order local effects in bending. Especially, differential thermal elongations of materials associated with second order geometrical effects may have an unfavourable effect on the load bearing capacity of composite columns. These phenomena are entirely neglected in available design method for composite columns. So, another design method based as an example on specific buckling curve and taking into account globally the effects of restrained thermal stresses and large transverse displacements of the column behaviour should be found. Consistently with the results of parametric study, it is quite logical that the relative slenderness  $\bar{\lambda}_\theta$  was evaluated at the ultimate temperature distribution using other reduction coefficients that those actually proposed in EN 1994-1-2, namely  $\varphi_{a,\theta}=1$  for steel, concrete  $\varphi_{c,\theta}=0.8$  for concrete and  $\varphi_{s,\theta}=1.0$  and reinforcement. Moreover, as the numerical results obtained at room temperature were shown close to the buckling curve "d" (see Figure 24), this curve has been chosen as a reference curve in the proposed design method.

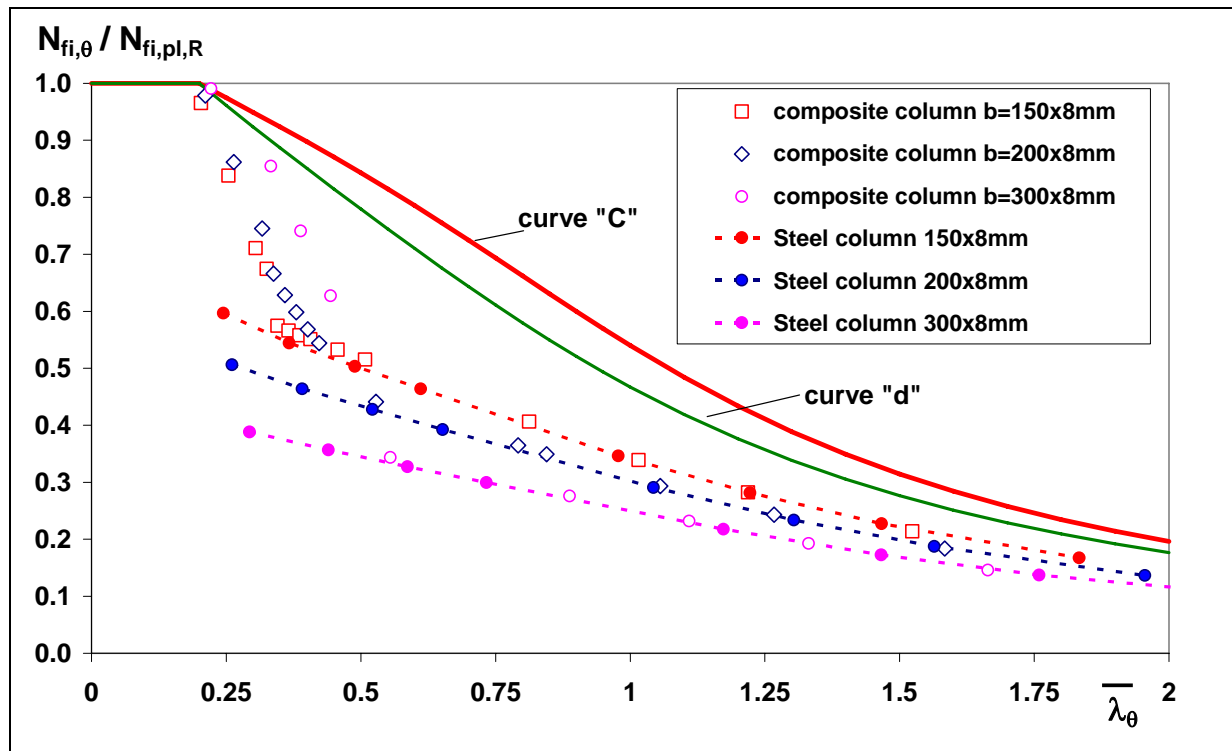


Figure 23 : Buckling coefficients of composite columns and geometrically identical steel columns

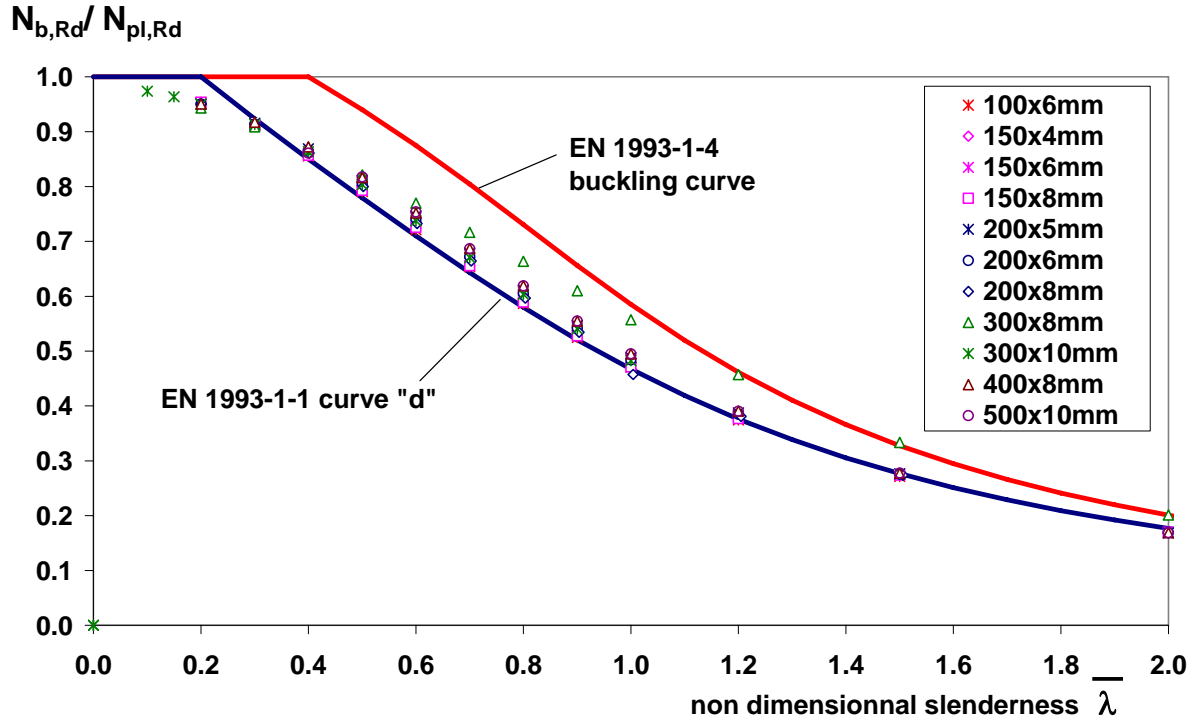


Figure 24 : Buckling coefficients of composite columns at room temperature

## 7.1.2 Proposed design method

The simplified design method follows the general flow chart specified in 4.3.5.1.1 of EN 1994-1-2 to check other types of composite columns but includes some specific characteristics which are presented hereafter.

### 7.1.2.1 Case of centric Load

For a given temperature distribution within the cross-section, the design axial buckling load of composite columns in fire situation,  $N_{fi,Rd}$ , is given by:

$$N_{fi,Rd} = \chi(\bar{\lambda}_\theta) \cdot N_{fi,pl,Rd} \quad (1)$$

where:

- $\chi$  is the reduction coefficient for buckling curve "d" of EN 1993-1-1 and depending on the non dimensional slenderness ratio at elevated temperature.
- $N_{fi,pl,Rd}$  is the design plastic resistance to axial compression in fire situation ;

The buckling reduction coefficient is expressed by the following relationships (familiar in steel construction)

$$\chi(\bar{\lambda}_\theta) = \frac{1}{\varphi + \sqrt{\varphi^2 - \bar{\lambda}_\theta^2}} \quad (2)$$

$$\text{with } \varphi = \frac{1}{2} \left( 1 + \alpha (\bar{\lambda}_\theta - \bar{\lambda}_0) + \bar{\lambda}_\theta^2 \right)$$

where  $\alpha=0.76$  and  $\bar{\lambda}_0 = 0.2$

The design value of the plastic resistance to axial compression in the fire situation is given by:

$$N_{fi,pl,Rd} = \sum_j (A_{a,j} \cdot f_{ay,\theta_j}) / \gamma_{M,fi,a} + \varphi_{c,\theta} \left( \sum_k (A_{s,k} \cdot f_{sy,\theta_k}) / \gamma_{M,fi,s} + \sum_m (A_{c,m} \cdot f_{c,\theta_m}) / \gamma_{M,fi,c} \right) \quad (3)$$

where:

- $A_i$  is the area of the element "i" of the cross-section;
- $f_{ay,\theta}$ ,  $f_{sy,\theta}$  and  $f_{c,\theta}$  are the characteristic strengths at elevated temperature of the steel of hollow section, the steel of reinforcing bars and the concrete respectively. For hollow section, the 0.2 % proof characteristic strength of stainless steel should be used.
- $\varphi_{c,\theta}$  is a reduction coefficient taking into account the differential effects of thermal stresses. it's the same coefficient as that used for the calculation of the effective flexural stiffness.

The relative slenderness of the column in fire situation is given by:

$$\bar{\lambda}_{\theta} = \sqrt{N_{fi,pl,R} / N_{fi,cr}} \quad (4)$$

where  $N_{fi,pl,R}$  is the value of  $N_{fi,pl,Rd}$  according to (3) with  $\gamma_{M,fi,a} = \gamma_{M,fi,c} = \gamma_{M,fi,s} = 1$ .

$N_{fi,cr}$  is the Euler elastic critical load effective flexural stiffness in fire situation:

$$N_{fi,cr} = \Pi^2 (EI)_{fi,eff} / l_{\theta}^2 \quad (5)$$

Where  $l_{\theta}$  is the buckling length of the column in fire situation.

The effective flexural stiffness of the cross-section,  $(EI)_{fi,eff}$ , is calculated as follows:

$$(EI)_{fi,eff} = \varphi_{a,\theta} \sum_j (E_{a,\theta_j} \cdot I_{a,j}) + \varphi_{c,\theta} \left( \sum_m (E_{c,\theta_m} \cdot I_{c,m}) + \sum_k (E_{s,\theta_k} \cdot I_{s,k}) \right) \quad (6)$$

where

- $E_{i,\theta}$  is the characteristic modulus of material "i" at the temperature  $\theta$ . For steel, it's the modulus of elasticity. For concrete,  $E_{c,\theta} = \frac{3}{2} \times E_{c,sec,\theta}$  where  $E_{c,sec,\theta}$  is the characteristic value for the secant modulus of concrete in the fire situation, given by  $f_{c,\theta}$  divided by  $\varepsilon_{cu,\theta}$ .
- $I_i$  is the second moment of area of material "i" related to the central axis (y or z) of the composite cross-section
- $\varphi_{a,\theta}$  (for steel wall) and  $\varphi_{c,\theta}$  (for concrete core including reinforcements) are reduction coefficients due to the differential effects of thermal stresses. Values resulting from numerical calibration appear rather different from those attributed to other types of composite cross-section.

Obviously, checking of the column consists in satisfying the condition:

$$N_{fi,Ed} \leq N_{fi,Rd} \quad (7)$$

where  $N_{fi,Ed}$  is the design value of the axial compression for the combination of actions considered in fire situation (according to EN 1991-1-2).

The coefficients  $\varphi_{a,\theta}$  and  $\varphi_{c,\theta}$  take the following values:

For hollow steel section:  $\varphi_{a,\theta}$  depends on the fire rating as given in Table 9.

Table 9 : Values of coefficient  $\varphi_{a,\theta}$

Fire Rating	R30	R60
$\varphi_{a,\theta}$	0.75	0.575

For concrete:  $\varphi_{c,\theta}$  is defined by means of six parameters  $L_{\theta,1}$ ,  $L_{\theta,2}$ ,  $L_{\theta,3}$ ,  $\varphi_{max}$ ,  $\varphi_{int}$  and  $\varphi_{min}$  depending on of the cross-section size (external size (b) and thickness (e) of the hollow steel section), the column buckling length  $L_{\theta}$ , the ratio of reinforcement  $A_s/(A_s+A_c)$  and the fire rating.

if  $L_{\theta} \leq L_{\theta,1}$ :

$$- \varphi_{c,\theta} = \varphi_{\max}$$

if  $L_{\theta,1} \leq L_{\theta} < L_{\theta,2}$ :

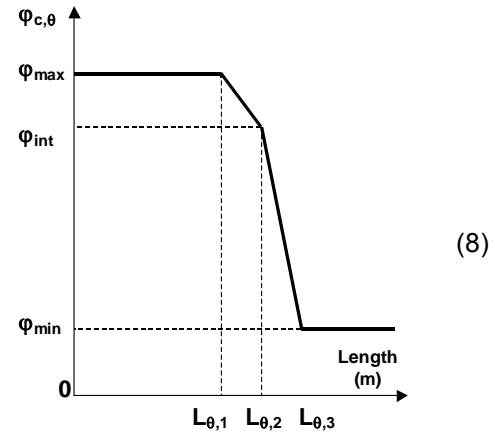
$$- \varphi_{c,\theta} = \frac{\varphi_{\max} - \varphi_{\text{int}}}{L_{\theta,1} - L_{\theta,2}} L_{\theta} + \frac{\varphi_{\text{int}} \times L_{\theta,1} - \varphi_{\max} \times L_{\theta,2}}{L_{\theta,1} - L_{\theta,2}}$$

if  $L_{\theta,2} \leq L_{\theta} < L_{\theta,3}$ :

$$- \varphi_{c,\theta} = \frac{\varphi_{\text{int}} - \varphi_{\min}}{L_{\theta,2} - L_{\theta,3}} L_{\theta} + \frac{\varphi_{\min} \times L_{\theta,2} - \varphi_{\text{int}} \times L_{\theta,3}}{L_{\theta,2} - L_{\theta,3}}$$

if  $L_{\theta,3} \leq L_{\theta}$ :

$$- \varphi_{c,\theta} = \varphi_{\min}$$



Values of parameters  $L_{\theta,1}$ ,  $L_{\theta,2}$  and  $L_{\theta,3}$  are given in the following table as function of cross-section size and ratio of reinforcement  $A_s/(A_s+A_c)$ . For intermediate values of the external size and thickness of hollow steel section, linear interpolation may be used to calculate  $L_{\theta,1}$ ,  $L_{\theta,2}$  and  $L_{\theta,3}$ .

Table 10: Values of parameters  $L_{\theta,1}$ ,  $L_{\theta,2}$  and  $L_{\theta,3}$  for fire ratings R30

ratio of reinforcement $A_s/(A_s+A_c)$ .	Cross-section size		Fire rating R30		
	b (mm)	e (mm)	$L_{\theta,1}$ (m)	$L_{\theta,2}$ (m)	$L_{\theta,3}$ (m)
0	100	4	0.50	0.70	1.25
		8	0.50	0.60	0.90
	250	4	1.90	2.90	4.00
		8	1.50	2.25	3.25
	500	4	8.25	9.40	9.75
		8	6.20	7.70	9.50
1 to 5	150	4	0.75	1.50	2.40
		8	0.60	1.20	2.00
	500	4	5.50	9.50	15.00
		8	5.00	8.00	12.00

Table 11: Values of parameters  $L_{\theta,1}$ ,  $L_{\theta,2}$  and  $L_{\theta,3}$  for fire ratings R60

ratio of reinforcement $A_s/(A_s+A_c)$	Cross-section size		Fire rating R60		
	b (mm)	e (mm)	$L_{\theta,1}$ (m)	$L_{\theta,2}$ (m)	$L_{\theta,3}$ (m)
0	150	4	0.50	0.90	1.80
		8	0.50	0.80	1.30
	300	4	2.40	3.20	3.50
		8	1.80	2.40	2.90
	400	4	4.80	5.50	6.00
		8	3.50	3.90	4.30
	500	4	7.70	8.60	9.20
		8	5.60	6.50	7.10
1	150	4	0.60	1.00	2.00
		8	0.60	0.80	1.25
	500	4	5.00	7.00	10.00
		8	3.50	5.50	9.00
2 to 5	150	4	0.70	1.12	2.45
		8	0.70	0.90	1.80
	500	4	4.50	6.25	11.00
		8	3.00	5.00	9.50

Values of parameters  $\varphi_{max}$ ,  $\varphi_{int}$  and  $\varphi_{min}$  are given in the following table as function of cross-section size and ratio of reinforcement  $A_s/(A_s+A_c)$ . For intermediate values of the external size and thickness of hollow steel section, linear interpolation may be used to calculate  $\varphi_{max}$ ,  $\varphi_{int}$  and  $\varphi_{min}$ .

Table 12: Values of parameters  $\varphi_{max}$ ,  $\varphi_{int}$  and  $\varphi_{min}$  for fire ratings R30

ratio of reinforcement $A_s/(A_s+A_c)$	Cross-section size b (mm)	Fire rating R30		
		$\varphi_{max}$	$\varphi_{int}$	$\varphi_{min}$
0	100	1	0.8	0
	500			
1	100	1	0.8	0.1
	500			0.15
2	100	1	0.8	0.12
	500			0.3
3	100	1	0.8	0.15
	500			0.45
5	100	1	0.8	0.2
	500			0.6

Table 13: Values of parameters  $\varphi_{\max}$ ,  $\varphi_{\text{int}}$  and  $\varphi_{\min}$  for fire ratings R60

ratio of reinforcement $A_s/(A_s+A_c)$	Cross-section size b (mm)	Fire rating R60		
		$\varphi_{\max}$	$\varphi_{\text{int}}$	$\varphi_{\min}$
0	150	1	0.85	0
	500			
1	150	1	0.85	0.05
	500			0.05
2	150	1	0.85	0.08
	500			0.20
3	150	1	0.85	0.10
	500			0.35
5	150	1	0.85	0.20
	500			0.60

#### 7.1.2.2 Case of eccentric load

For a load eccentricity  $\delta$ , the design buckling resistance  $N_{\text{fi,Rd},\delta}$  is obtained from:

$$N_{\text{fi,Rd},\delta} = \phi N_{\text{fi,Rd}} \quad (9)$$

Where:

- $\phi$  is a correction factor depending on the relative eccentricity  $\bar{\delta} = \delta/b$ . For intermediate values of the relative eccentricity, linear interpolation may be used to calculate  $\phi$ .

Table 14: Values of coefficient  $\phi$

Relative eccentricity $\bar{\delta}$	0.0625	0.125	0.25	0.5
$\phi$	0.85	0.75	0.65	0.5

- $N_{\text{fi,Rd}}$  is the design axial buckling resistance obtained from (1) but using appropriate values of the reduction coefficient  $\varphi_{c,\theta}$  to calculate the effective flexural stiffness of the cross-section  $(EI)_{\text{fi,eff}}$  and the plastic resistance to axial compression  $N_{\text{fi,pl,Rd}}$ .

In case of eccentric load, the reduction coefficient for concrete core  $\varphi_{c,\theta}$  takes the following value:

$$\varphi_{c,\theta} = \beta \varphi_{c,\theta,\text{ref}} \quad (10)$$

where  $\beta$  is a correction factor depending on the relative eccentricity  $\bar{\delta} = \delta/b$  as follows:

Table 15: Values of coefficient  $\beta$

relative eccentricity $\bar{\delta}$	0.0625	0.125	0.25	0.5
$\beta$	0.85	0.75	0.65	0.5

For non-reinforced column  $\varphi_{c,\theta,\text{ref}}$  is calculated according to (8) with the following parameters:



Fire rating	Size b (mm)	$L_{\theta,1}$ (m)	$L_{\theta,2}$ (m)	$L_{\theta,3}$ (m)	$\varphi_{\max}$	$\varphi_{\text{int}}$	$\varphi_{\min}$
R30	100	0.6	0.8	1.25	1	0.8	0
	500	1.75	3.50	9.25			
R60	150	0.75	1.00	2.00	1	0.85	0
	500	1.50	2.25	7.25			

Table 16: Values of mains parameters to calculated  $\varphi_{c,\theta}$  in the case of eccentric load

For reinforced column  $\varphi_{c,\theta,\text{ref}}$  is taken as the reduction coefficient calculated for centric load.

### 7.1.3 Field of application

The extensive parametric investigation which the simplified design method is based on allows to propose the following fields of application:

- stainless steel grades EN1.4301, EN1.4401 and EN1.4571;
- buckling length :  $\ell_0 \leq 30b$  ( or  $d$  ) ;
- size of hollow section:  $100 \text{ mm} \leq b$  ( or  $d$  )  $\leq 500 \text{ mm}$  ;
- thickness of hollow steel section:  $e \leq 8 \text{ mm}$
- concrete class from C20/25 to C60/75 ;
- percentage of reinforcement :  $0\% \leq A\% \leq 5\%$  ;
- axially loaded column or eccentrically loaded column such as relative eccentricity :  $0.0625 \leq \delta = d / ( b \text{ or } d ) \leq 0.5$  ;
- standard fire resistance from R30 and R60

### 7.1.4 Comparison between the proposed design method and the numerical model

An exhaustive comparison between the proposed simplified design method and the numerical model cannot be carried out here. However, to show the quite acceptable accuracy of the simplified method, some figures are shown hereafter. In these figures, the marks of ratio  $N_{fi,Rd} / N_{fi,pl,Rd}$  are arranged as a function of the relative slenderness calculated at elevated temperature in accordance with (4),  $N_{fi,Rd}$  is the correct buckling load given by the advanced numerical model and  $N_{fi,pl,Rd}$  is the value of the plastic resistance according to (3).

It can be noted that the proposed design method is in general on the safe side when comparing to the numerical results, except in the case of columns with intermediate buckling lengths where some points are slightly on the unsafe side (but less than 15%). Globally, the difference between the simplified method and the numerical model does not exceed 10% on the unsafe side, which is fully acceptable.

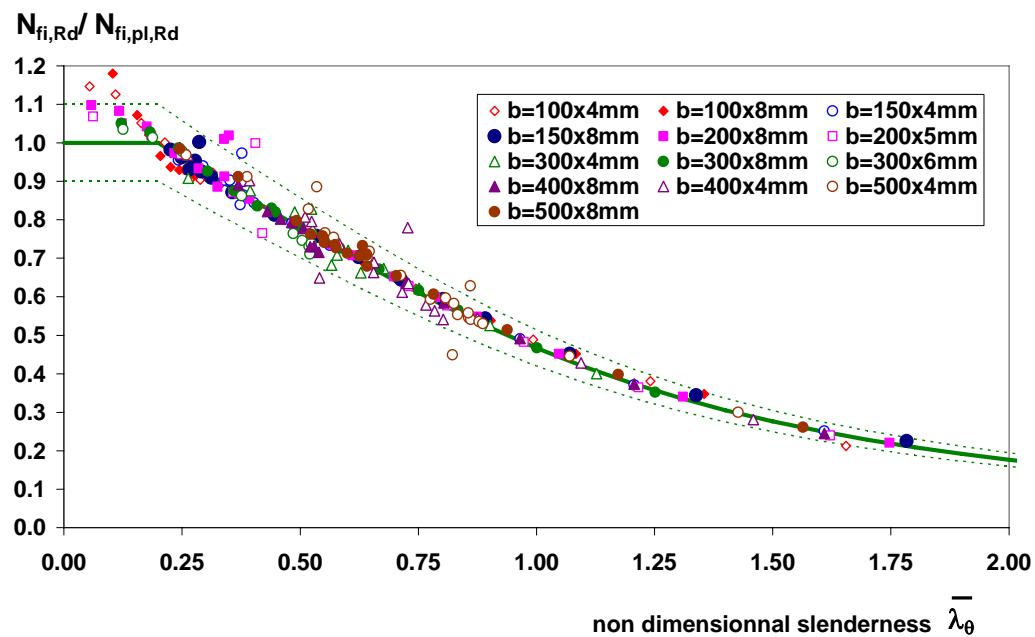


Figure 25 : Comparison between numerical results and simplified method for axially loaded non-reinforced columns and fire rating R30

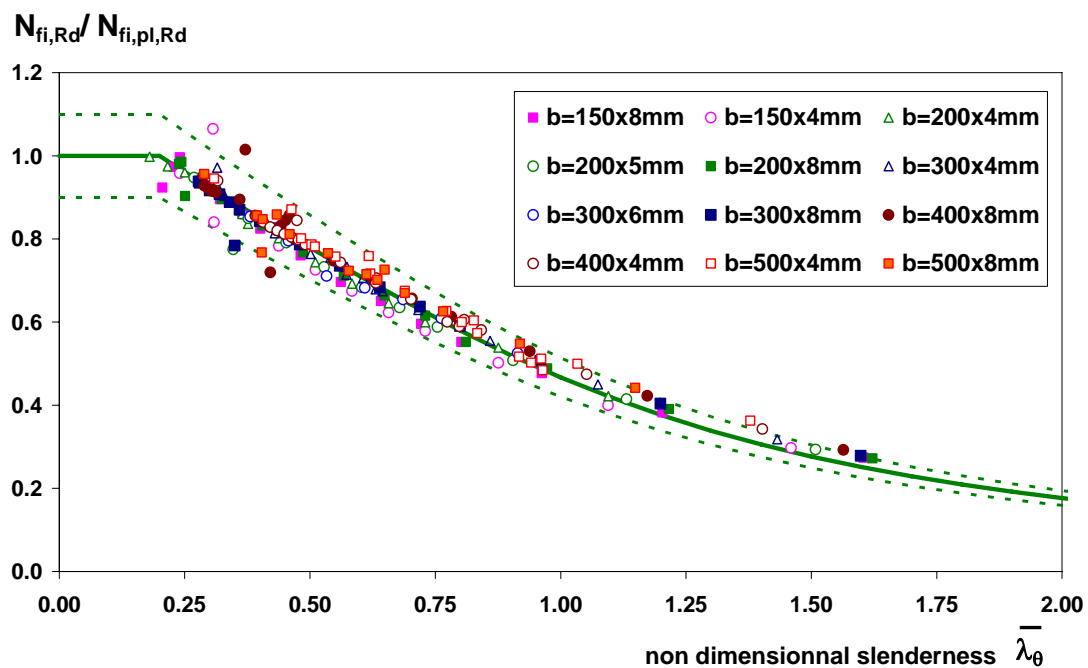


Figure 26: Comparison between numerical results and simplified method for axially loaded non-reinforced columns and fire rating R60

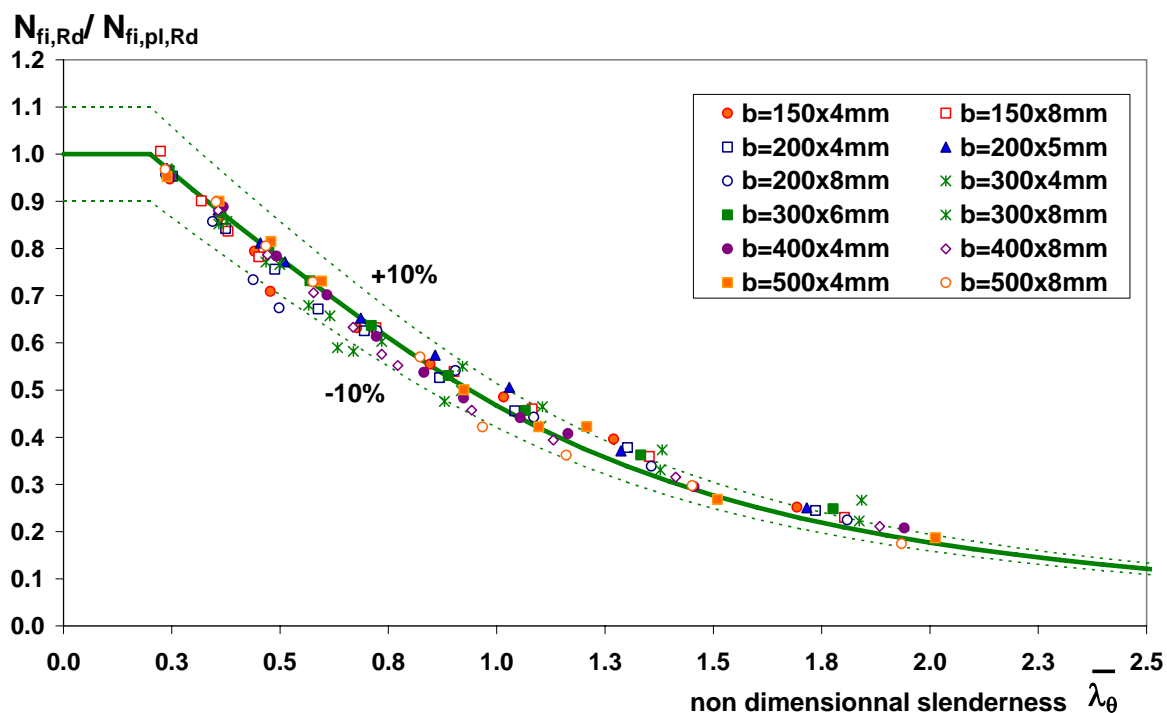


Figure 27: Comparison between numerical results and simplified method for axially loaded reinforced columns (using 2% of reinforcing bars) and fire rating R30

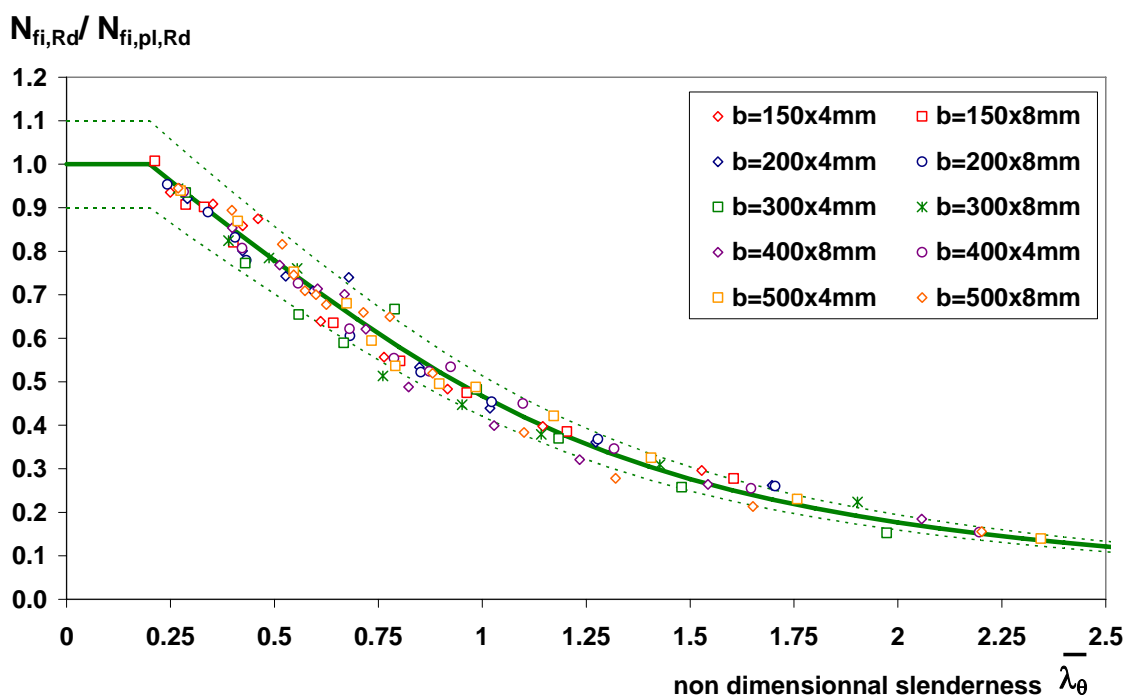


Figure 28: Comparison between numerical results and simplified method for axially loaded reinforced columns (using 3% of reinforcing bars) and fire rating R60

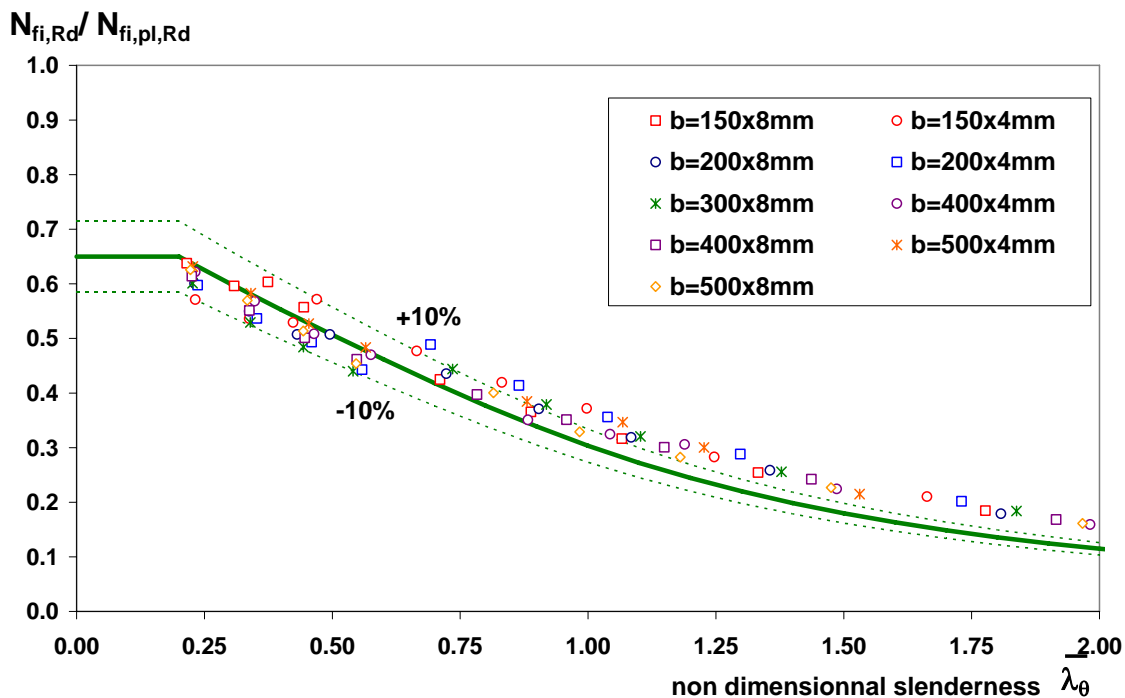


Figure 29: Comparison between numerical results and simplified method for eccentrically loaded reinforced columns (with a relative eccentricity  $\bar{\delta} = 0.25$  and using 3% of reinforcing bars) and fire rating R30

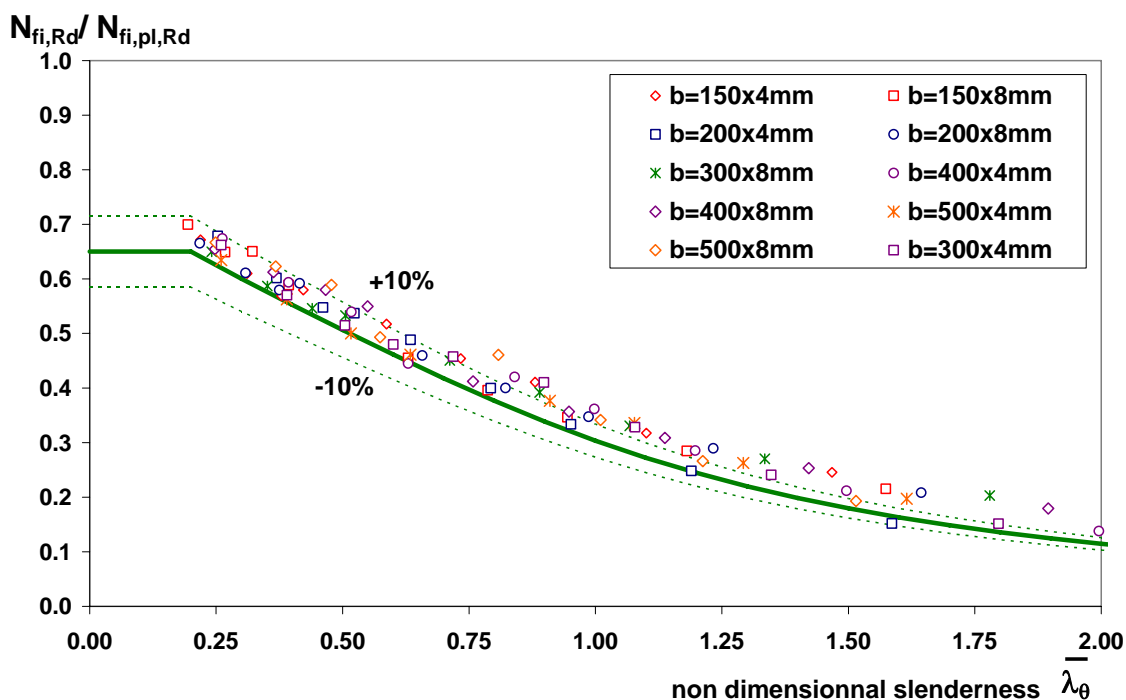


Figure 30: Comparison between numerical results and simplified method for eccentrically loaded reinforced columns (with a relative eccentricity  $\bar{\delta} = 0.25$  and using 3% of reinforcing bars) and fire rating R60

### 7.1.5 Comparison between fire test results and simplified method

Moreover, to assert the validity of the simplified method, a comparison between fire tests and corresponding calculation results has been performed.

To evaluate the accuracy of the simplified method against experimental results, the buckling resistance should be estimated at the ultimate temperature distribution corresponding to the failure time obtained from tests (ranging between 42 and 71 minutes). However, the proposed design method allows to check composite columns for the standard fire ratings R30 and R60 only. So, for intermediate fire duration, ultimate buckling loads have been linearly interpolated between the ultimate loads obtained for the two standard fire ratings. When the failure time of columns was higher than 60 minutes, comparison has been made with the ultimate load calculated for R60.

Buckling resistance thus calculated are reported in **Table 17** and compared to test loads. It should be noticed that calculations have been performed using the measured mechanical properties of materials reported in the same table. It appears clearly that the simplified calculation method gives a good agreement with the standard fire test. Globally, the difference between buckling resistances calculated analytically and test loads does not exceed 15% as illustrated in Figure 31. Moreover, it can be noted that the unsafe results have been obtained for columns which have failed after 60 minutes of standard fire exposure. Of course, if these columns were failed at time close to 60 minutes, the difference between numerical model and design method would have been better and in the safe side.

Table 17: Ultimate loads of composite columns

Column	Characteristic Materials strengths (N/mm <sup>2</sup> )			Failure time (min)	Test conditions Load/ eccentricity	Calculated buckling load (KN)	Ratio Calculated load/ Test Load
	Stainless steel	Concrete	Rebars				
N°1	340	41.5	450.0	42	400 / 5 mm	357.0	0.90
N°2	305			59.5	240 / 0.25×b**	235.0	0.98
N°3	380			56	630 / 5 mm	570.0	0.90
N°4	305			71	240 / 0.25×b**	276.0	1.15
N°5	313			38	750 / 0.5×b**	715.0	0.95
N°6	313			70.5	1000 / 0.125×b**	1020.0	1.02
N°7	313			62	800 / 0.25× b**	837.0	1.04

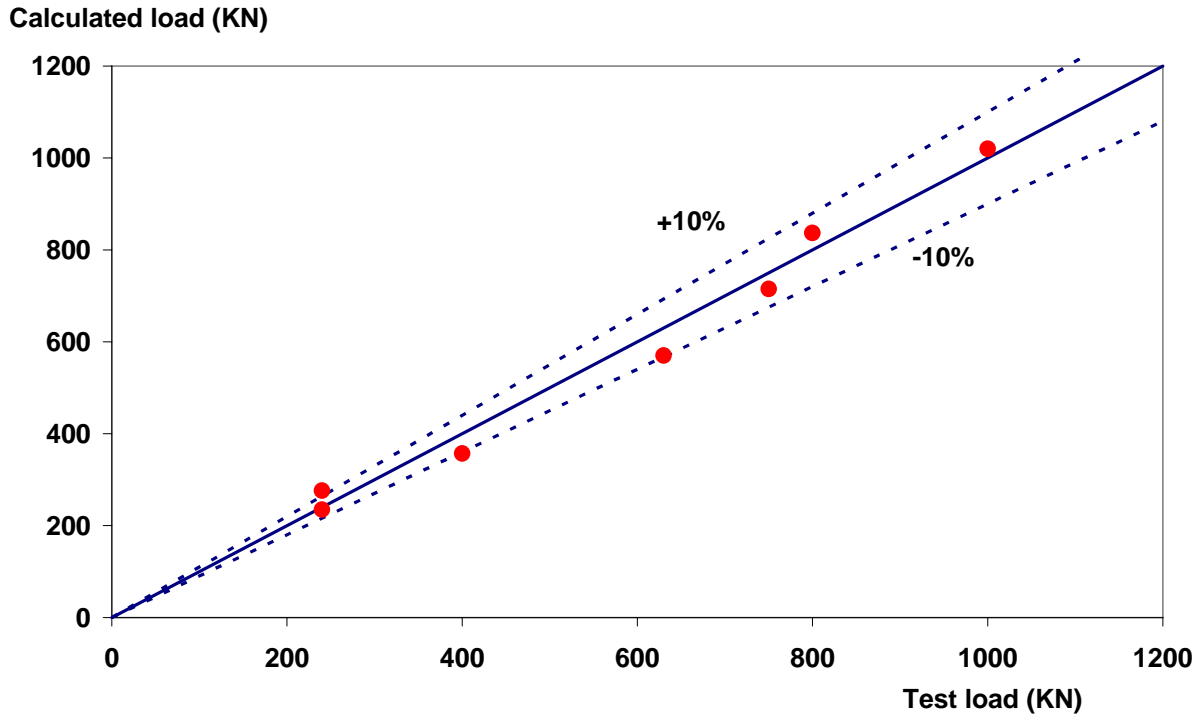


Figure 31: Comparison of ultimate loads between the simplified method and tests

## 7.2 FLOOR BEAMS WITH CONCRETE FIRE PROTECTION

### 7.2.1 Preliminary parametric study

In order to make easier the fire design of floor beams with concrete fire protection, 2D thermal analysis using computer code ANSYS were carried out to establish simplified temperature distributions for exposure to ISO standard fire up to 30 minutes.

Investigated beams, corresponding mesh and boundary condition are illustrated in **Figure 32**. Only one half of the beam was modelled to reduce the size of the model and cross-section was meshed using Plane55 finite element. Boundary conditions were introduced by means of Surf151 finite element.

In calculations, non linearities due to temperature dependency of materials properties have been taken into account. It has been assumed that conduction is the main heat transfer mechanism in the steel section and the concrete slab. Convection and radiation act essentially for heat transfers from fire to both stainless steel plate and exposed side of the concrete slab. As a simplification, direct heat transfer was assumed between the stainless steel plate and the upper flange or/and the concrete slab. Thus, possible gaps which can occur between the different parts of the beam have been neglected.

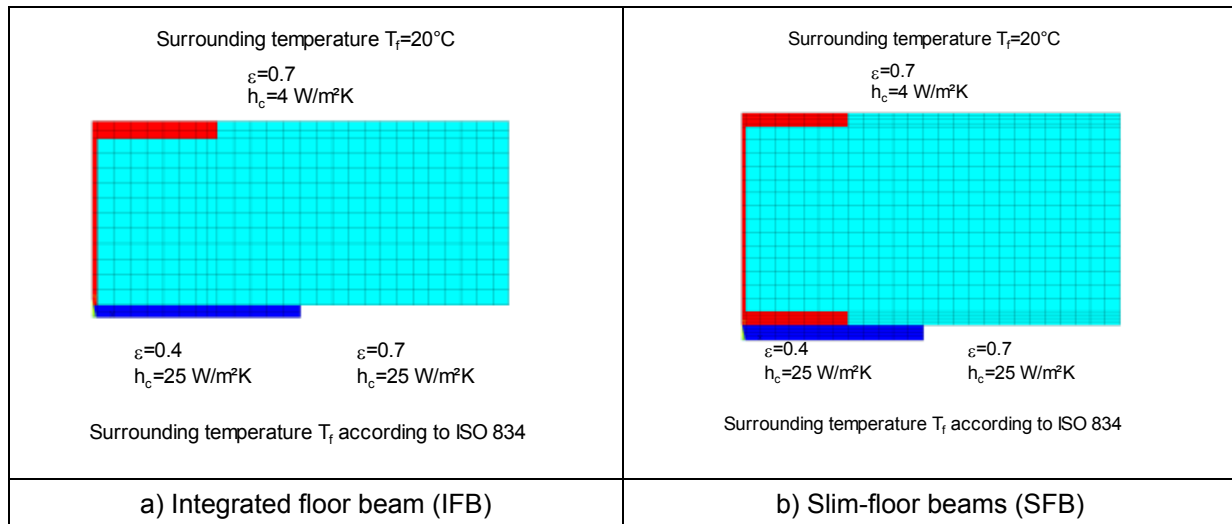


Figure 32 : Section mesh and boundary conditions

Parametric study has been carried out, adopting the following parameters:

- Height IFB cross-sections (carbon steel profile- stainless steel plate) : ½ IPE400 – 380x10, IPE500 - 400x12, HEB300 – 500x15, HEB600 500x20, ½ HEA 450 – 500x15, ½ HEM220 – 430x10, ½ HEM 340 500x30, ½ HEM650-500x35;
- Seven SFB cross-sections (carbon steel profile- stainless steel plate): HEB140 – 340x10, HEB200 - 360x15, HEB240 – 440x15, HE280 480x20, HEM200 – 410x10, HEM 220 430x20, HEM260-470x15; It should be noted that the dimensions of the chosen beams are close to the IF and SF beams product by ARCELOR.
- The net heat flux transferred to the slim floor beam by convection and radiation was calculated basing on a convection coefficient  $h_c = 25 \text{ W/m}^2\text{K}$  and an emissivity of 0.4 for stainless steel plate and 0.7 for concrete slab accordingly to EN 1991-1-2 and EN 1993-1-2.
- The thermal materials properties of the concrete as a function of temperature were taken in accordance with EN 1994-1-2, assuming upper limit for thermal conductivity. Moisture content in concrete is taken as 4%;
- Stainless steel and carbon steel material models were taken from EN 1993-1-2;

As an example, **Figure 33** shows the temperature fields obtained in the integrated floor beam n°1 after 30 and 90 minutes of standard fire exposure.

**Figure 34** and **Figure 35** give temperature distributions calculated along the depth of the beams (stainless steel plate and carbon steel profile) at 30, 60, 90 and 120 minutes exposure to standard fire.

From these figures, it can be observed that:

- A large temperature gradient occurs in the beam cross-section due to the encasement of the concrete. Moreover, there is always an appreciable difference between the mean temperature of the stainless steel plate and the mean temperature of the bottom flange (SF beam) or the temperature at the bottom of the web (IF beam).
- The temperature in the carbon steel profile remains below  $400^\circ\text{C}$  after 30 minutes of fire exposure. As the full strength of steel can be expected for this temperature, it appears clearly that 30 minutes fire resistance can be easily achieved by investigated beams. After 60 minutes, the temperature of the carbon steel profile above approximately one quarter of the web depth from the lower flange (SF beam) or bottom edge of the web (IF beam) is higher than  $400^\circ\text{C}$ . After 120 minutes, one half of the carbon steel profile is heated more than  $400^\circ\text{C}$ .
- On the unexposed side of the floor, the temperature remains lower than  $100^\circ\text{C}$  after 120 minutes of standard fire exposure. The insulation criteria seem to be always satisfied with this type of structural members.

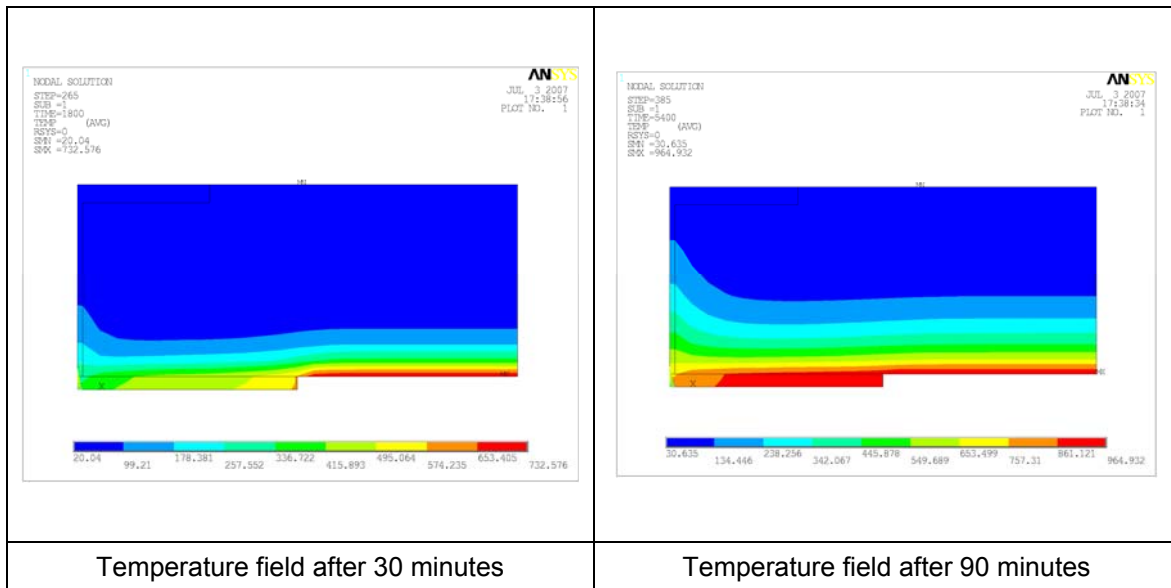


Figure 33: Cross-section heating of the IF beam n°1 (1/2 HEA450 and 500x15 stainless steel plate)

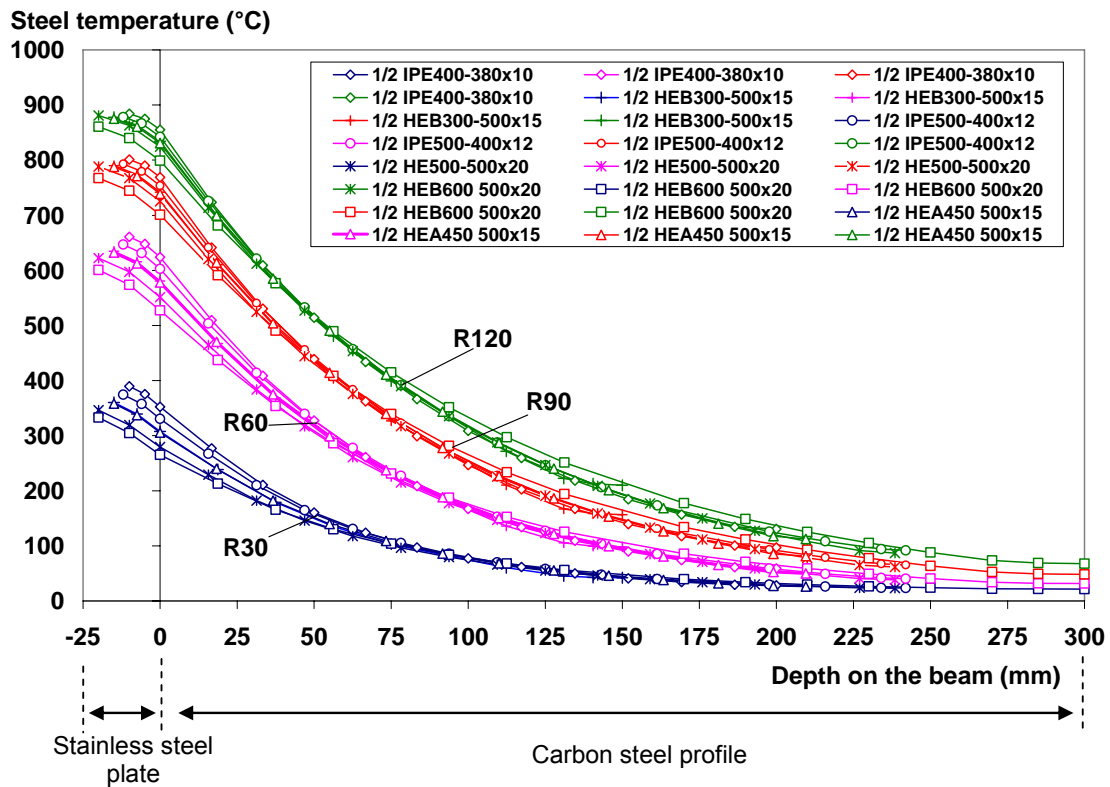


Figure 34: Temperature distribution along the depth of IF Beams from 30 to 120 minutes of standard fire exposure



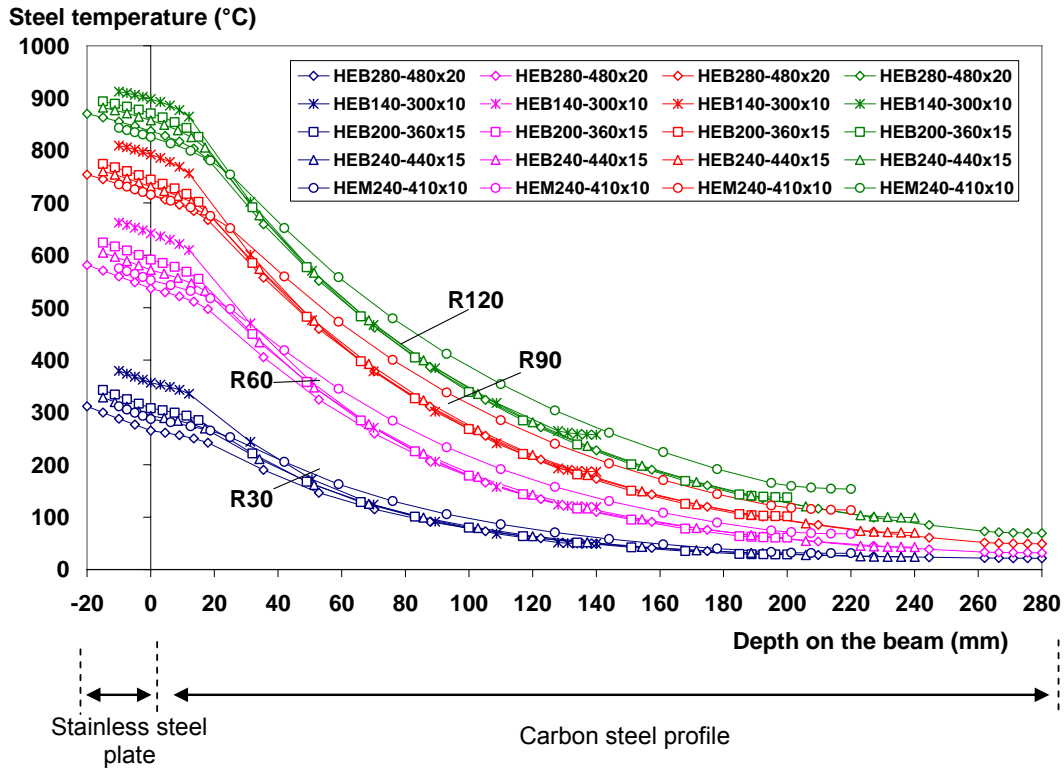


Figure 35: Temperature distribution along the depth of SF Beams from 30 to 120 minutes of standard fire exposure

## 7.2.2 Proposed design method for simply supported beams

The proposed design method is based on the simple plastic moment theory. It requires the calculation of the neutral axis and corresponding moment resistance taking into account temperature distribution through the cross-section and corresponding reduced material strength.

The following simplifying assumptions have been made:

- The concrete does not contribute to the load bearing capacity at elevated temperatures and thus may be ignored.
- Failure of beams occurs when maximum mechanical strain exceeds 2% on the exposed stainless steel plate.

The plastic neutral axis of the beam is determined such that the tensile and compressive force acting in the section are in equilibrium:

$$\sum_{i=1}^n A_i k_{y,\theta,i} \left( \frac{f_{y,i}}{\gamma_{M,f,i,a}} \right) = 0 \quad (10)$$

where  $f_{y,i}$  is the nominal yield strength  $f_y$  for the elemental steel area  $A_i$  (stainless steel plate, both carbon steel flanges and web), taken as positive on the compression side of the plastic neutral axis and negative on the tension side.

The design moment resistance  $M_{f,t,Rd}$  may be determined from:

$$M_{f,t,Rd} = \sum_{i=1}^n A_i z_i k_{y,\theta,i} \left( \frac{f_{y,i}}{\gamma_{M,f,i}} \right) \quad (11)$$

where  $z_i$  is the distance from the plastic neutral axis to the centroid of the elemental area  $A_i$ .

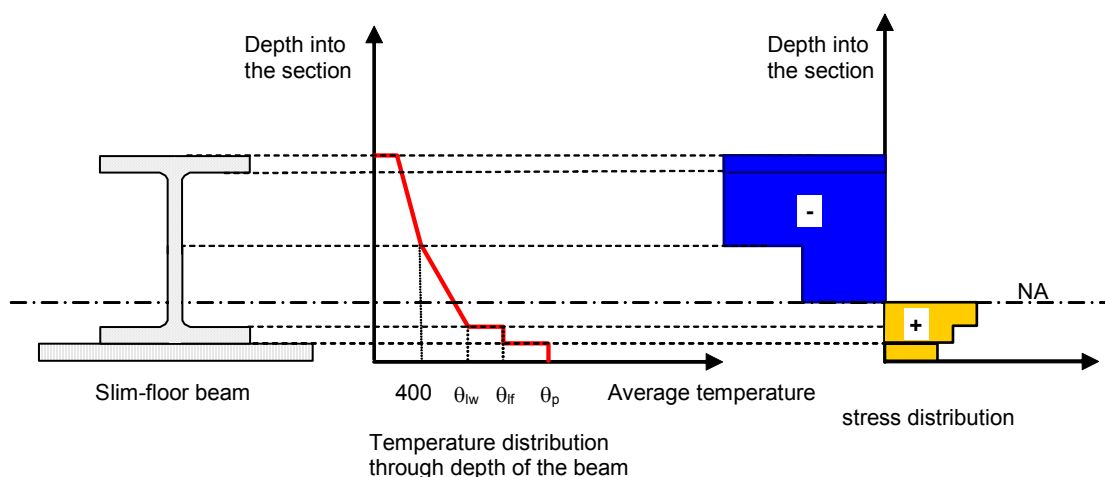


Figure 36: Temperature and stress distributions along the depth of beam

For the calculation of the design value of the moment resistance, the cross-section of the beam is divided into various components, namely:

- the stainless steel plate,
- the lower flange of the carbon steel profile (when used);
- the web of the steel profile;
- the upper flange of the carbon steel profile.

To each of these parts of the cross-section, simple rules are given below which defines the effect of temperatures and allow calculating the reduced characteristic strength in function of the standard fire resistance R30, R60, R90 or R120.

#### Stainless steel plate:

- Full area:  $A_p = e_p \times b_p$
- Uniform temperature  $\theta_p$  defined in function of the stainless steel plate thickness  $e_p$  and the flange thickness  $e_f$  as follows:
  - For IF beam:  $\theta_p = \theta_o - a \times e_p$  (12)
  - For SF beam:  $\theta_p = \theta_o - a \times (e_p + e_f)$

Where  $e_p$  and  $e_f$  are the thickness of the stainless steel plate and the lower flange respectively;  $\theta_o$  and  $a$  are empirical coefficients given in Table 18.

Table 18: Values of parameters  $\theta_o$  and  $a$

Fire rating	IF beam		SF-beam	
	$\theta_o$	$a$	$\theta_o$	$a$
30	570	7	500	3
60	830	6	775	
90	920	3	930	
120	980	2	1025	

- Reduced strength according to the previously predicted temperature:

$$f_{sy,\theta p} = k_{2,\theta p} \times f_{sy,20}$$

where  $k_{2,\theta}$  is the reduction factor for the strength at 2% total strain at temperature  $\theta_p$ . The reason of using the 2% strain strength of steel is due to the fact that for fire design of carbon steel, this strength is considered as the characteristic design strength.

Lower flange (when used):

- Full area:  $A_{lf} = e_f \times b_f$
- Uniform temperature distribution  $\theta_{lf}$  estimated for the required fire resistance class as follows:

$$\theta_{lf} = b \times \theta_p \quad (13)$$

where  $b$  is a empirical coefficient given in Table 19.

Table 19: Values of parameter  $b$

Fire rating	30	60	90	120
$b$	0.75	0.85	0.90	0.95

- Reduced strength distribution according to previously predicted temperature

$$f_{sy,\theta_{lf}} = k_{y,\theta_{lf}} \times f_{ay,20} \quad (14)$$

where  $k_{y,\theta_{lf}}$  is the reduction factor for the yield strength of the steel at temperature  $\theta_{lf}$ .

web:

The web of the steel beam is divided into two parts. The upper part of the web possesses the full yield stress  $f_{ay,20^\circ C}$ , where the yield stress of the lower part is assumed to reduce linearly from the yield stress of the upper part to the reduced yield stress at the bottom edge of the web.

- Upper part of the web:  $h_u$ 
  - Area:  $A_{wl} = e_w \times h_l$
  - Remain at temperature lower than  $400^\circ C$
  - For steel temperature not exceeding  $400^\circ C$ , no strength reduction is considered ( $f_{ya,20^\circ C}$ )
- Lower part of the web (part of the web with the height  $h_l$  and starting at the inner edge of the flange or at stainless steel plate) Area:  $A_{wl} = e_w \times h_l$ 
  - Only for fire rating higher than R30, strength changes linearly from  $f_{ya,20^\circ C}$  at its top edge to  $K_a f_{ya,20^\circ C}$  at its bottom edge.
  - The height  $h_l$  changes with fire rating

The height  $h_l$  of the lower part of the web is calculated to:

$$h_l = -\sqrt{\frac{2\alpha t}{\beta}} \ln\left(\frac{380}{\theta_{lw} - 20}\right) \quad (15)$$

Where

- $t$  is the time (s)
- $\beta = 12.25$
- $\alpha = \rho_a / \rho_a C_a$  ( $\lambda_a = 45 \text{ W/mK}$ ,  $C_a = 600 \text{ J/KgK}$ ,  $\rho_a = 7850 \text{ Kg/m}^3$ )
- $\theta_{lw} = \phi \theta_s$  is the mean temperature at the bottom edge of the web,  $\theta_s$  is the temperature of the stainless steel plate according to (12) and  $\phi$  is a reduction factor given in the following table:

Table 20: Values of parameters  $\phi$

Fire rating	60	90	120
IF-beam	0.77	0.83	0.87
SF-beam	0.76	0.81	0.84

The reduced yield strength to be considered in the lower part of the web is given by:

$$f_{sy,\theta} = f_{ay,20} \times (1 + k_{y,\theta lw})/2 \quad (16)$$

where  $k_{y,\theta lw}$  is the yield strength of steel at the steel temperature  $\theta_{lw}$

### 7.2.3 Comparison between the proposed design method and the numerical model

A comparison was made between advanced numerical model and the proposed simple calculation method for investigating the precision and the validity of the latter.

Five beam cross-section, with respectively standard hot rolled steel profiles HEA450, HEB200, HEB280 HEB300 and HEB600, and three fire rating, from 60 to 120 minutes, were taken in the comparison. Main structural details of investigated simply-supported beams are reported in **Figure 37**. Steel grade of carbon steel profile is S235. Stainless steel grade is EN1.4404 with a 0.2% proof strength  $f_{0.2p} = 240$  Mpa and an ultimate strength,  $f_u = 2.04 \times f_{0.2p}$ .

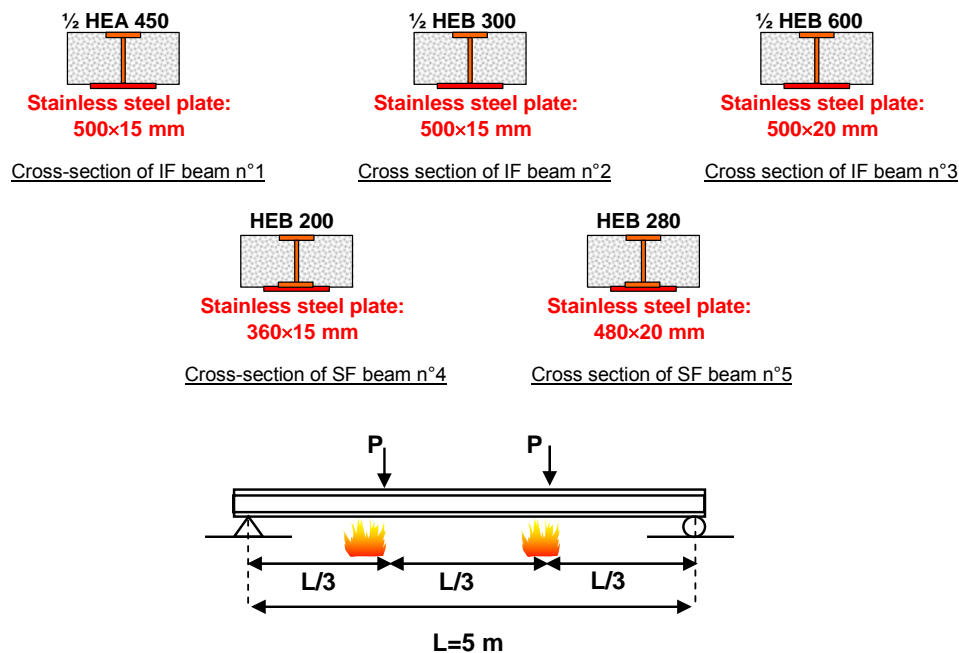


Figure 37: Characteristics of beams used in comparison

Using the numerical SISMEF, ultimate bending moment of the beam was calculated by firstly submitting the beam to the ISO fire curve until the expected fire, 60, 90 or 120 min. Once this time was reached, the corresponding temperature distribution in the cross section was kept constant and vertical load P was applied incrementally to the beam up to failure. To improve the accuracy of this failure load (which leads only to an approximate value of the effective ultimate bending moment of the beam), neighbouring vertical loads, more or less increased or reduced, were applied at room temperature and the beam was heated progressively under constant loads until the required fire resistance was obtained.. In calculation, failure of beams was assumed to occur when the maximum mechanical strain in stainless steel plate exceeds 2%. As illustrated in **Figure 38**, this assumption leads generally to a maximal deflection ranging from span/15 to span/10.

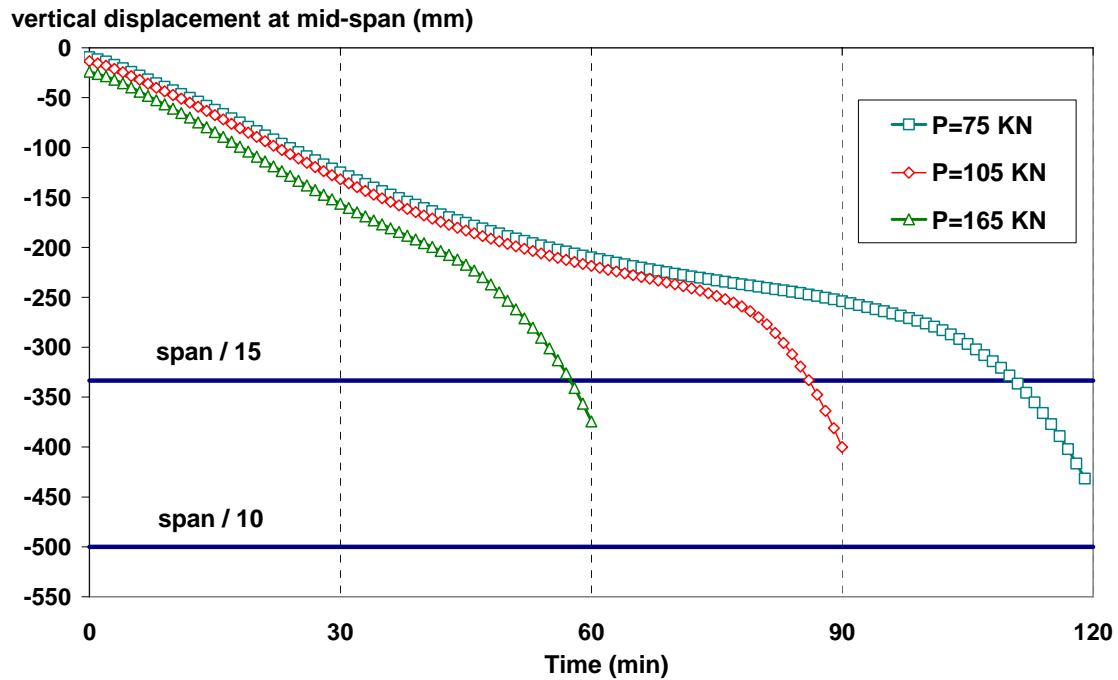



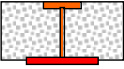


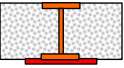
Figure 38: Vertical displacement calculated at mid-span of beam n°1 (1/2 HEA 450 - 500x15 stainless steel plate)

**Table 21** gives the moment resistance based on the proposed design method. They are compared with the ultimate bending moment (produced by vertical applied load) given at the ultimate limit state by the numerical model.

It can be seen that:

- The proposed design method gives good agreement with the numerical model. As shown in **Figure 39**, the difference between the simplified method and the numerical model remain lower than 10%.
- 60 minutes fire resistance can be easily achieved if the load ratio is lower than 0.7. Moreover, it appears clearly that IF-beams can achieve without difficulty 90 minutes fire resistance when the load ratio is lower than 0.5. SF-beams can achieve 120 minutes fire resistance for the same load ratio without any applied fire protection.

Table 21: Comparison of the proposed design method with numerical model

Beam	Fire rating	Ultimate bending moment (KN m)		Ratio $M_{SM} / M_{NM}$	Load ratio*
		Proposed design method ( $M_{SM}$ )	Numerical Model ( $M_{NM}$ )		
<b>½ HEA 450</b>  <b>Stainless steel:</b> <b>500×15 mm</b>	R60	267.0	275.0	0.97	0.72
	R90	180.70	175.0	1.03	0.46
	R120	136.32	125.0	1.09	0.33
<b>½ HEB 300</b>  <b>Stainless steel:</b> <b>500×15 mm</b>	R60	219.3	216.7	1.05	0.75
	R90	184.6	175.0	1.07	0.45
	R120	112.0	105.0	1.06	0.31
<b>½ HEB 600</b>  <b>Stainless steel:</b> <b>500×20 mm</b>	R60	542.9	558.3	0.97	0.73
	R90	401.3	366.7	1.09	0.48
	R120	297.4	275.0	1.08	0.36
<b>HEB 200</b>  <b>Stainless steel:</b> <b>360×15 mm</b>	R60	176.9	170.0	1.04	0.89
	R90	131.3	141.7	0.94	0.74
	R120	95.0	100.0	0.95	0.52
<b>HEB 280</b>  <b>Stainless steel plate:</b> <b>480×20 mm</b>	R60	421.8	400.00	1.05	0.92
	R90	354.6	333.3	1.06	0.77
	R120	257.4	250.0	1.03	0.58

\* the load ratio is defined as  $M_{NM} / M_{Rd}$ , where  $M_{Rd}$  is the bending moment resistance given at room temperature by the numerical model.

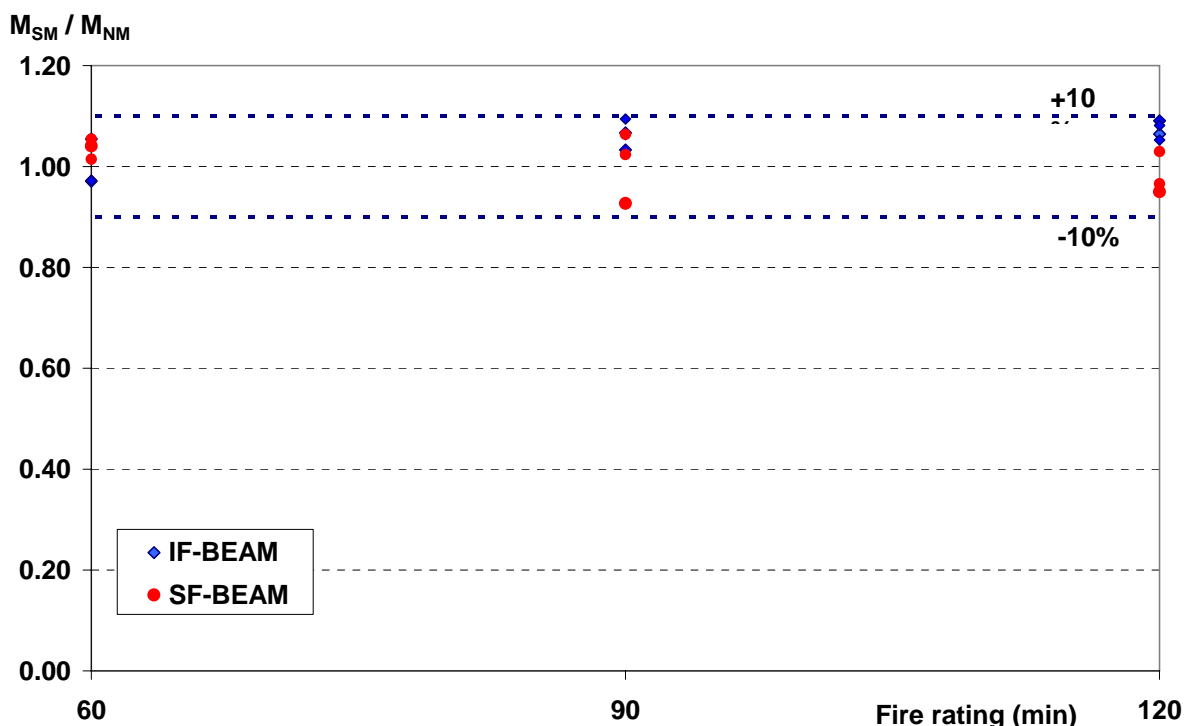


Figure 39: Comparison of the proposed design method with numerical model

## 8 COMPARAISON BETWEEN STAINLESS STEEL AND CARBON STEEL

To confirm advantages of composite members with stainless steel with regard to the fire resistance, comparisons have been made with S235 carbon steel composite members without any applied fire protection. Beams and columns adopted in this comparison study are illustrated in **Figure 40**. Concerning column, stainless steel becomes an interesting solution only if no reinforcing bars are needed to achieve the required fire resistance. As a result, comparisons have been performed for non-reinforced columns only. Moreover steel grade of stainless steel EN1.4401 was adopted because it is the most commonly used in construction.

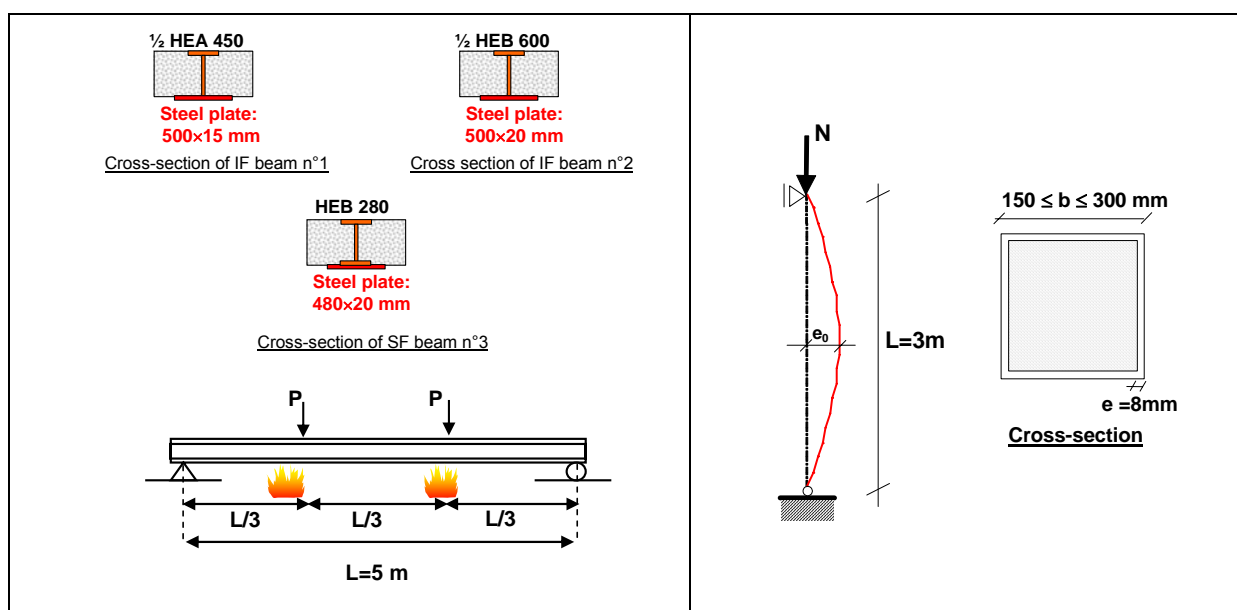


Figure 40: Details of beams and columns used for comparison

For the purpose of comparison, the temperature rise in beams and columns were previously calculated using the same assumptions that those adopted for the numerical analyses of fire tests. Moreover, it should be noted that temperatures of members where exposed steel part (plate or hollow section) is carbon steel have been computed adopting an emissivity of 0.7 for carbon steel.

**Figure 41** illustrates the temperature rises thus calculated through the cross-section of the integrated floor beam n°1. The curves of point 1 and 2 represent the temperature rise of the exposed steel plate. The curves of point 2 and 3 give the temperature rise at one quarter and one half of the web depth respectively. The curve of point five give temperature rise of the upper flange. As it can be seen, the beam where the exposed plate is stainless steel heated lower than the carbon steel cross-section. After 60 minutes of fire exposure, the maximum temperature obtained in the exposed steel plate is 835°C for stainless steel in comparison to 877°C for carbon steel. After 120 minutes, the maximum plate temperatures are 1000°C and 1020°C for stainless steel and carbon steel, respectively. This is mainly due to the fact that stainless steel has a lower emissivity than carbon steel, namely 0.4 compared to 0.7. For the same reason, temperature rise of the concrete encased carbon steel profile is lower where plate is stainless steel.

Same temperature comparisons are given in **Figure 42** for square composite column b=200x8mm.

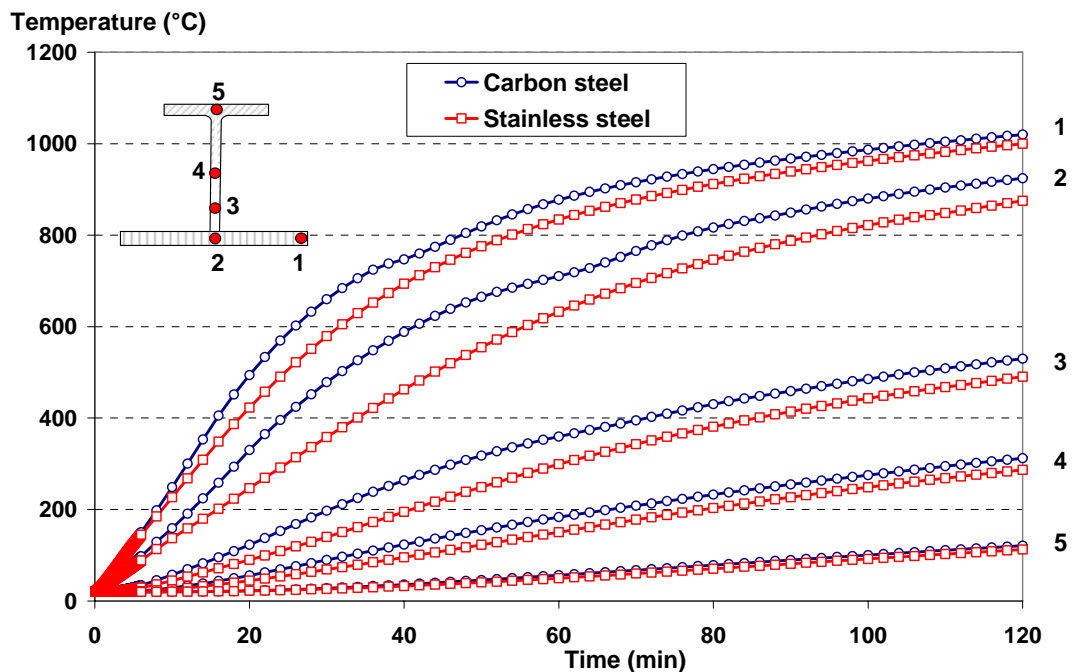


Figure 41: Temperature rise of IF beam n°1 according to steel grade of exposed steel plate



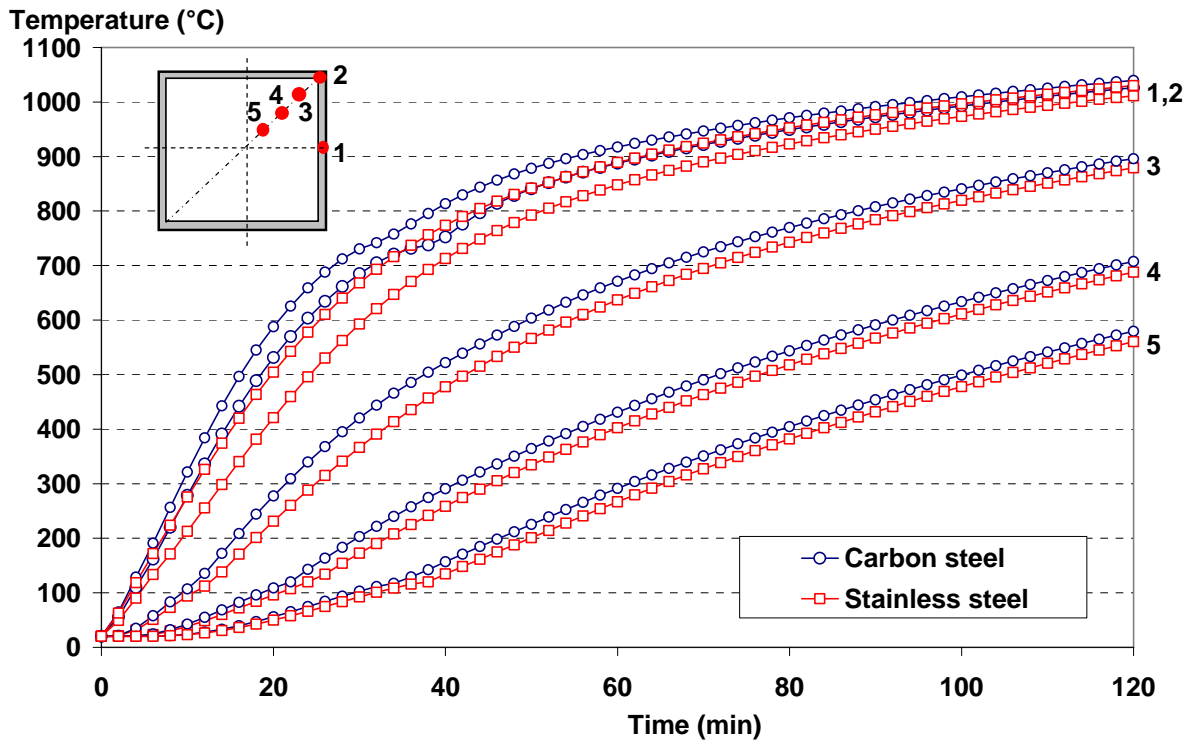


Figure 42: Temperature rise of square column b=200x8mm according to steel grade

**Table 22** compares the moment resistance and corresponding load ratio given at the ultimate limit state for all investigated beams (with exposed carbon or stainless steel plate). **Figure 43** to **Figure 45** show the vertical displacements calculated at mid-span of the same beams.

From these results, the following comments can be drawn:

- Differences between fire resistances are important according to steel grade. With the same fire rating, the bending moment resistance of carbon steel beams is always lowest than moment resistance calculated for the same beam but with exposed stainless steel plate. As an example, a moment resistance of 275 kN m was obtained for the stainless steel beam n°1 while the moment resistance of the same carbon steel beam was only 98.4 kN m.
- 120 minutes fire resistance can be easily achieved by the IF beam with exposed stainless steel plate where the load ratio is lower than 0.3. In contrast to this, carbon steel beam can only achieved a fire resistance of 60 minutes with the same maximum load ratio.
- 120 minutes fire resistance can be easily achieved by the SF beam with exposed stainless steel plate where the load ratio is lower than 0.5. In contrast to this, carbon steel beam can only achieved a fire resistance of 60 minutes with the same maximum load ratio.




**Table 23** gives the fire buckling resistance of each composite column and corresponding maximum load ratio according to steel grade (stainless steel or carbon steel).

It can be seen that:

- Stainless steel columns perform better than carbon steel columns: Carbon steel columns buckle at a lower load than the stainless steel column with identical size and length.
- For a given fire rating, maximum load ratio of stainless steel columns increases when increasing cross-section size. This is mainly due to the lower temperature rise of the large cross-section in comparison to smaller cross section.
- Maximum load factors of stainless steel columns are always higher than those obtained for carbon steel columns. As an example, for a fire rating of 30 minutes, the maximum load factor of the stainless steel column with mean cross-section size ( $b=200 \times 8 \text{ mm}$ ) is 0.35 in comparison to 0.15 for identical carbon steel column. In fact, the stainless steel column can achieve 60 fire minutes resistance with the same maximum load ratio.

Numerical results confirm the best fire behaviour of composite columns with stainless steel hollow section. The improved behaviour is mainly explained by the enhanced material properties and the favourable relationship between strength and stiffness that makes stainless steel less prone to buckling in fire. Indeed, slenderness of stainless steel column tends to reduce when increasing elevated what improve the flexural buckling behaviour of column by lowering lateral deflections, and therefore reducing second-order effects.

Table 22: Comparison of moment resistance of beams with exposed stainless or carbon steel plates

Beam	Fire rating	Beam with stainless steel plate		Beam with carbon steel plate	
		Moment resistance (KN m)	Load level	Moment resistance (KN m)	Load level
<b><math>\frac{1}{2}</math> HEA 450</b>  <b>Steel plate: 500x15 mm</b>	R60	275.0	0.72	98.4	0.27
	R90	175.0	0.46	66.7	0.17
	R120	125.0	0.33	56.7	0.15
<b><math>\frac{1}{2}</math> HEB 600</b>  <b>Steel plate: 500x20 mm</b>	R60	558.3	0.73	233.3	0.31
	R90	366.7	0.48	163.3	0.22
	R120	275.0	0.36	98.3	0.13
<b>HEB 280</b>  <b>Steel plate: 480x20 mm</b>	R60	400.00	0.92	266.67	0.55
	R90	333.3	0.77	136.67	0.28
	R120	250.0	0.58	104.17	0.22

\* the load ratio is defined as ratio between the moment resistance at the fire ultimate state and the moment resistance at room temperature.

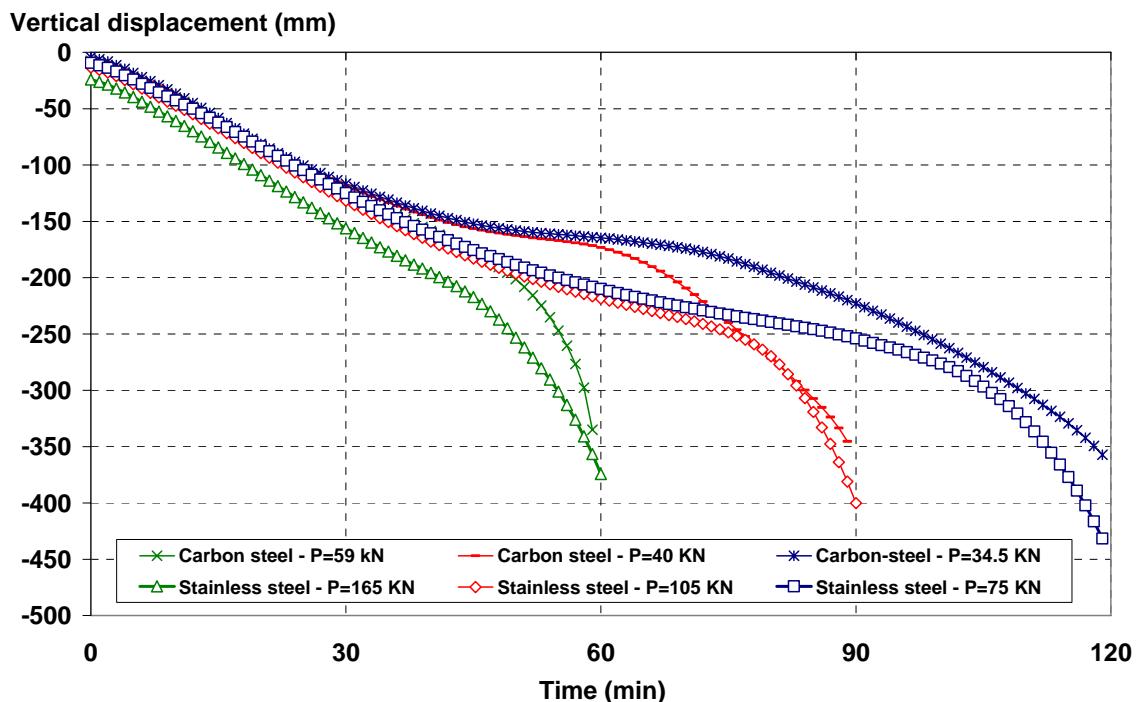


Figure 43: Vertical displacement at mid-span of the IF beam n°1 as function of applied load and steel grade of exposed steel plate

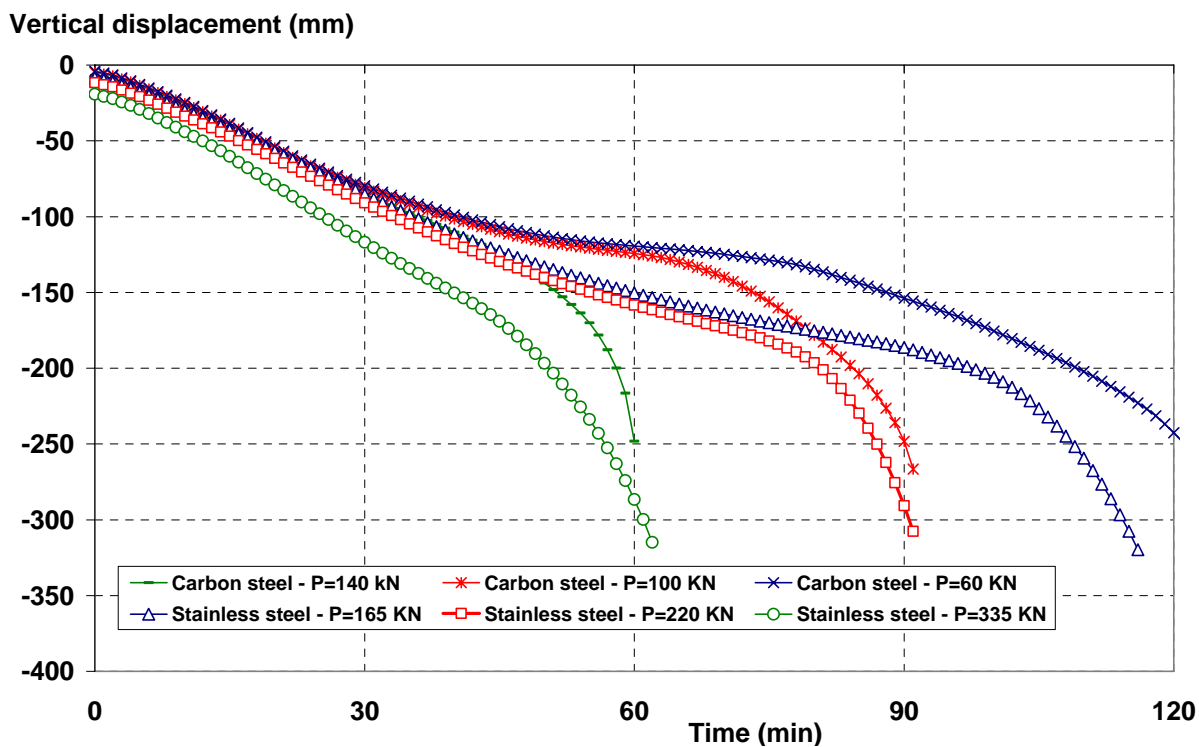


Figure 44: Vertical displacement at mid-span of the IF beam n°2 as function of applied load and steel grade of exposed steel plate

Vertical displacement (mm)

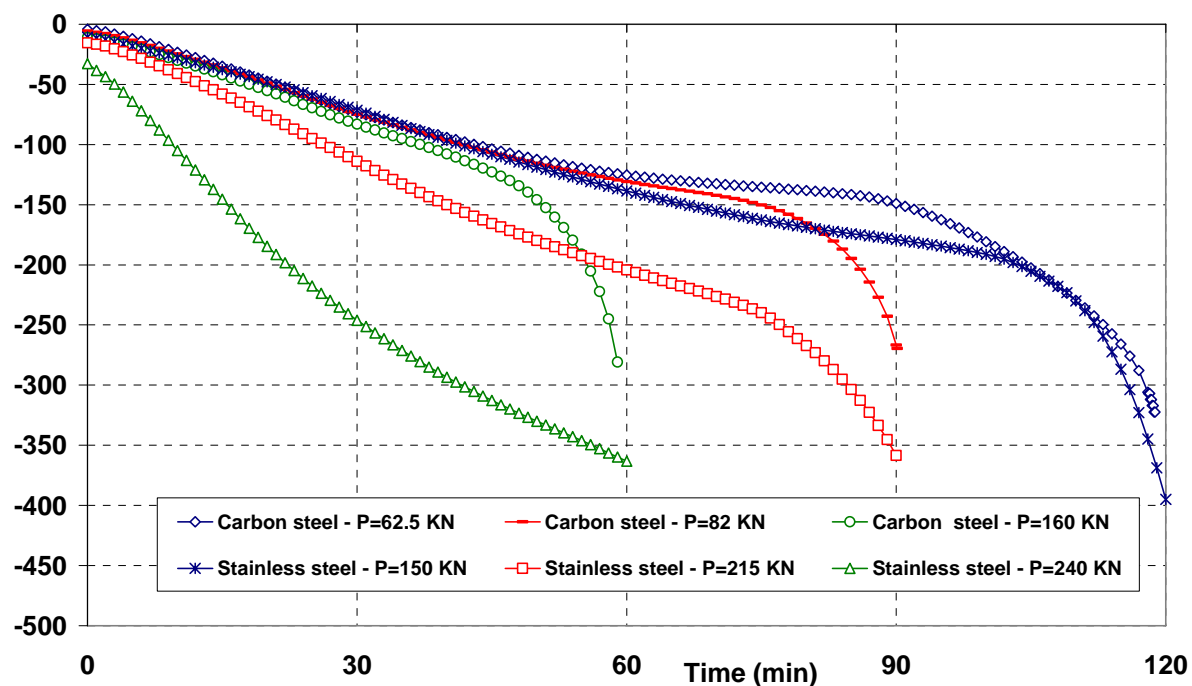


Figure 45: Vertical displacement at mid-span of the SF beam n°3 as function of applied load and steel grade of exposed steel plate

Table 23: Comparison of buckling resistance of columns with hollow stainless steel section

Column	Fire rating	Stainless steel column		Carbon steel column	
		Buckling resistance (KN)	Load level	Buckling resistance (KN)	Load level
b=150x8	30	413.3	0.36	117.2	0.15
	60	184.1	0.16	46.6	0.04
b=200x8	30	721.9	0.36	306.3	0.15
	60	325.6	0.16	113.9	0.06
b=300x8	30	2737.5	0.65	1950.0	0.47
	60	1220.0	0.29	626.7	0.15

\* the load ratio is defined as ratio between the buckling resistance at the fire ultimate state and the buckling resistance at room temperature obtained from numerical model.

## 9 CONCLUSIONS

Using numerical model SISMEF, the fire resistances of seven composite columns with hollow stainless steel sections and two partially protected floor beams with exposed part in stainless steel have been calculated and compared with test results. These comparison demonstrate that the model SISMEF is capable of predicting the behaviour of composite members with stainless steel (failure time, displacements, ...) with a good accuracy.

Then, the fire behaviour of previous composite members has been investigated with a wide range of parametric simulations. Referring to this base of numerical results, simple design methods consistent with the general flow chart used in EN 1994-1-2 to check the other types of composites members but including some specific characteristics have been proposed. It has been shown through the comparison with numerical results that the simple design method are capable of predicting with a quite good accuracy the fire resistance of composite columns with hollow stainless steel section and partially protected slim-floor beams.

## 10 RECOMMANDATIONS FOR FURTHER WORKS

Further investigations could be made to extend the simplified design method developed for composite columns to hollow section with thickness higher than 8mm.

## 11 REFERENCES

- [1] EN 1991-1-2 - Eurocode 1 " Actions on structures " – Part 1-2: General Actions – Action on structures exposed to fire, CEN, 2005;
- [2] EN 1993-1-1. Eurocode 3: Design of steel structures – Part 1-1: General rules and rules for buildings, CEN, 2005;
- [3] EN 1993-1-2,. Eurocode 3: Design of steel structures – Part 1.2: General rules – Structural fire design, CEN, 2005
- [4] prEN 1994-1-2, Eurocode 4 "Design of Composite Steel and Concrete Structures: Structural Fire Design", CEN, 2004;
- [5] ANSYS, "ANSYS User's Manual for Revision 8.0 – Volume IV – Theory", Swanson Analysis SYSTEM, INC., Houston USA, 1992;
- [6] RENAUD, C. Modélisation numérique, expérimentation et dimensionnement pratique des poteaux mixtes avec profil creux exposés à l'incendie, Thèse de Docteur en génie civil, INSA de Rennes, France, 2003;

- [7] RENAUD, C., ARIBERT, J.M., and ZHAO, B, Advanced numerical model for the fire resistance of composite columns with hollow steel section, Steel and composite structures, Vol. 3, 75-95, No. 2., 2003;
- [8] ZHAO, B. and ARIBERT, J.M. Finite Element Method For Steel-Concrete Composite Frames Taking Account of Slip and Large Displacements, European Journal of Finite Element, Vol. 5, n°2, 221-249, 1996;
- [9] ZHAO B. 1994. Modélisation numérique des poutres et portiques mixtes acier-béton avec glissements et grands déplacements, Thèse de docteur en Génie Civil, INSA de RENNES, Franc, 1994;
- [10] CTICM, Fire test on non-reinforced composite column with square hollow stainless steel section "Test report 06-U-297", 2006;
- [11] CTICM, Fire test on non-reinforced composite column with square hollow stainless steel section "Test report 06-U-298", 2006;
- [12] CTICM, Fire test on reinforced composite column with square hollow stainless steel section "Test report 06-U-300", 2006;
- [13] CTICM, Fire test on reinforced composite column with square hollow stainless steel section "Test report 06-U-303", 2006;
- [14] CTICM, Fire test on non-reinforced composite column with square hollow stainless steel section "Test report 06-U-323", 2006;
- [15] CTICM, Fire test on reinforced composite column with square hollow stainless steel section "Test report 06-U-330", 2006;
- [16] CTICM, Fire test on reinforced composite column with square hollow stainless steel section "Test report 06-U-335", 2006;
- [17] CTICM, Fire test on Integrated-Floor beam with exposed stainless steel plate "Test report 06-U-348", 2006;
- [18] CTICM, Fire test on Slim-Floor beam with exposed stainless steel plate "Test report 06-U-355", 2006;

## ANNEX A

### Photographs of tested columns



Figure 46 : View of composite column after test n°2



Figure 47 : View of composite column after test n°3





Figure 48 : View of composite column after test n°4



Figure 49 : View of composite column after test n°5



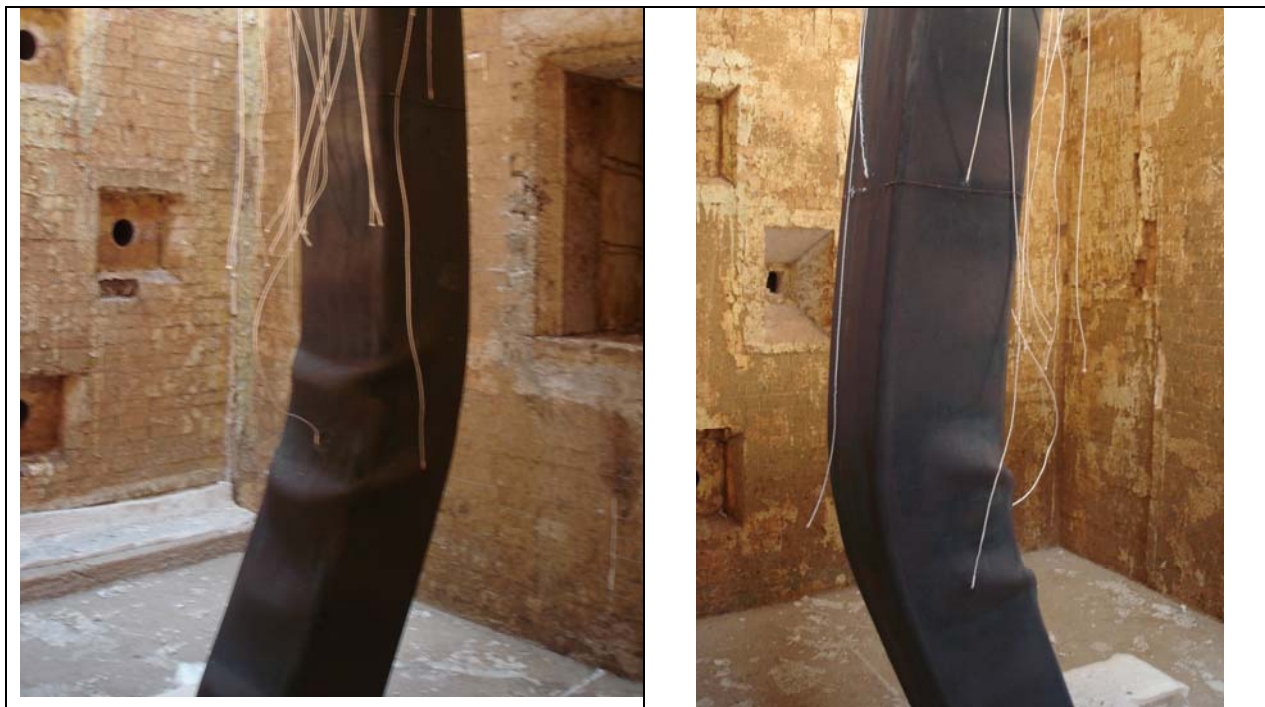


Figure 50 : View of composite column after test n°6



Figure 51 : View of composite column after test n°7

## ANNEX B

### Temperature development in columns: Comparison of the fire tests and the FE analyses

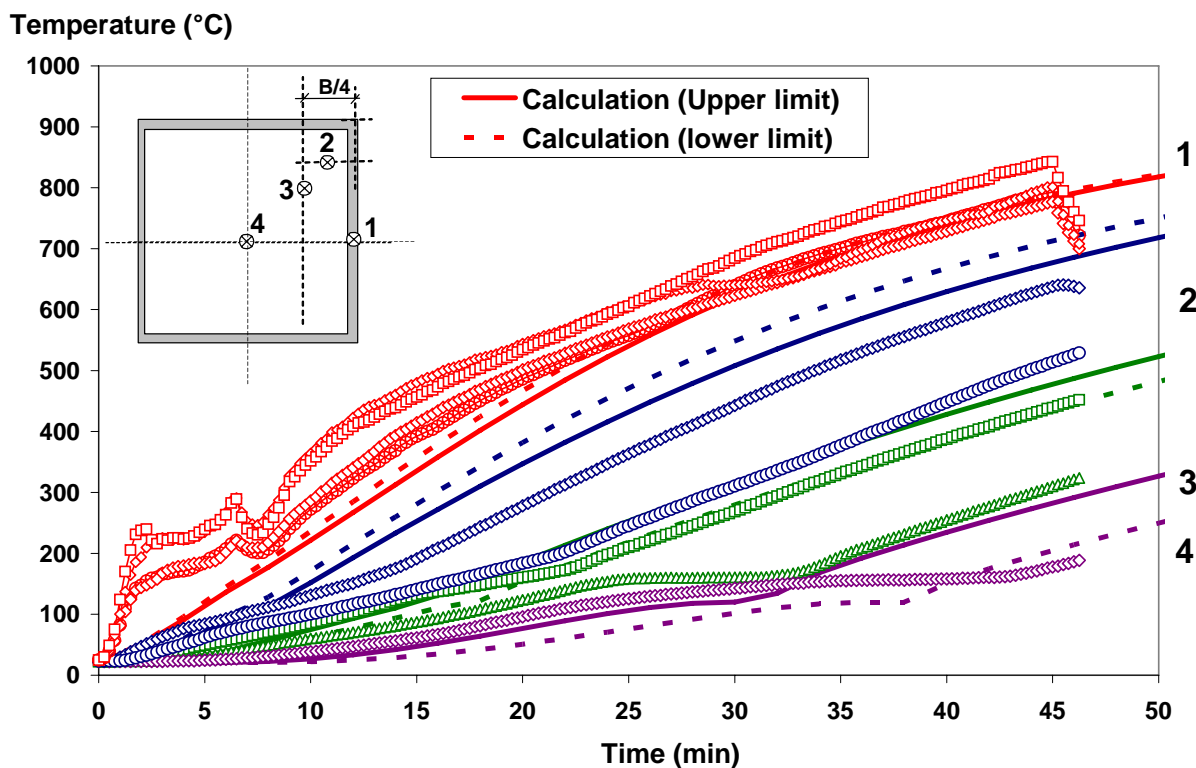


Figure 52 : Calculated and measured temperatures in the column cross-section n°1 of test n°1

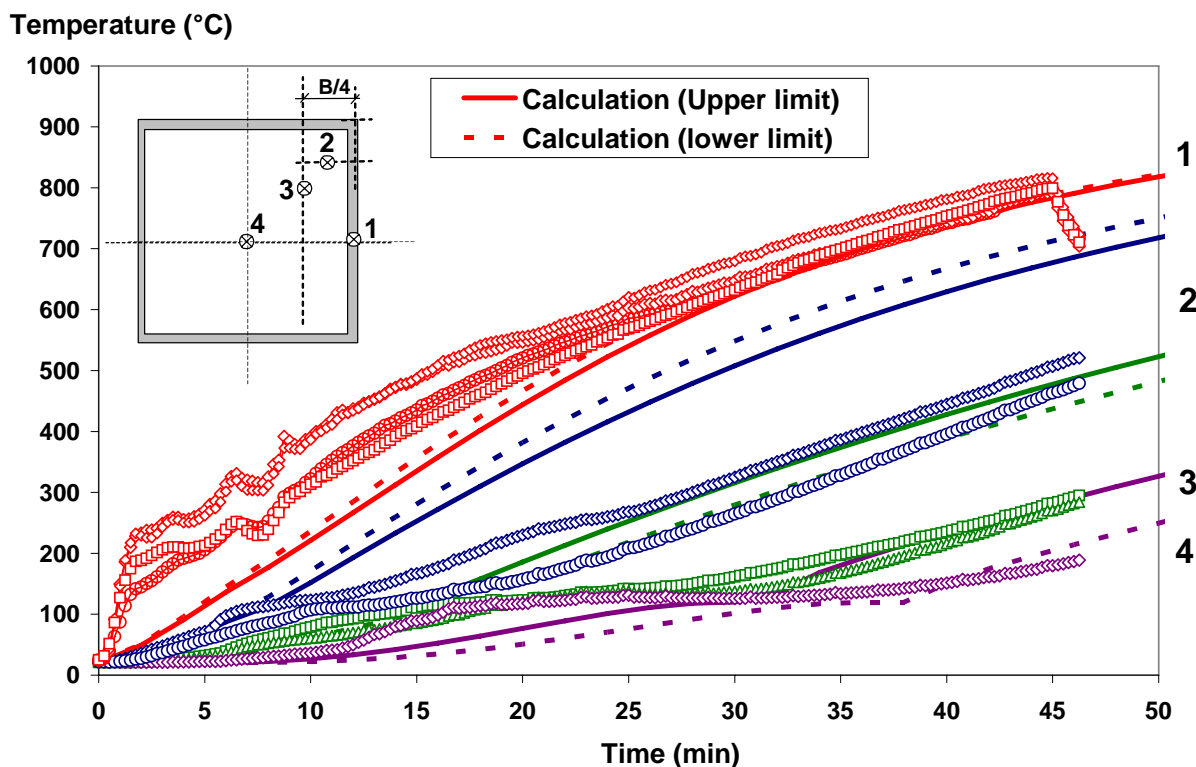


Figure 53 : Calculated and measured temperatures in the column cross-section n°3 of test n°1

Temperature (°C)

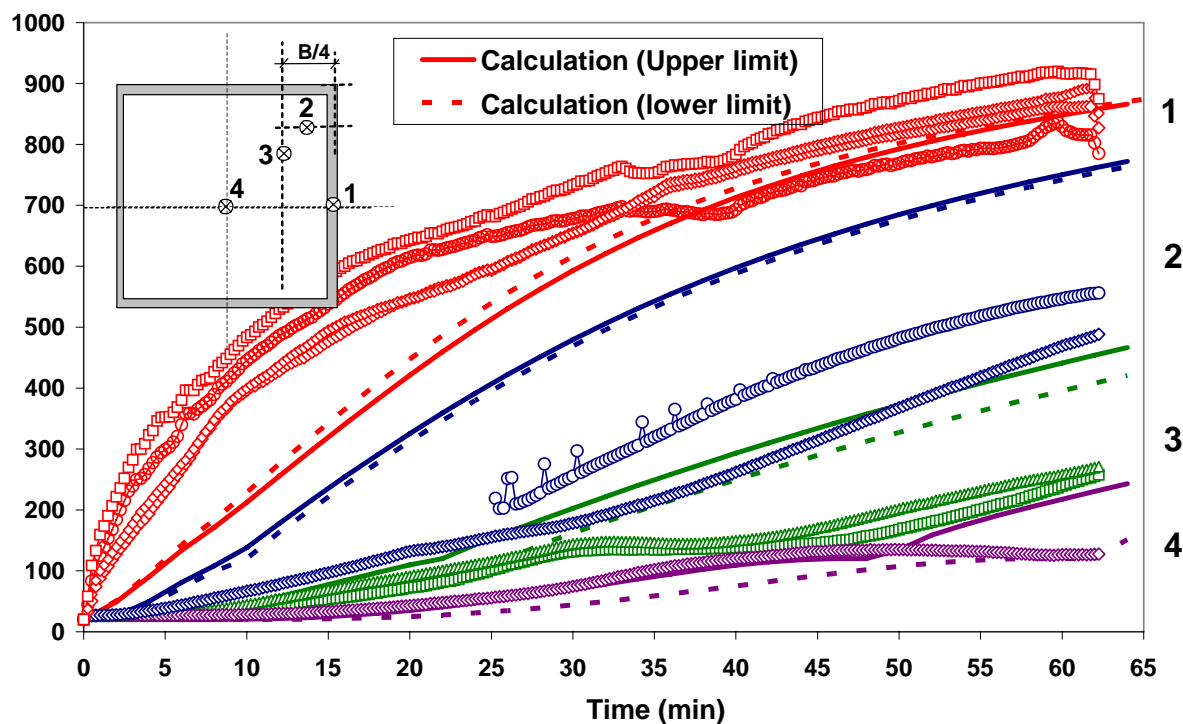


Figure 54 : Calculated and measured temperatures in the column cross-section n°1 of test n°2

Temperature (°C)

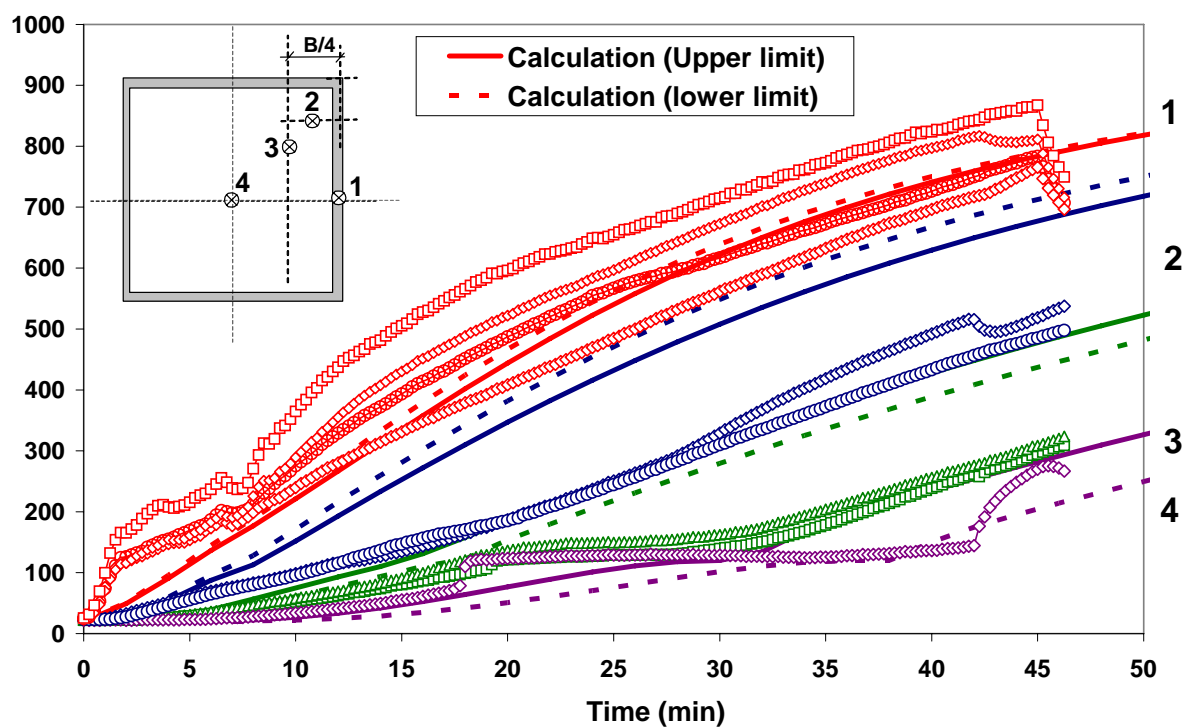


Figure 55: Calculated and measured temperatures in the column cross-section n°2 of test n°1

Temperature (°C)

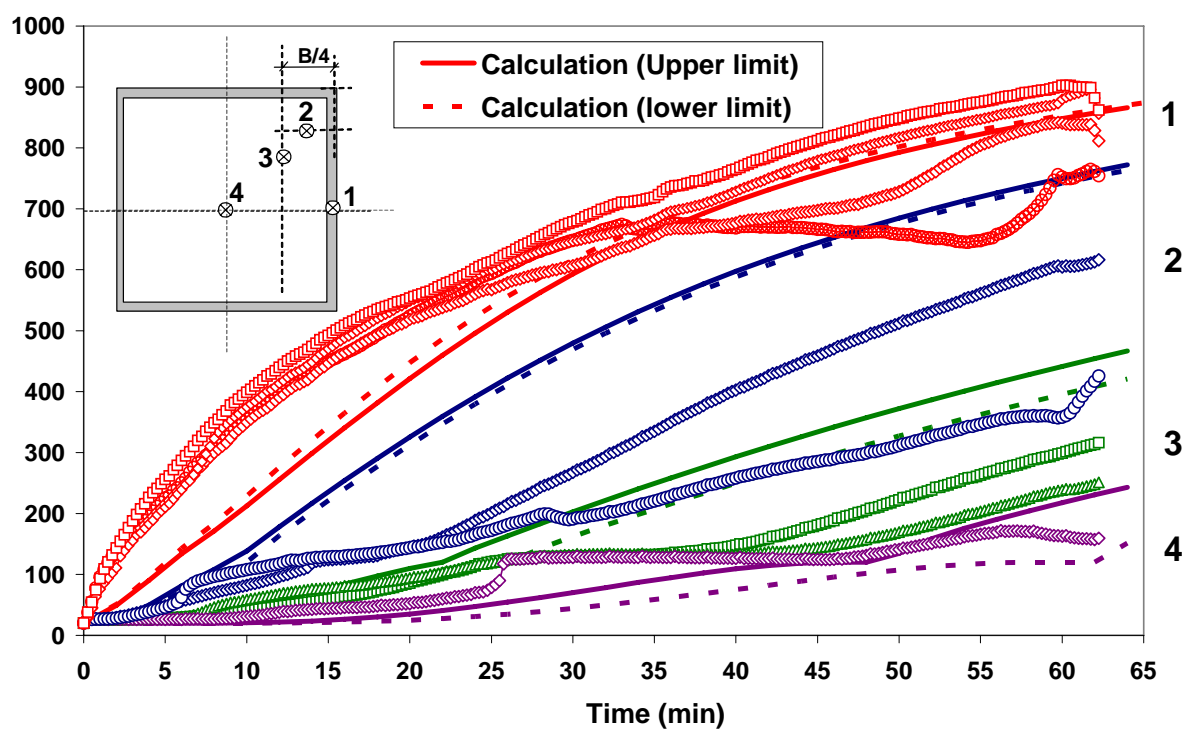


Figure 56 : Calculated and measured temperatures in the column cross-section n°2 of test n°2

Temperature (°C)

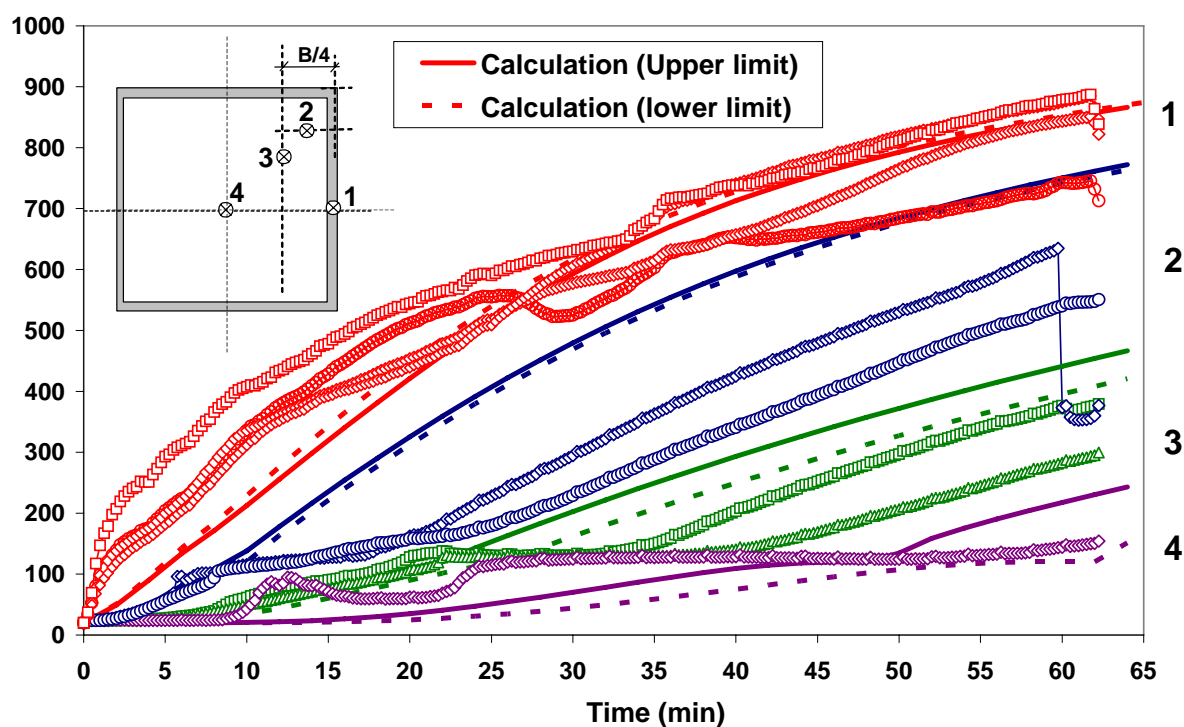


Figure 57 : Calculated and measured temperatures in the column cross-section n°3 of test n°2



Temperature (°C)

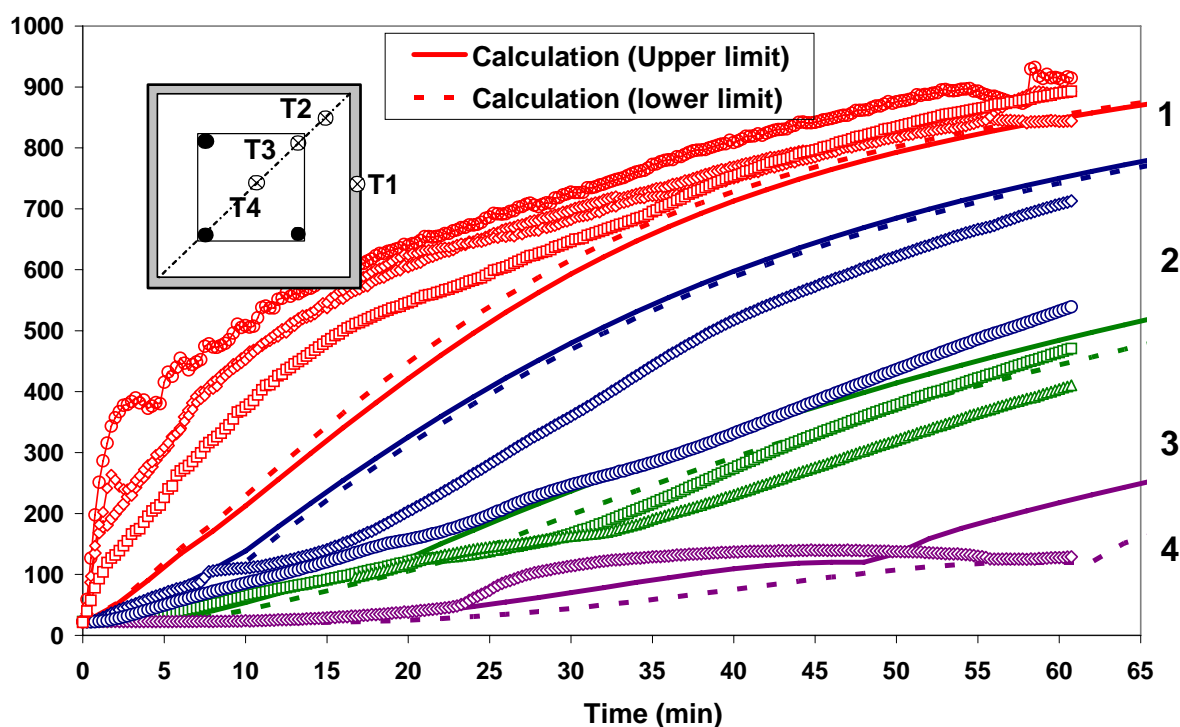


Figure 58 : Calculated and measured temperatures in the column cross-section n°1 of test n°3

Temperature (°C)

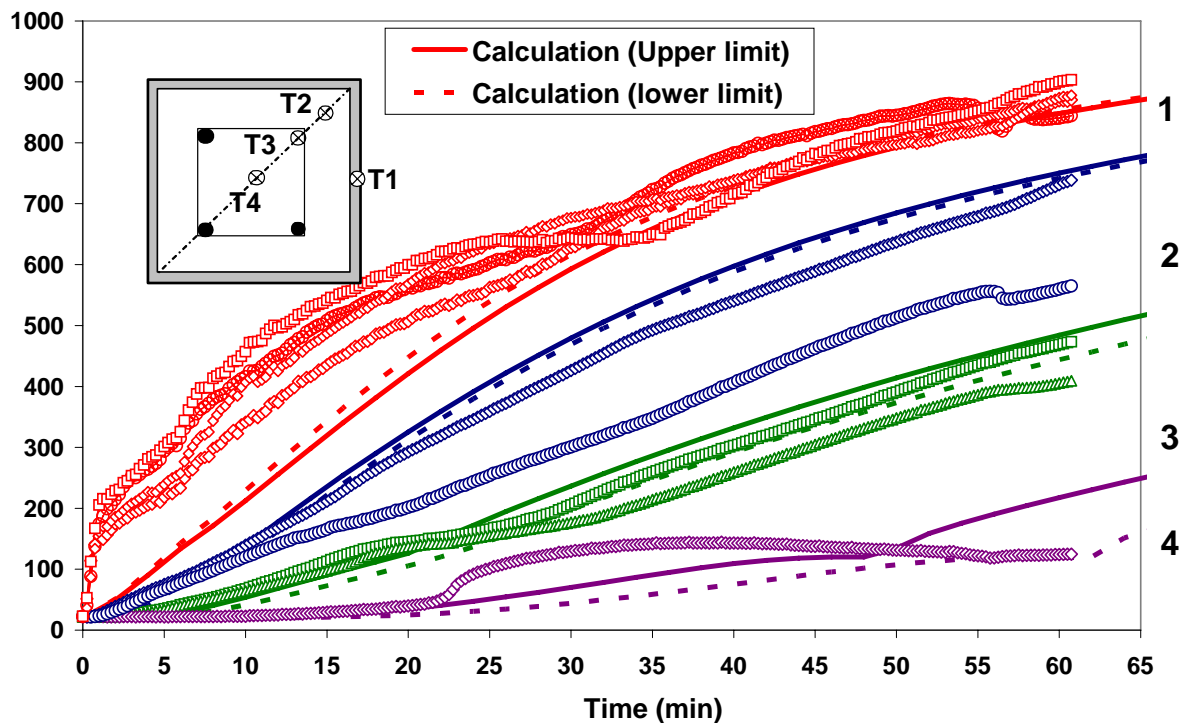


Figure 59: Calculated and measured temperatures in the column cross-section n°2 of test n°3

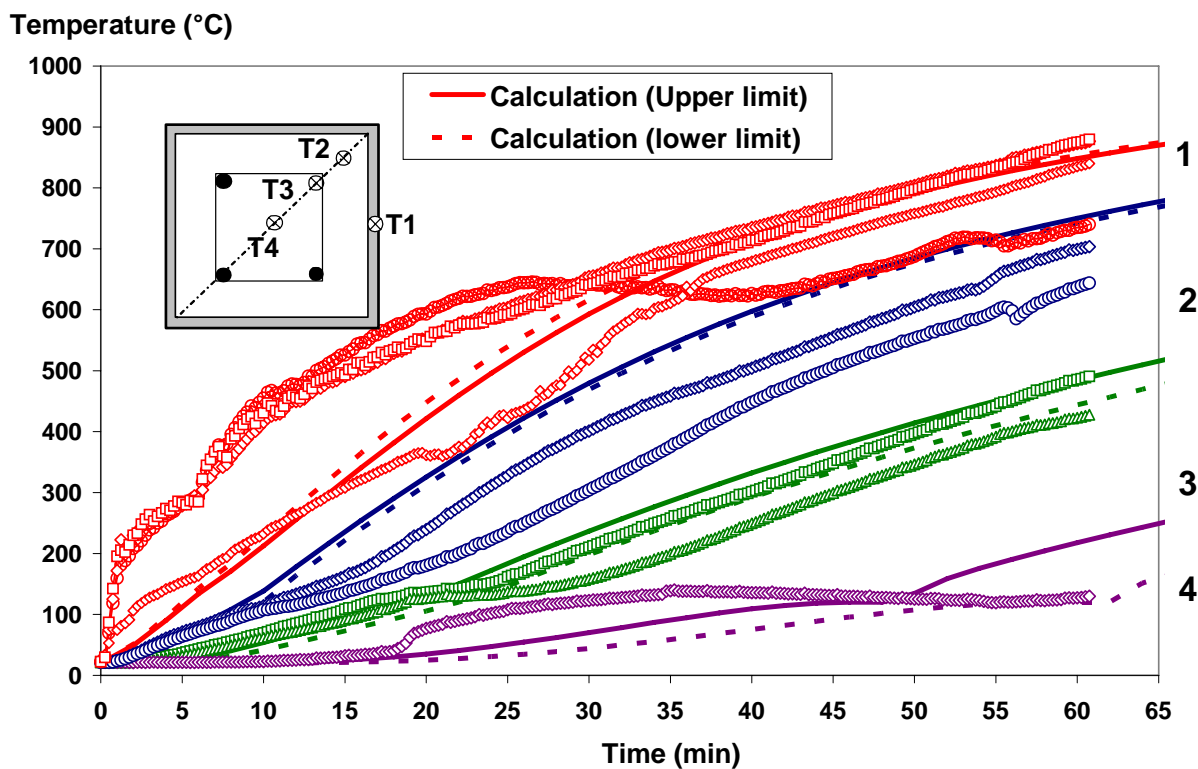


Figure 60 : Calculated and measured temperatures in the column cross-section n°3 of test n°3

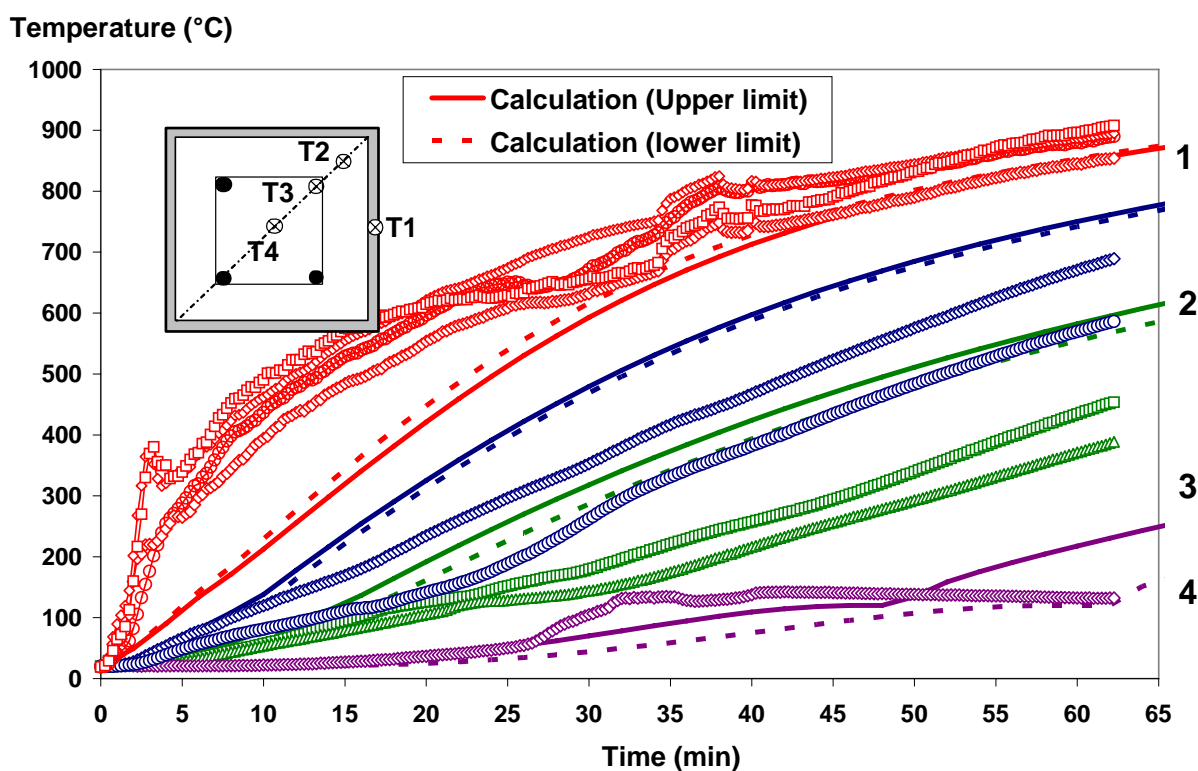


Figure 61 : Calculated and measured temperatures in the column cross-section n°1 of test n°4

Temperature (°C)

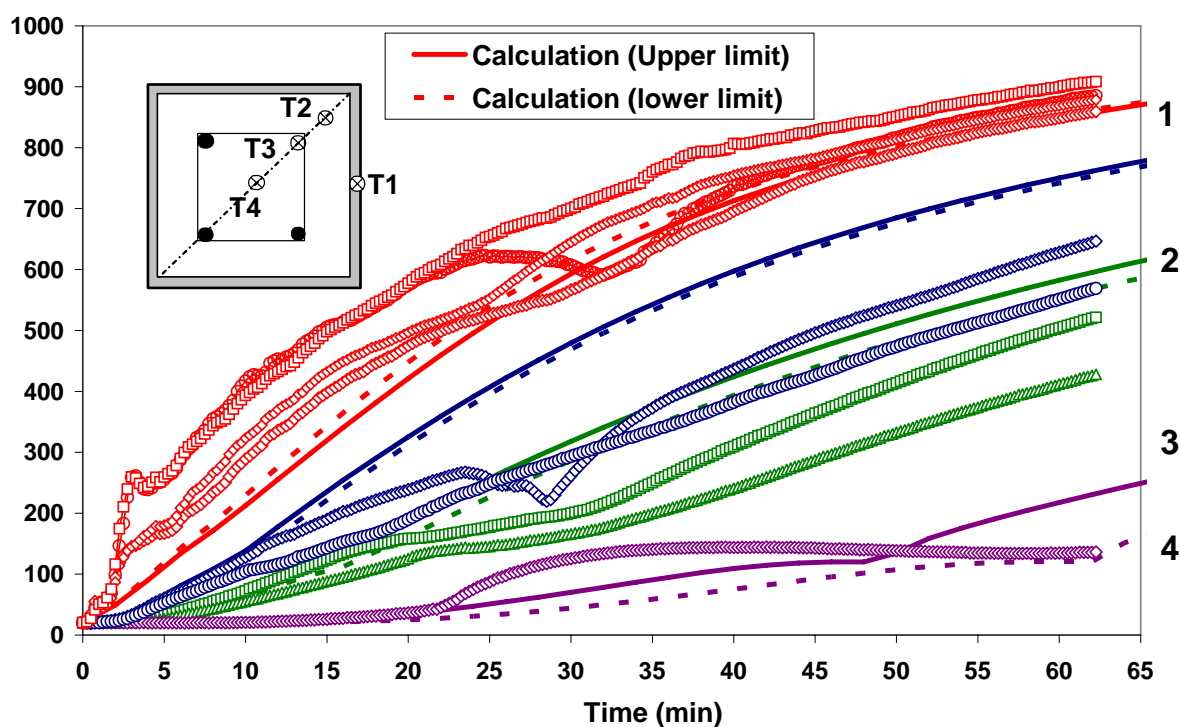


Figure 62 : Calculated and measured temperatures in the column cross-section n°2 of test n°4

Temperature (°C)

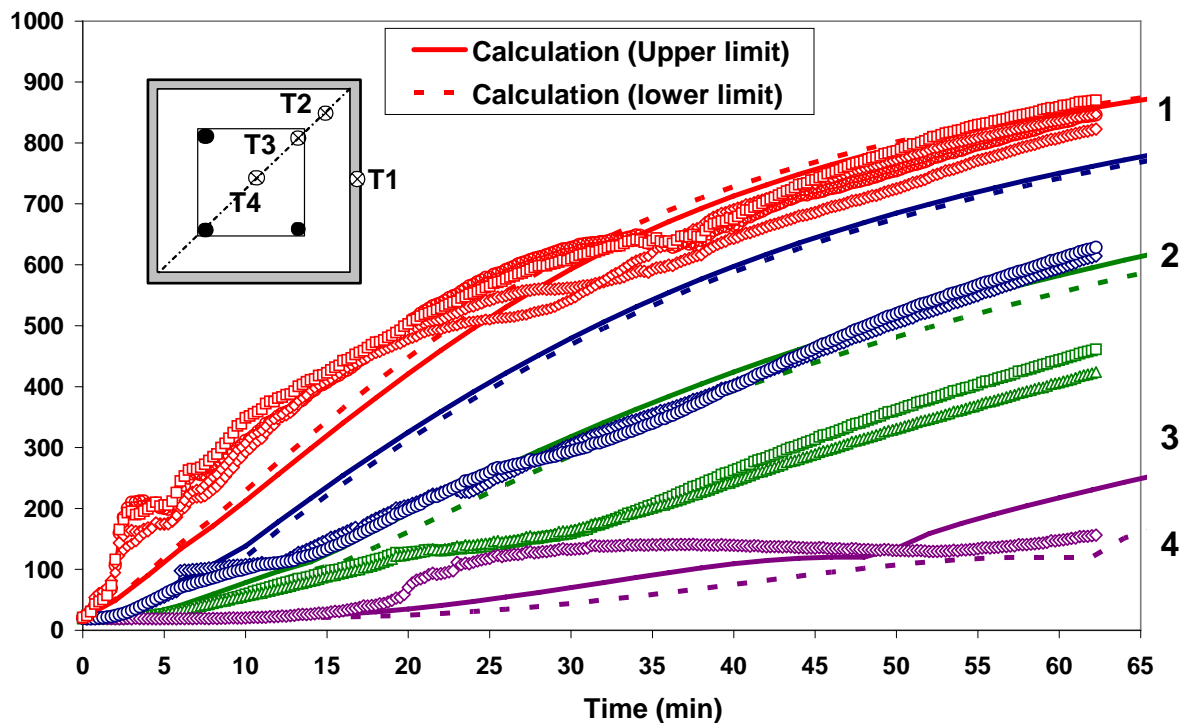


Figure 63 : Calculated and measured temperatures in the column cross-section n°3 of test n°4

Temperature (°C)

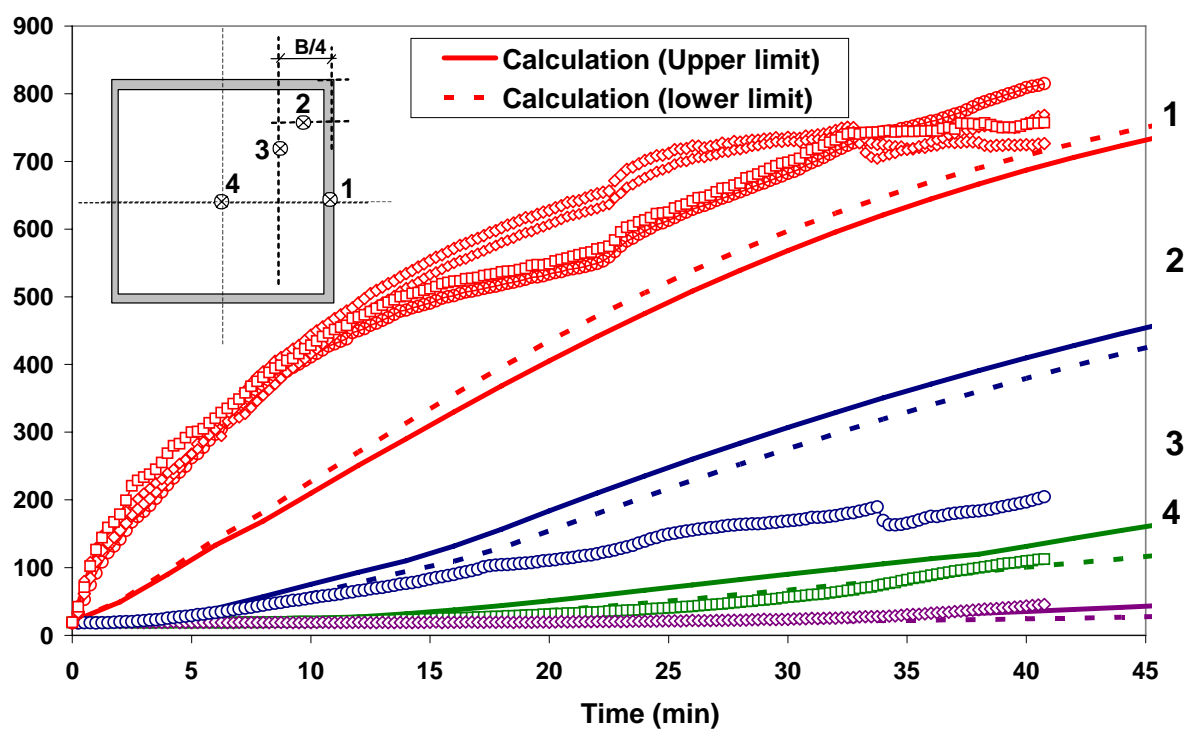


Figure 64 : Calculated and measured temperatures in the column cross-section n°1 of test n°5

Temperature (°C)

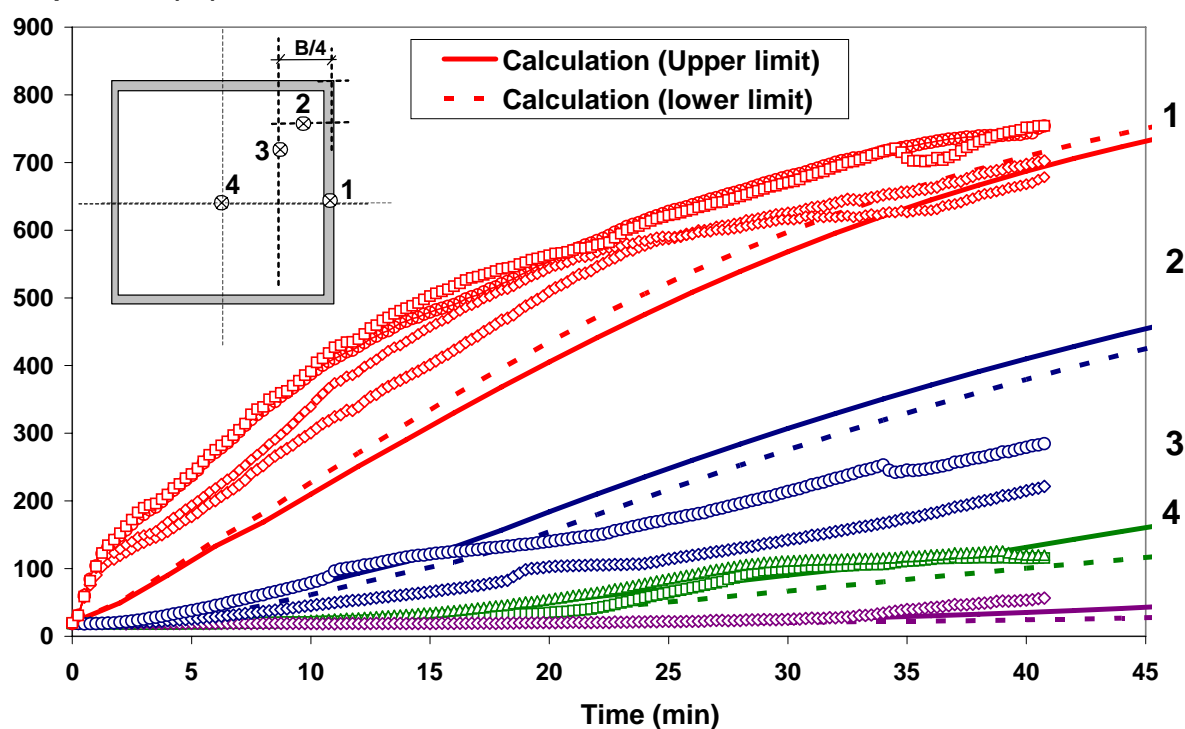


Figure 65 : Calculated and measured temperatures in the column cross-section n°2 of test n°5



Temperature (°C)

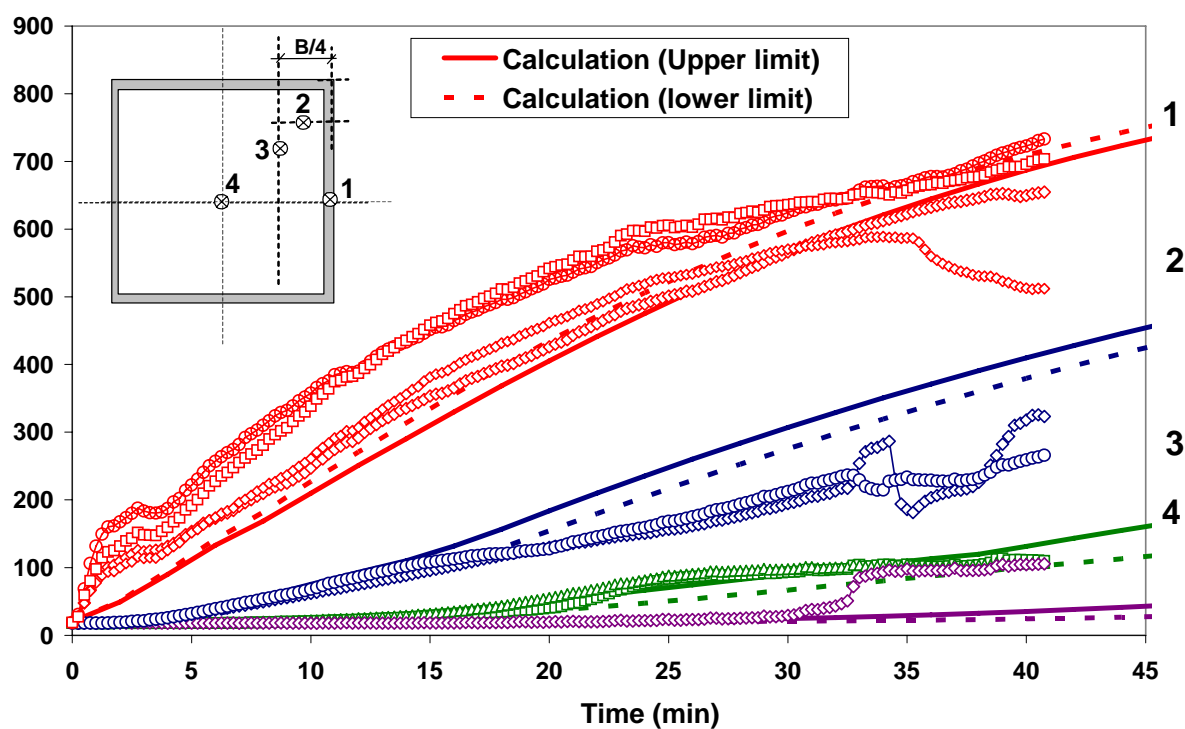


Figure 66 : Calculated and measured temperatures in the column cross-section n°3 of test n°5

Temperature (°C)

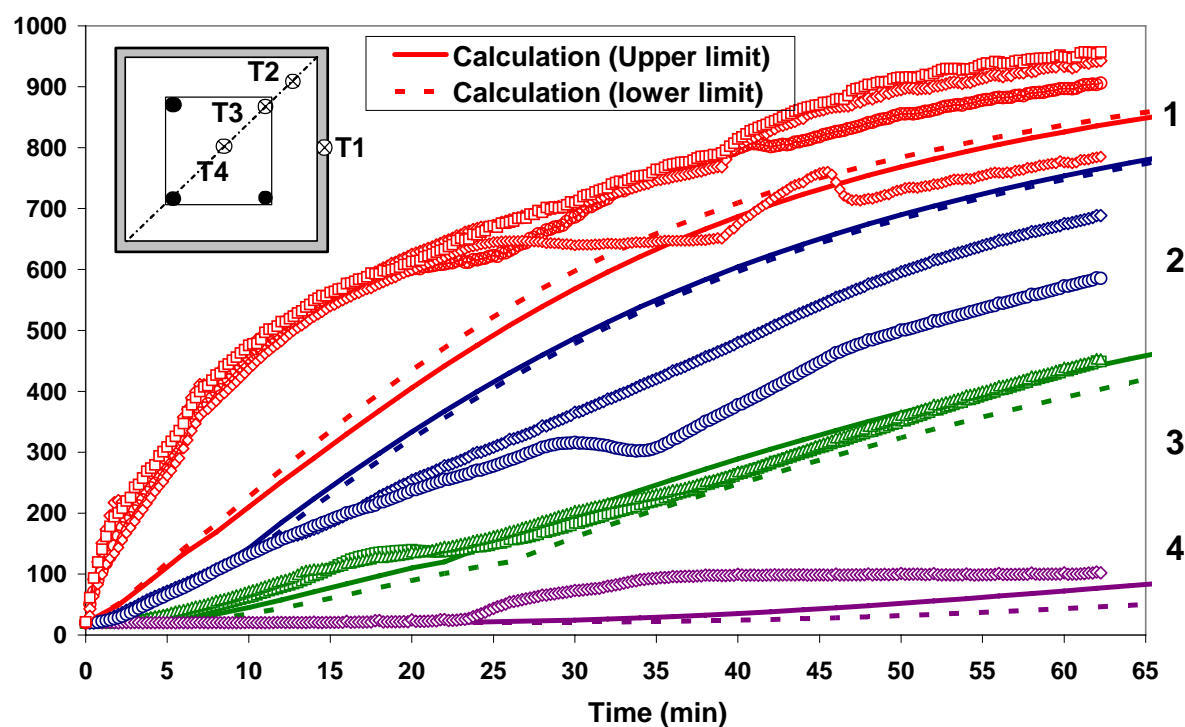


Figure 67 : Calculated and measured temperatures in the column cross-section n°1 of test n°6

Temperature (°C)

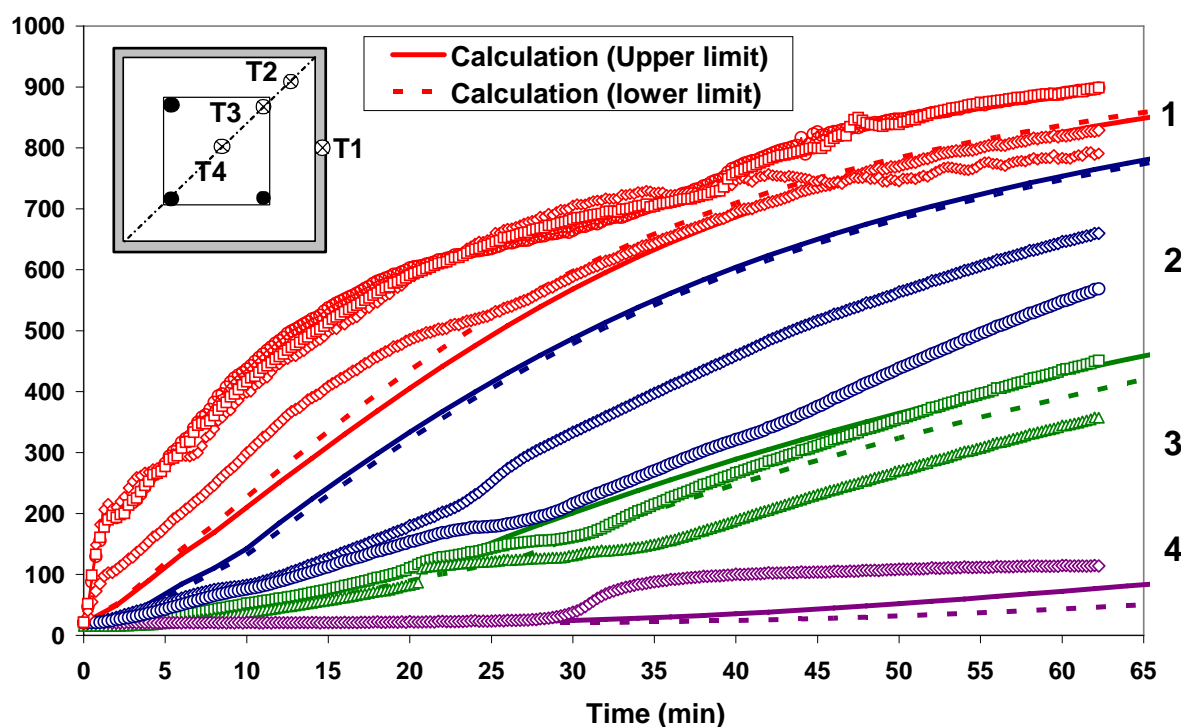


Figure 68: Calculated and measured temperatures in the column cross-section n°2 of test n°6

Temperature (°C)

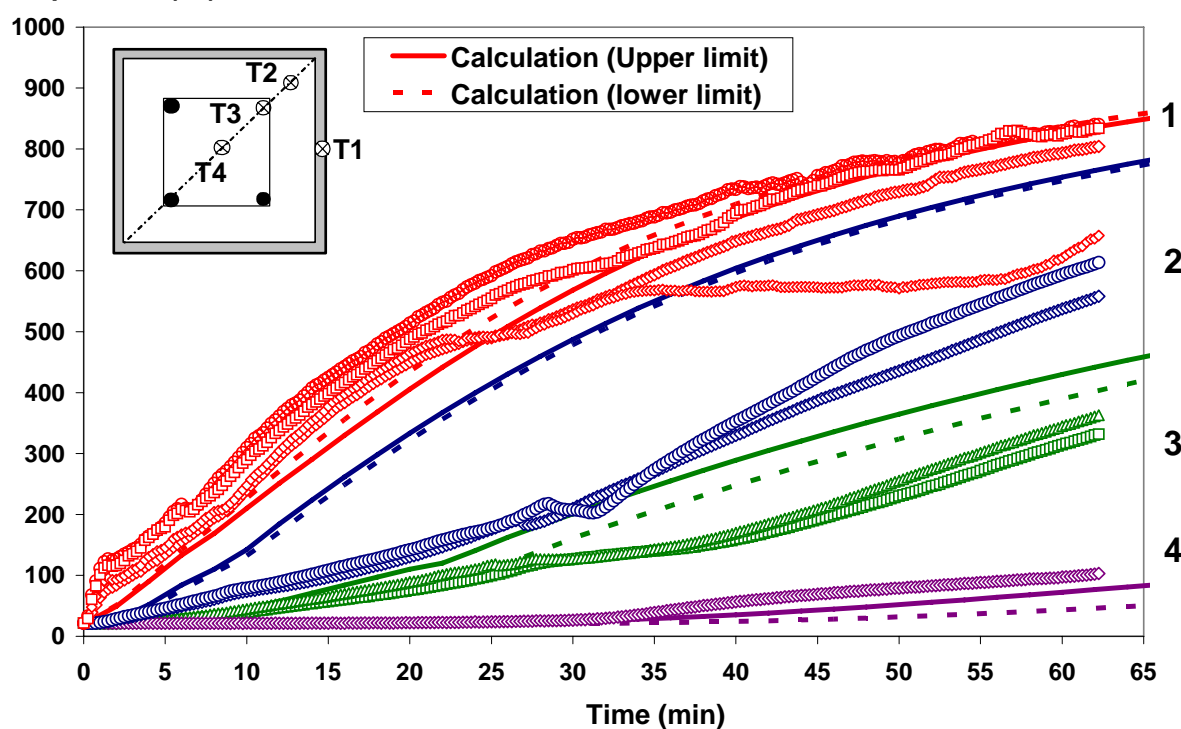


Figure 69 : Calculated and measured temperatures in the column cross-section n°3 of test n°6

Temperature (°C)

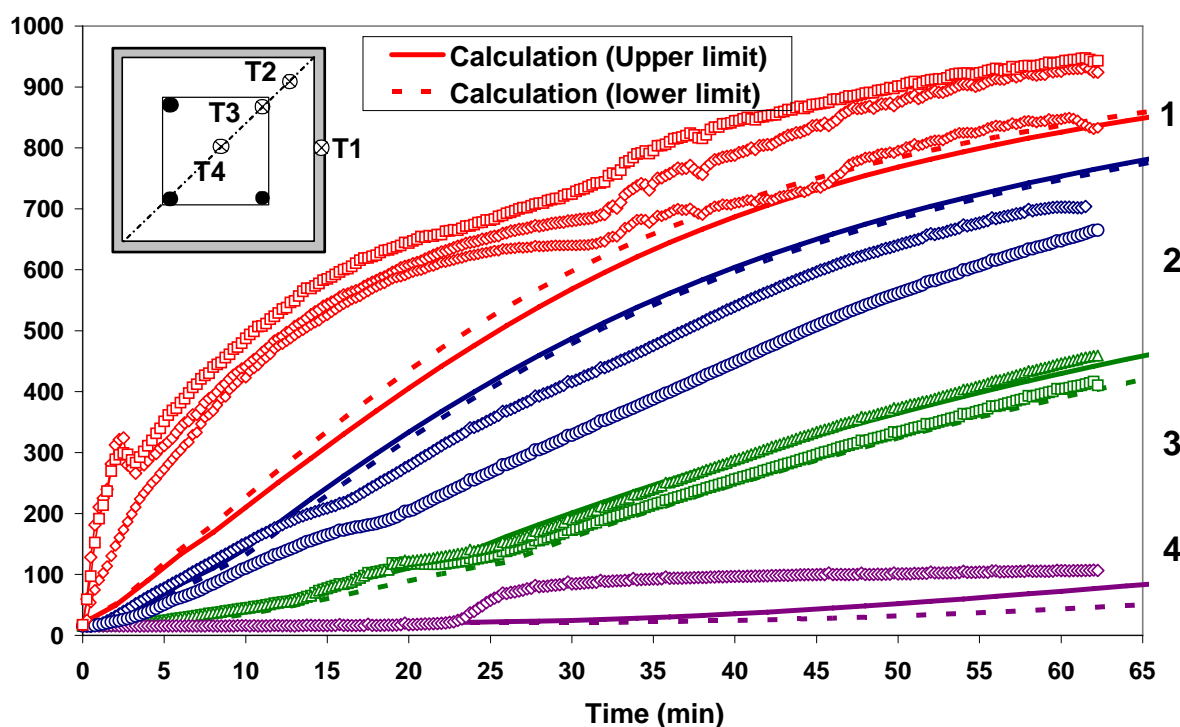


Figure 70 : Calculated and measured temperatures in the column cross-section n°1 of test n°7

Temperature (°C)

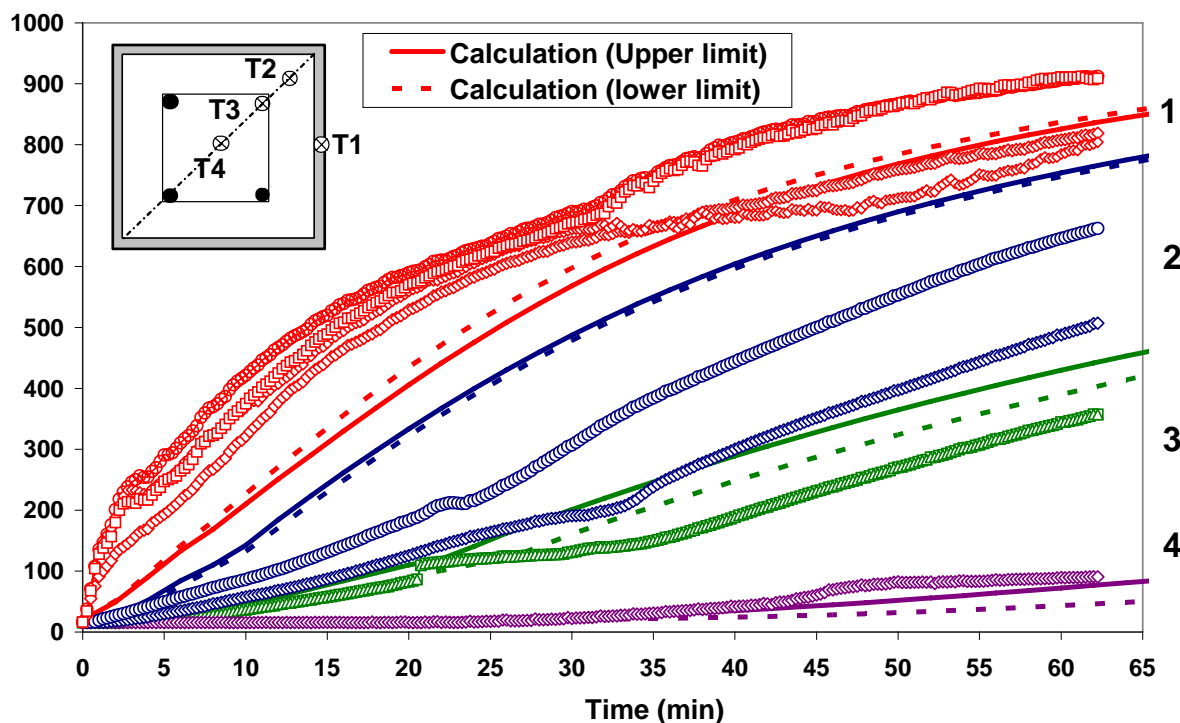


Figure 71: Calculated and measured temperatures in the column cross-section n°2 of test n°7

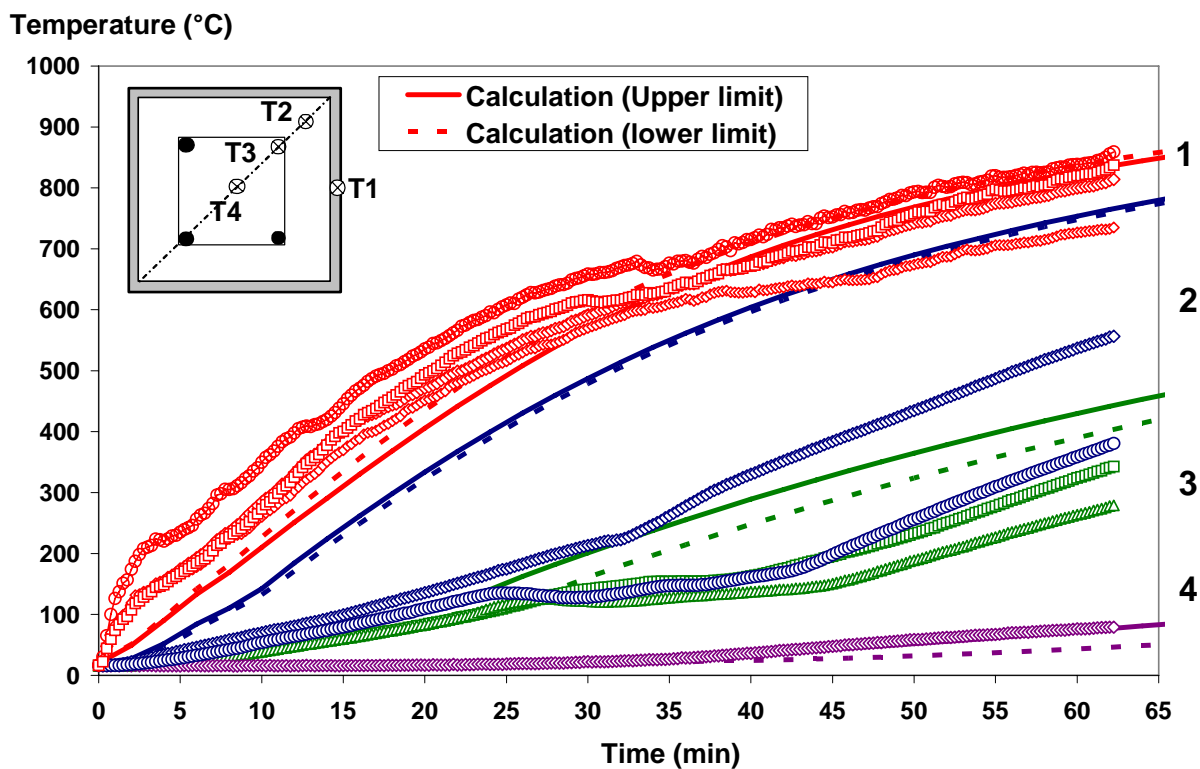


Figure 72 : Calculated and measured temperatures in the column cross-section n°3 of test n°7

## ANNEX C

### Comparison of the fire tests and the FE analyses

Vertical displacement (mm)

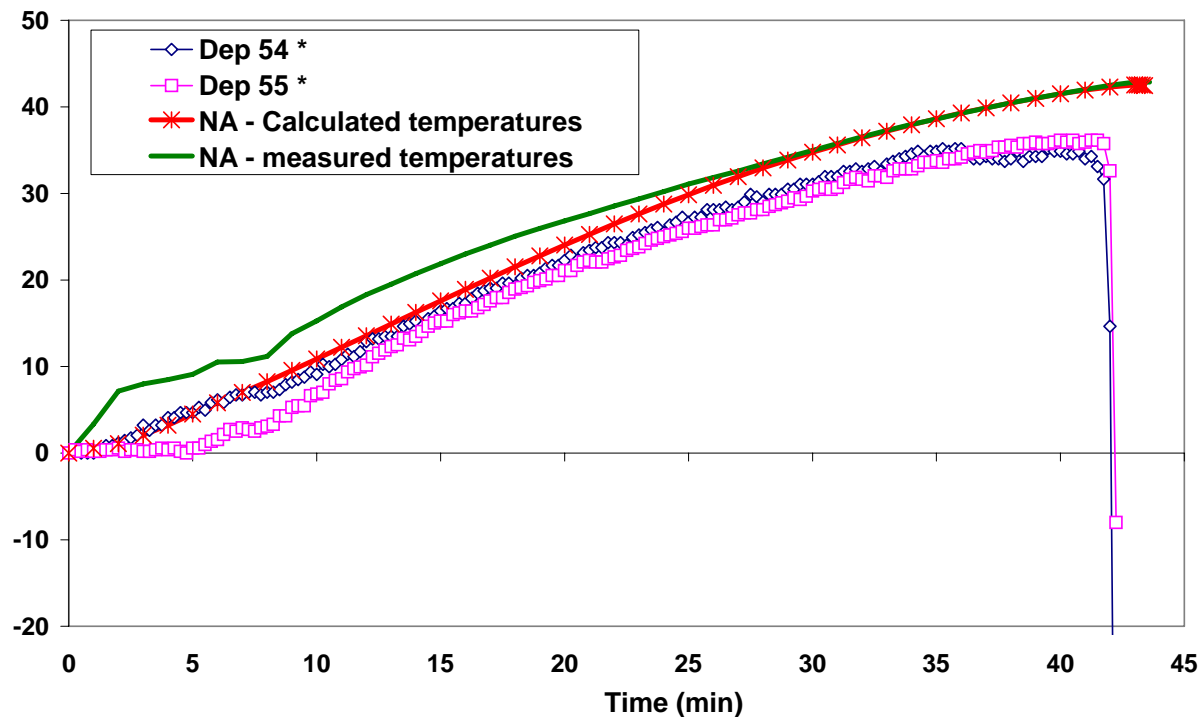


Figure 73: Vertical displacement at the column top of test n°1

Vertical displacement (mm)

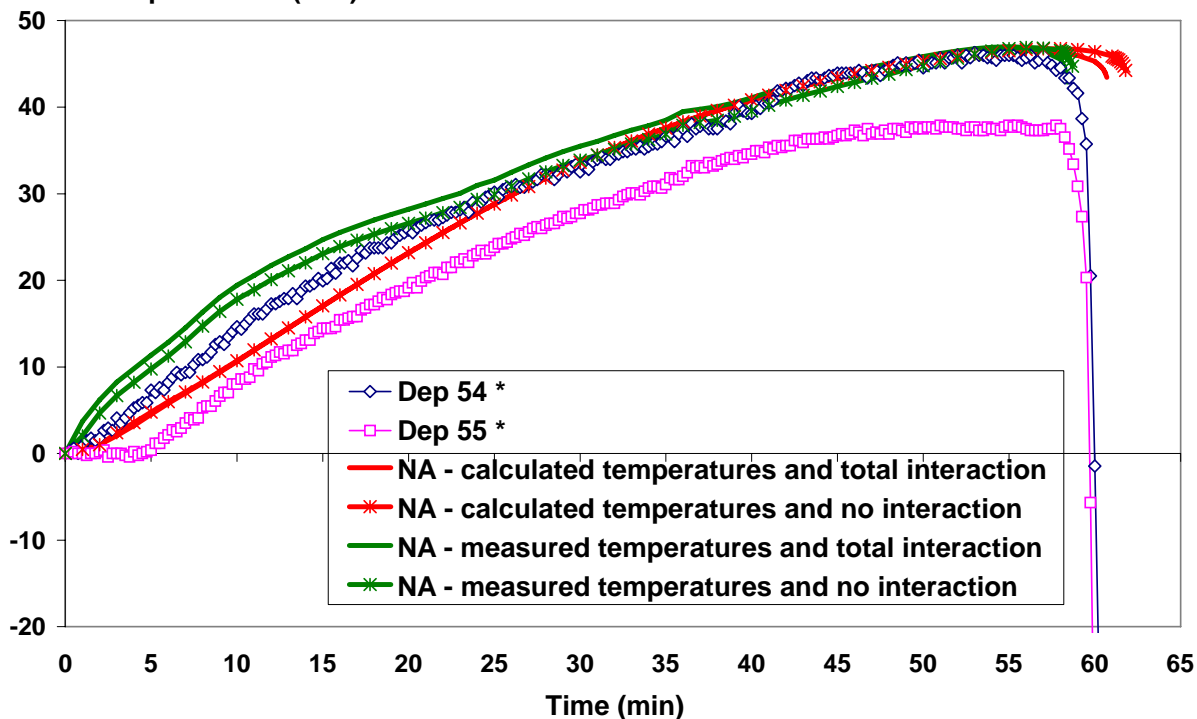


Figure 74::Vertical displacement at the column top of test n°2

Vertical displacement (mm)

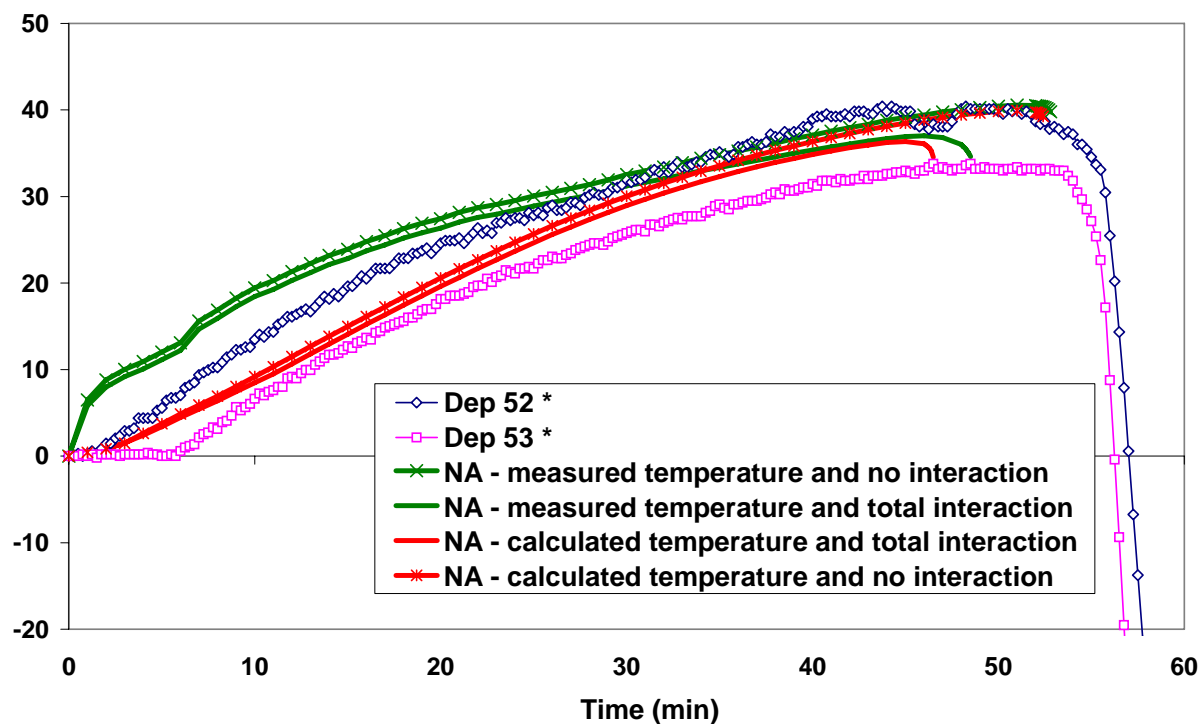


Figure 75: Vertical displacement at the column top of test n°3

Vertical Displacement (mm)

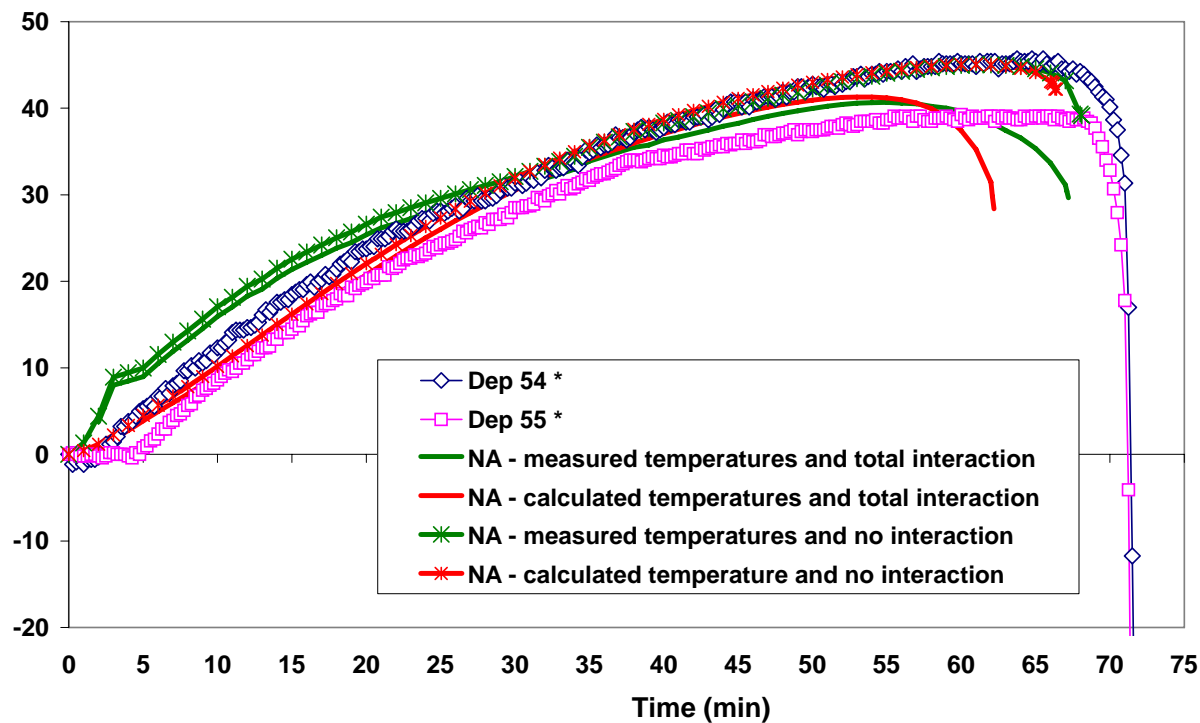


Figure 76 : Vertical displacement at the column top of test n°4

Vertical displacement (mm)

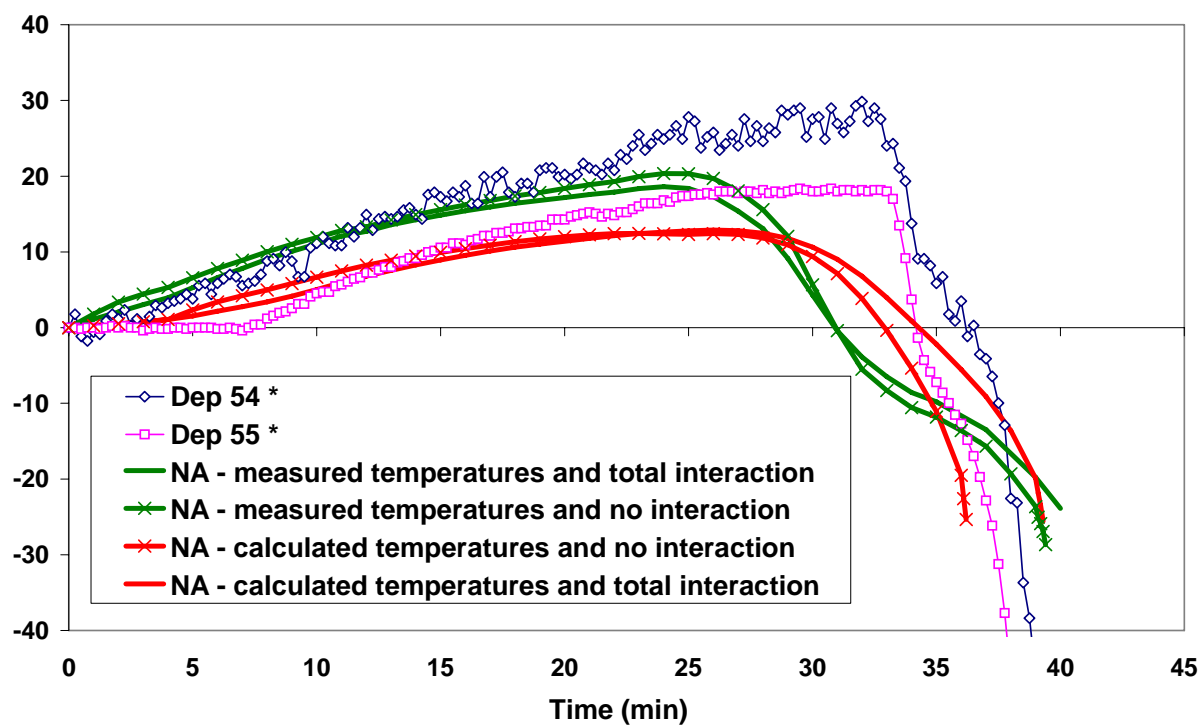


Figure 77 : Vertical displacement at the column top of test n°5

Vertical displacement (mm)

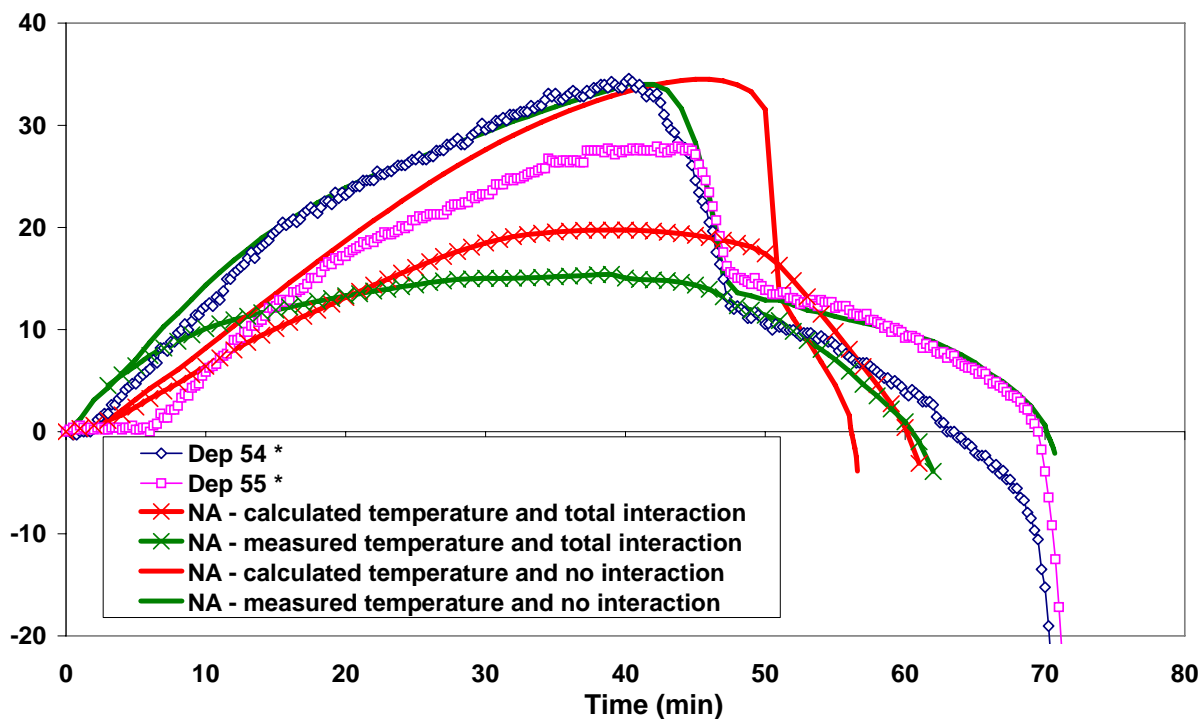


Figure 78 : Vertical displacement at the column top of test n°6

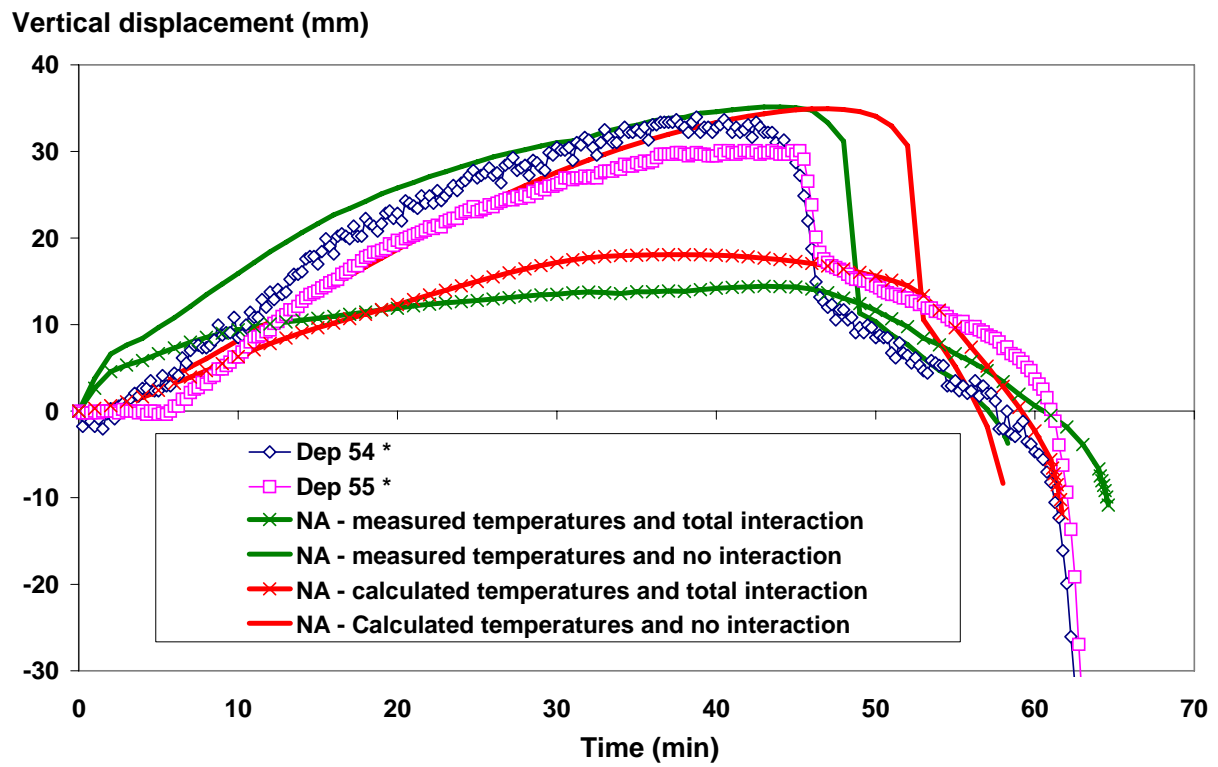


Figure 79 : Vertical displacement at the column top of test n°7